UNIVERSITÀ DEGLI STUDI DI MILANO BICOCCA

PhD School in Chemical Science

INTERACTIONS BETWEEN ATMOSPHERIC PARTICULATE MATTER AND STONE SURFACES

BY MEANS OF LABORATORY AND IN FIELD STUDIES

PhD dissertation by

Marco Casati

Supervisor

Prof. Ezio Bolzacchini

Academic year 2014/2015

Contents

Chapter 4
Study of potential decay-effects on stone substrates of each size fractions of atmospheric PM and single-salts PM. **129**

Chapter 5
Concluding Remarks **156**

Bibliographical Notes

CHAPTER 1

Introduction

1.1 Effects of Particulate Matter on Stone Materials

The outdoor exposed materials may show signs of weathering and decay. The damage can be purely aesthetic or it can affect the artefacts deeper inside their original material. The decay factors can be classified based on the different type of interactions with the substrates:

- Physical factors, which produce damage with pure physical mechanisms i.e. thermal shocks, wind erosion, frost and thaw cycles, dissolution and crystallization of salts.

- Chemical factors, which produce damage through chemical or physical chemical mechanisms i.e. acids pollutants, oxidants, chelating agents and solubilizers.

- Biodeteriogens, both autotrophic and heterotrophic, that can induce damage as a consequence of their growth on the materials surfaces (*Zanardini et al., 2000*).

The actual decay phenomena that can be observed on exposed artefacts are often the result of a combination of these three types of factors, which may also act synergistically. However, the atmosphere with its variations of temperature and humidity and the pollutants contained therein, may play a crucial role to establish the main mechanisms in action and the rate of the decay. Generally, the interactions between the material and the atmosphere lead to the formation of surface layers which cause damage to the original material (*Sabbioni, 1995*). Several atmospheric pollutant can have a fundamental role respect to stone materials decay. Particulate matter (PM) is one of the most studied pollutants (*Camuffo et al., 1982; Ferm et al., 2006; Ghedini et al., 2011; Grossi et al., 2003*) and, from this point of view, in the last years PM, NO_x and O_3 are receiving a growing attention due to the decreasing concentrations of other gas-phased acid pollutants such as SO_2 (*Ferm et al., 2005; Ghedini et al., 2011; Kucera et al., 2007; Urosevic et al., 2012*).

Atmospheric PM is defined as a suspension of fine solid or liquid particles in a gas (*Seinfeld and Pandis, 2006*). More properly, the term aerosol refers to the sum of airborne solid and liquid particles while the acronym PM is used to

indicate the dried out particles. Aerosol can be present in the atmosphere since it is directly emitted (primary aerosol) from natural or anthropogenic sources, otherwise it can be formed by gas-to-particle conversion processes (secondary aerosol). The range in size of atmospheric aerosol is considered to be from few nanometers (nm) to tens of micrometers (μm) (*Seinfeld and Pandis, 2006*). Therefore, PM is a complex mixture of substances with different origin and chemical composition, which results to be highly variable in space and time. In urban areas PM is often characterized by a carbonaceous core with the presence of organic and inorganic compounds eventually absorbed on its surface (*Gualtieri et al. 2011*). Each PM chemical fraction has been associated with specific decay phenomena.

The water-soluble inorganic fraction of PM contains water-soluble compounds i.e. nitrates, sulphates, chlorides, ammonium. The chemical composition of the water-soluble inorganic fraction can vary according to the seasons (*Perrone et al 2012*). Water-soluble inorganic compounds can be responsible of the so-called "salts-weathering". The atmospheric deposition is not the only source of salts for a stone surfaces, but it can represent a significant source under certain conditions (*Chabas et al., 2000; Ferm et al, 2006; Maro et al., 2014; McAlister et al., 2008*). The hygrometric variations may cause crystallization-hydration cycles of the salts. These cycles can promote the presence of

moisture on stone surfaces or causing mechanical stress during crystallization. This latter action is particularly dangerous for porous materials (*Charola, 2000 and references therein; Doehne, 2002 and references therein; Espinosa et al., 2008; Franzen & Mirwald, 2009; Grossi et al 2011; Linnow et al, 2006; Steiger 2005; Steiger & Asmussen, 2008*). In addition to this, acid compounds can be found in the water-soluble fraction of PM (*Behera et al, 2013; Pathak et al, 2004*) and these compounds will impact on various types of surfaces (*Potgieter-Vermaak et al., 2012*). In the water-soluble fraction can be also found some organic compounds like i.e. carboxylic acid (*Sabbioni et al., 2003; Tsai et al., 2008*). As well as an acid action, these compounds can have hygroscopic properties (*Speer at al., 2003*). Also oxalates can be found in the water-soluble fraction of PM (*Ma et al., 2013*). Oxalates are one of the most common compounds associated with weathering layers. The origin of the presence of oxalates so common is still subject of debate (*Sabbioni et al., 2003*), and the atmospheric deposition of soluble oxalates on carbonate stones can lead to the formation of calcium oxalates: whewellite, weddellite, caoxite (*Conti et al., 2010; Conti et al., 2014; Conti et al., 2015*). However, the so-called oxalate patina tend be compact and resistant to water and acidity, so much so that it was proposed the use of oxalates (i.e. ammonium oxalate) as conservative treatments (*Doherty et al., 2007; Conti et al.; 2011; Conti et al., 2013*).

The organic fraction of PM may contain several kind of chemical compounds and considering the wide variety of these organic compounds, a complete characterization of the organic matter in the PM is rather complicated. However, aliphatic hydrocarbons, polycyclic aromatic hydrocarbons, diterpenoids, fatty acids and phthalates were identified in weathered layers (*Saiz-Jimenez, 1993*). The organic matter may play a role in several decay processes, for example, the activity of heterotrophic bacteria on stone is governed by the availability of suitable organic matter (*Saiz-Jimenez, 1993; Zanardini et al., 2000*). Atmospheric depositions can help to increase the availability of organic matter on stone surfaces.

Carbonaceous particles are another relevant constituent of PM. This fraction can be indicated with different names, depending on the analytical techniques used for its determination: elemental carbon (EC), black carbon (BC), soot (*Andreae & Gelencsér, 2006*). A first issue deriving from the deposition of BC is the surface blackening, since BC is characterized to be strongly light-absorbing. In this respect, a relationship between the total suspended particles amount and the chromatic variations in term of lightness of the exposed surfaces was found (*Grossi et al., 2003; Urosevic et al., 2012*). It was also proved that carbonaceous particles have a catalytic role in the formation processes of the black crusts (*Ghedini et al., 2000; Rodriguez-Navarro &*

Sebastian, 1996; Sabbioni et al., 1992). Grey-to-black crust formation is produced by gypsum crystals and atmospheric deposition. Carbonaceous particles, because of their high specific surfaces, act as catalytic support to the heterogeneous oxidation of SO_2 (*Ghedini et al., 2000*), and play a decisive role as nucleation point (*Rodriguez-Navarro & Sebastian, 1996*) promoting the formation of gypsum on carbonate substrates. The reaction can be represented by the following steps (*Giavarini et al., 2008*):

$$SO_2 + \tfrac{1}{2}\ O_2 \rightarrow \quad SO_3 \qquad\qquad\qquad (1.1)$$

$$SO_3 + H_2O \rightarrow \quad H_2SO_4 \qquad\qquad\qquad (1.2)$$

$$H_2SO_4 + CaCO_3 + H_2O \ \rightarrow\ CaSO_4{\cdot}2H_2O + CO_2 \qquad (1.3)$$
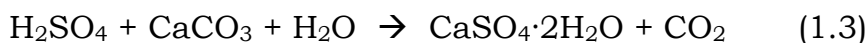
Carbonaceous particles are often associated with transition and heavy metals i.e. Fe, Mn, Zn, Cu, Pb, Ti, V, Cr, Ni, Pt, Rh (*McAlister et al., 2008; Rampazzi et al., 2011; Sabbioni 1995*), which contribute at the catalytic activity. Observing the reactions (1.2) and (1.3) it is clear that water has a key-role in the process. As well as salts, hydrophilic organic compounds and carbonaceous particles, other components of the PM like i.e. clay minerals, can help to retain moisture and prevent quick evaporation. This action may promote gypsum formation.

PM can be removed from the atmosphere through dry and wet deposition processes, and these are also the ways in which PM can deposit on the surfaces of the built

cultural heritage. Wet deposition takes place during rain events and dry deposition all the rest of the time. Wet deposition is due to the retention of the particles which impact the surfaces together with the precipitation, either if it is direct (as occurs on unsheltered horizontal surfaces), or wind-driven (as occurs on less sheltered vertical surfaces). Sheltering conditions can strongly influence the magnitude of this kind of deposition (*Camuffo et al., 1982*). Aerosol dry deposition on surfaces results from the combination of several processes such as Brownian diffusion, impaction and interception due to the turbulent motions, gravitational sedimentation, thermophoresis, diffusiophoresis, electrostatic attraction, etc. Gravitational sedimentation is expected to play no role in dry deposition on vertical surfaces, and in this scenario it is assumed that turbulent diffusion is the main mechanism, but in the vicinity of building facades the structure of turbulent flows and the value of turbulent diffusivity are still a matter of uncertainties and debates (*Maro et al. 2014*).

The study of the decay of cultural heritage stone material is a very complex issue, and it is even more complex study the role of PM in the decay processes since also PM is a complex pollutant. Even if the role of PM in some decay process, like i.e. the formation of black crust, was well highlighted and understood, such a knowledge derived mainly from the analytical study of real decayed layers, and

it is not simple to derive patterns or mathematical models that may be of general application (see section 1.2). In addition to this, urban PM is subject to changes, some depending on the climate and thus they could be linked to climate changes, other changes may depend on the environmental and energy policies. Therefore it is fundamental improve the knowledge about the PM-induced stone decay and improve the ability to predict the effects of climate and pollution changes for the cultural built heritage.

1.2   Analysis of the literature approaches

A large literature about stone decay and the effects of atmospheric pollutants on the surfaces of the built heritage has been produced. It is possible to identify two different approaches to the problem: an "empirical" approach as well as a "modellistic" approach.

It could be considered as empirical approach the direct analysis of monuments and their decayed layers, the so-called "diagnostic" phase of the restoration activities and the exposure tests of new specimens of stones (or other materials) with the prospect to observe their decay after a certain amount of time. This kind of approach has the advantage to allow the evaluation of the complexity of the decay phenomena. In fact, the decay of stone materials can take different morphologies, depending on the chemical and physics characteristics of stone material as well as the specific environment in which it is exposed. As a matter of fact, the decay is the result of complex interactions of many variables. It often occurs that different entities and different morphologies of decay can be observed in different points of a single zone of a single monument (see section 1.1*, Camuffo et al 1982, Maravelaki-Kalaitzaki & Biscontin 1999)*. To understand this complexity is a hard challenge. The analysis of decay layers of monuments and the diagnostic related to the restoration activities are of fundamental importance to document the possible

morphologies of decay and to create a suitable background of case-studies. However, this is an ex-post approach and the information thus obtained are often case-specific. With such approach it is not simple to fully understand the causes of observed decay (*Smith et al., 2008*), and obtain generally applicable information. In fact, monuments can have a troubled history, which is often almost unknown. The decay due to the atmospheric pollution is added to that due to improper restoration activities, traumatic events, carelessness and abandonment of the buildings. For these reasons, a potentially more fruitful approach is to perform exposure tests (*Butlin et al., 1992*; *Realini et al., 1995; Tzanis et al., 2011; Zappia et al., 1998*). The problem is that stones durability performance cannot be satisfactorily predicted trough short-term tests (*Smith et al., 2008*). Consequently, an exposure test of a building material needs a very long time horizon, with consequent high costs and difficulties related to the managing of research projects lasting several years (*Tidblad et al., 2012*). Even if the exposure of a fresh stone specimen allows to simplify some of the variables which underlie the occurrence of the decay phenomena, conditions in terms of sheltering or exposure are difficult to reproduce. In any real exposure, environmental variables (i.e. temperature, relative humidity, wind, pollutants etc) act in an unique way and it is not possible to understand the contribution of a single variable to the total of the observed decay.

With a modellistic approach it is attempt to develop quantitative relationship between some environmental parameter and the effects in terms of material decay. Usually this kind of relationship tries to assess the contribution of the single environmental variables to the decay. In this way, if the environmental variables of a certain place are known, it is possible to predict the decay which is subject the heritage exposed in that place. This kind of approach has the advantage to provide a predictive tool, which is nowadays of fundamental importance to understand the effects of climate changes on built heritage (*Bonazza et al., 2009; Brimblecombe et al., 2010; Sabbioni et al., 2010*). For example, several functions were proposed to predict the surface recession of carbonate stone (*Bonazza et al., 2009*). These functions are listed in table 1.2, according to the summary proposed by Bonazza et al. (2009).

Table 1.2: Models for surface recession on carbonate stone. Reworked from Bonazza et al. 2009

REFERENCE	FUNCTION	
LIPFERT (1989)	$R = 18.8 \cdot R + 0.016 \cdot [H^+] + 0.18 \cdot (V_{DS}[SO_2] + V_{DN}[HNO_3])$	**(1.4)**
LIVINGSTON (1992)	$\Delta[CA^{2+}] = \Delta[SO_4^=] + \{10^{-11.6}(1/\gamma_{RO}[H^+]_{RO} + 1/\gamma_0[H^+]_0) - \frac{1}{2}([H^+]_{RO} - [H^+]_0)\} + \{10^{-11.6}(1/\gamma_0[H^+]_0 + 1/\gamma_R[H^+]_R) - \frac{1}{2}([H^+]_0 - [H^+]_R)\}$	**(1.5)**
WEBB ET AL. (1992)	$S.L.(mol) = ADV_{DS}C_{SO2} + (K_H K_1 P_{CO2}/2[H^+]_R) \, 3\Sigma(A_I R - E_{VAP}) + ([H^+]_I/2) \, 3\Sigma(A_I R)$	**(1.6)**
BAEDECKER ET AL. (1992)	$S.L.(mmol/L) = 0.16[1.0 - 0.015T + 0.0000922T^2] / 0.683 + 0.49[H^+]$	**(1.7)**
TIDBLAD ET AL. (1998; 2001)	$R = 2.7[SO_2]^{0.48} \, EXP\{f_{P1}(T)\} \, t^{0.96} + 0.019 Rain[H^+] \, t^{0.96} \, f_{P1}(T) = -0.018T$	**(1.8)**
KUCERA ET AL. (2007)	$R = 3.95 + 0.0059[SO_2]RH_{60} + 0.054 Rain[H^+] + 0.078[HNO_3] RH_{60} + 0.0258 PM_{10}$	**(1.9)**

In Lipfert (1989) model (1.4):

L = surface recession per year (μm year^{-1});

18.8 = term based on the solubility of $CaCO_3$ in equilibrium with 330 ppm of CO_2 (μm m^{-1});

R = precipitations (m year^{-1});

0.016 = constant valid for precipitation pH in the range 3–5;

$[H^+]$ = hydrogen ion conc. (μmol l^{-1}) evaluated from rain yearly pH;

0.18 = conversion factor from (cm s^{-1}) (μg m^{-3}) to μm;

V_{dS} = deposition velocity of SO_2 (cm s^{-1}) and $[SO_2]$ = conc. (μgm^{-3});

V_{dN} = deposition velocity of HNO_3 (cm s^{-1}) and $[HNO_3]$ = conc. (μgm^{-3}).

In Livingstone (1992) model (1.5):

$\Delta[Ca^{2+}]$ **and** $\Delta[SO_4^{=}]$ = differences in concentration (mol l^{-1}) of the ions Ca^{2+} **and** $SO_4^{=}$ between rainwater and runoff water;

$[H^+]_0$ = effective hydrogen ion concentration (mol l^{-1}) of the rainwater in the absence of anthropogenic pollutants ($10^{-5.6}$);

$[H^+]_r$ = effective hydrogen ion concentration (mol l^{-1}) of rain;

$[H^+]_{ro}$ = hydrogen ion concentration (mol l^{-1}) of the runoff;

γ = activity coefficient

In Webb et al. (1992) model (1.6):

S.L. = Stone Loss (mol)

C_{SO2} (μm m^{-3}) = mean SO_2 concentration during the exposure of duration (D);

VdS = deposition velocity (cm s^{-1}) of SO_2;

A = surface area of the exposed stone;

A_i = rainfall interception area;

$[H^+]_r$ **and** $[H^+]_l$ = volume–weighted mean hydrogen ion concentrations of the runoff and rainfall (mol l^{-1}), respectively;

E_{vap} **(mm^3)** = volume of rainfall evaporating from the stone sample;

K_H **and** K_1 = equilibrium constants of carbonate and bicarbonate in equilibrium with atmospheric concentration of 350 ppm CO_2 (Henry constant and first dissociation constant respectively)

R = amount of rainfall (mm).

In Baedecker et al. (1992) model (1.7):

S.L. = Stone loss (mmol/l);

T = temperature (°C);

$[H^+]$ = hydrogen ion concentration (mol l^{-1}).

In Tidblad et al. (1998 and 2001) model (1.8):

R = surface recession per year (μm year^{-1});
$[SO_2]$ = concentration (1-83 μm m^{-3});
T = temperature (2-19°C);
$Rain$ = amount of rainfall (327-2144 mm);
$[H^+]$ = concentration (0.0006-0.13 mg l^{-1})
t = time (1-8 years)

In Kucera et al. (2007) model (1.9):

R = surface recession per year (μm year^{-1});
$[SO_2]$ = concentration (μm m^{-3});
RH_{60} = measured relative humidity when RH>60% otherwise 0;
$Rain$ = amount of rainfall and $[H^+]$ is the H^+ conc. (0.0006-0.13 mg l^{-1})
$[HNO_3]$ = HNO_3 concentration (μm m^{-3});
PM_{10} = particulate matter concentration (μg m^{-3})

Looking at these functions, two main issues can arise. First of all, some of these functions were derived from the observation of exposed limestone, or they can be postulated for generic calcite, like i.e. Lipfert (1989) model (*Bonazza et al., 2009*). The built heritage can be formed by a wide range of carbonate lithotypes, with different characteristics in terms of structure, porosity, homogeneity, accessory minerals etc.; also the manufacturing can affect some property like surface roughness. This problem is even more evident in the case of artificial stone materials, some of which can have a carbonate matrix. Stones with different petrophysical characteristics are subject to different decay rates and it follows that is unlikely that a single function can model properly the surface recession of such wide category of different materials. A second issue regards the

variables chosen to build the functions. Some models use variables that are difficult to predict, with the consequent difficulties in using the models with predictive purposes. For example Livingstone (1992) and Webb (1992) models need data about the composition of runoff water, and up to not it is not possible to make projections about the composition of the runoff water (*Bonazza et al., 2009; Grossi et al., 2008*). In addition to this, the most of the models were developed considering the SO_2 dominating situations Current and future scenarios are considered to be multi-pollutant situations, in which SO_2 is not longer dominant and other pollutants like ozone, PM and nitrogen compounds are receiving a growing attention respect to decay and corrosion phenomena (*Kucera et al., 2007*). For example, Lipfert (1989) function, which is one of the most used (*Bonazza et al., 2009; Brimblecombe & Grossi, 2009; Grossi et al., 2008*), recognized three main mechanisms for material loss: karts effects, acid rain effect and dry deposition. Only Kucera (2007) function introduced a term about PM, and it considers the PM_{10} atmospheric concentration. As stated in section 1.1, and more in detail in case of the Po Valley in section 1.3, PM can have a complex chemical composition and a complex dimensional pattern, which can strongly vary with space and time. Therefore, it arises that the simple PM_{10} atmospheric concentration cannot be a proper estimator of the role of PM in stone decay processes.

Similar consideration are also valid in the case of the functions predicting the surface blackening. In fact, some functions are available to predict the black soiling, considering as the decreasing in the L^* coordinate of the Lab colour space, after a certain time. For example, Grossi et al. (2003) proposed the following simple relation:

$$L_t^* = L_i^* - SC\sqrt{TSP\,t} \quad (Eq.\,1.10)$$

L_t^* and L_i^* = L^* coordinate in the Lab color space at final and initial time
SC = soiling coefficient which is characteristics of each stone, according to Grossi et al. (*2003*)
TSP = Total Suspended Particles
t = time

Another similar model was proposed by Brimblecombe and Grossi (*2009*):

$$L_t^* = (L_0^* - L_\infty^*)\cdot\exp(-SC\cdot TSP\cdot t) + L_\infty^* \quad (\text{Eq.}\,1.11)$$

Where L_∞^* is the lightness after infinite soiling. The most difficult parameter to constrain these equation is TSP, and even more challenging is to estimate the portion of TSP responsible for the blackening, which is commonly associated with Elemental Carbon or Black Carbon (*Urosevic et al. 2012*).

In conclusion, with a modellistic approach only one single kind of decay can be modelled at time, as in the case of surface recession or black soiling. The more complex decay phenomena, like i.e. the black crust formation, which are

due to several mechanisms acting synergically having a non-linear behaviour (*Smith et al* 2008), cannot be modelled. In addition to this complex pollutants, like PM, are not describable with only one single simple variable so it is difficult to make a proper evaluation of the role of PM in decay processes with a modellistic approach.

1.3 The situation in the Po Valley

Northern Italy is one of the most industrialized and populated regions in western Europe and is characterized by high levels of atmospheric pollution (*Perrone et al., 2012*). The Po Valley is considered as an European hot spot regarding the problem of atmospheric PM pollution. This is due to the high density of anthropogenic PM sources, low mixing layer height, poor ventilation and secondary PM formation (*Carbone et al., 2010; Ferrero et al., 2012; Rodriguez et al., 2007*). From this point of view, Italian legislation (D. Lgs. 155/2010) transposes European regulation (2008/50/CE) establishing an annual limit of $PM_{2.5}$ at 25 $\mu g \cdot m^{-3}$ starting from 2015 and a daily limit of PM_{10} at 50 $\mu g \cdot m^{-3}$ has not to be exceeded more than 35 days in a year. The annual limit of PM_{10} concentration is 40 $\mu g \cdot m^{-3}$. Considering the case of the metropolitan area of Milan, which is the main city in the Po valley, in 2014 the daily limit of PM_{10} was exceeded not less than 53 days, in some parts of the city the limit was exceeded for more than 60 days, and 2015 was even worse. Despite this, the 2014 annual average concentration of PM_{10} stands at 34 $\mu g \cdot m^{-3}$ and it is under the regulatory limits. The annual average of $PM_{2.5}$ is of 26 $\mu g \cdot m^{-3}$ in accordance to the reducing target for this pollutants. By observing the trends of annuals averages of several atmospheric pollutants in the city of Milan, it can be noticed that some of them show a clear downward trend

i.e. SO_2 and benzene. In the case of PM_x this trend is less evident, confirming that the PM pollution is still an unsolved problem in the city of Milan and in the whole Po Valley.

In Milan, the fine fraction of PM represent a large part of the total PM. The ratio $PM_{2.5}/PM_{10}$ is about 80% in the last decade (*Casati et al; 2015*), and data from local protection agency (ARPA Lombardia) indicate that this ratio stands at 76% in 2014. PM concentrations in Milan are higher during the cold season and lower during the warm season. This seasonal trend is typical in all the Po Valley and it is due to the seasonal meteorology: during the cold season conditions of atmospheric stability with low mixing layers cause very high concentrations of atmospheric pollutants at ground levels (*Ferrero et al., 2010*). Conversely, the warm season is characterized by higher average wind speed and broader mixing layer thus improving the atmospheric dispersion of the pollutants (*Perrone et al. 2012*). Also the chemical composition of PM changes with season, as it can be seen in figure 1.1 (*taken from Perrone et al., 2012*)
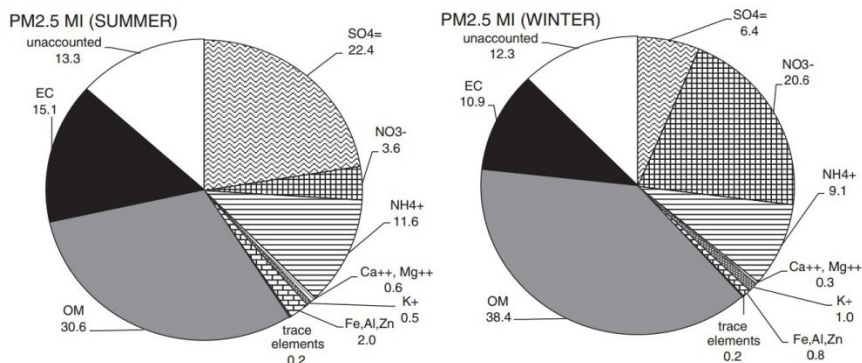
Figure 1.1: PM$_{2.5}$ average chemical composition in Milan.– Taken from Perrone et al. Sci. Total Environ. (2012).

Organic Matter (OM) explains 30-40% of the total PM$_{2.5}$ mass, The Elemental Carbon (EC) explains the 10-15% and the 12-13% is unaccounted. The main seasonal difference is in the composition of the inorganic ions fraction, which accounts for about the 40% of the total mass. NH$_4^+$, NO$_3^-$, SO$_4^=$ are the main inorganic ions and represent more than 95% of the total inorganic ions. A nitrates-predominance occurs during the cold season while there is a sulphates-predominance during the warm season (*Ferrero et al., 2013; Perrone et al., 2010, 2012, 2013 and references therein; Sangiorgi et al., 2011*). During the warm season, PM$_{2.5}$ is rich in sulphates because they are formed mainly by photochemical reaction (*Vecchi et al., 2008*) starting from gaseous precursor SO$_2$. On the other hand, during the cold season PM$_{2.5}$ is rich in nitrates because NO$_3^-$ is mainly present as ammonium nitrate which is semivolatile. Therefore, the low temperature of the cold season promotes

its condensation in the particulate phase (*Schaap et al., 2002*). Ammonium is the main cation and it does not show a significant seasonal trend.

The Po Valley represents an unique situation not only by the point of view of the air quality but also as regards the huge amount of cultural heritage that lies in it. It is believed that in Italy it is conserved a large part of the Word Cultural Heritage, the Italian "Risk Chart" drafted in 1996 (*Accardo et al., 2002 and 2003*) lists no less than 57000 cultural assets, 5000 of which are archaeological and 52000 are architectural. Looking at the regional distribution of these cultural assets (Figure 1.2), it can be noticed that most of them are placed in the regions of the Po Valley.
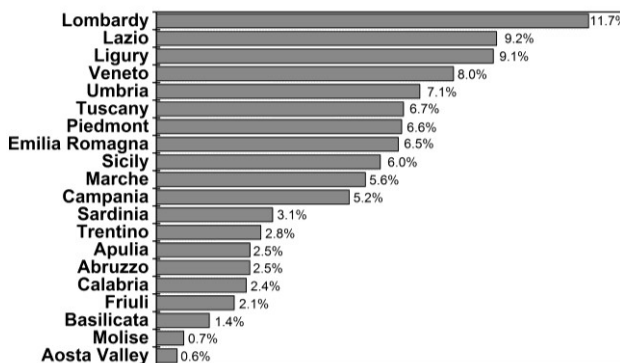
Figure 1.2: Regional distribution of the Italian Cultural Heritage according to the "Italian Risk Map" – Reworked from http://www.cartadelrischio.it/

Lombardy is in the first place, as it counts 7316 cultural assets representing the 11,7% of the total, but also the other regions of the Po Valley: Veneto, Piedmont and Emilia Romagna, are in the upper part of the list.

Essentially, Po Valley represents a unique laboratory in order to study the effects of air pollution on Cultural Heritage. In fact, several literature's works in this topic were performed in the Po Valley. Limiting to the case of Milan, it is possible to cite works about the analysis of real damage layers on buildings and monuments (*Bonazza et al., 2005; Bugini et al., 2000; Cappitelli et al., 2007; Fermo et al., 2014a; Gulotta et al., 2012; Pedrazzani et al., 2006*) as well as exposure tests of stone and buildings materials specimens (*Realini et al., 2005; Kucera et al., 2007; Tidbald et al., 2012; Zanardini et al., 2000; Zappia et al., 1998*) and modellistic approaches (*Casati et al., 2015*; *Screpanti and De Marco, 2009*).

CHAPTER 2

Evaluation of the Stone Decay Hazard related to Atmospheric Particulate Matter Pollution using an Heritage Climatology approach

2.1   Theoretical Background

The decay of outdoor-exposed materials may heavily depend on factors related to climate and pollution (*Sabbioni 1995; Bonazza et al. 2009; Ghedini et al. 2011; Urosevic et al. 2012*). As concerned the relationship between certain type of climate and the possible decay mechanisms that can be took place therein, the wording "heritage climatology" has been proposed to identify this field of study. The concept of "heritage climatology" has been recently proposed by Brimblecombe, and in some of his works it can be found applications of this concept (*Brimblecombe 2010;*

Grossi et al. 2011). The proposal of a specific wording to identify the study of heritage's decay in relationship to climate highlights the growing attention that climate and its changes are having in the scientific community.

As stated, decay may depend on climate but also on pollution and by this point of view, PM is one of the most relevant air pollutant concerning stone decay (*Camuffo et al., 1982; Grossi et al., 2003; Ferm et al., 2006*). PM can cause damage to outdoor-exposed stone materials after deposition on stone surface and its role in materials-decay processes is receiving growing attention due to the decreasing concentrations of other gas-phased acid pollutants such as SO_2 (*Ferm et al., 2005; Kucera et al., 2007; Ghedini et al., 2011; Urosevic et al., 2012*). Even if several studies highlighted the role of some single PM's components in specific stone-decay processes (*Saiz-Jimenez et al. 1993; Rodriguez-Navarro and Sebastian 1996; Torfs et al. 1997; Chabas et al. 2000; Zanardini et al. 2000; McAlister et al. 2008; Stefanis et al. 2009; Ozga et al. 2011; Potgieter-Vermaak et al. 2012*) PM is a complex mixture of substances (*Perrone et al. 2012*), and few works have tried to assess the potential decay impact of PM considering its comprehensive chemical-physics properties and its behaviour during climatic variations. A similar approach can fills the gaps concerning the quantification of the hazard for heritage

stone substrates due to the synergic effect of climate and atmospheric PM pollution.

Several indicators were proposed in literature for the evaluation of the hazard for outdoor-exposed stone substrates. Some authors (*Brimblecombe et al. 2006; Bonazza et al. 2009*) have focused their attention on the time of wetness (TOW) that represent the time fraction during which liquid water could be present on a stone surface. Liquid water can trigger a large number of decay processes, such as solid-liquid reactions, acid attack, penetration of salts solutions in the porosity of materials and biofilms formation. Thus, the TOW describes the hazard that a stone could be exposed to because of "chemical" decay-mechanisms (*Camuffo 1995; Cardell-Fernandez et al. 2002; Dohene 2002*). Another indicator was introduced by Grossi et al. (2011) who focused their attention on the phase-transition events. They proposed the number of crystallization-dissolution cycles (Ncy) as a stone hazard indicator that describes the number of phase transitions (from solid to solution, and back to solid) of soluble stone contaminants due to ambient RH variations. As a consequence, Ncy indicates the hazard that a stone could be exposed to because of "mechanical" decay-mechanism due to the stress induced when crystallization occurs.

Even if TOW and Ncy appear as promising indicators of the hazard for stone substrates, their quantification was conducted just using simplified approaches. Concerning TOW, the computation algorithm assumed the wetting of surfaces when RH is greater than 80% and temperature is greater than 0°C (*Brimblecombe et al. 2006; Bonazza et al. 2009*). Other authors (*Ponziani et al. 2012*) used the Distance to Dew Point (DDP) index and the Kelvin equation to assess the condensation events frequency. As stated by Camuffo (1995) all these methods are valid for non-reactive surfaces, and the presence of contaminants may cause deviations from such a quite simple model. A similar situation occurs for the Ncy computation: most of the literature studies exploited the equilibrium humidity point of pure salts to assess the number of phase transitions in function of ambient RH variations (*Doehne 2002; Steiger 2005; Grossi et al. 2011*).

Considering the situation of PM deposited on stone surfaces, its hygroscopicity could be one of the most relevant properties concerning stone decay hazard (*Camuffo et al. 1982; Camuffo 1995; McAlister et al. 2008*). In the case of complex mixture as PM is, hygroscopicity can be described by two key-parameters: the deliquescence relative humidity (DRH) and the crystallization relative humidity (CRH). These are the thresholds at which a phase change of

the PM water-soluble fraction occurs: from solid to a saturated solution at DRH, and vice versa at CRH (*Potukuchi and Wexler 1995a, b; Martin 2000; Speer et al. 2003; Seinfeld and Pandis 2006*). CRH is generally lower than DRH, thus generating a hysteresis loop in the hydration levels (*Seinfeld and Pandis 1998; Martin 2000; Martin et al. 2003; Randriamiarisoa et al. 2006; Ferrero et al. 2013a, 2014*). DRH and CRH both depend on the whole PM chemical composition, which changes in time and space because of PM sources variability and atmospheric reactivity. These parameters may be different for PM from different sites and seasons and, this may result in a different hazard for exposed stone materials.

As a consequence, an accurate knowledge of both DRH and CRH is required for an appropriate calculation of TOW and Ncy in the case of an ideal PM deposit . This procedure allows proper assessment of the hazards for stones substrates considering the site-specific synergy between PM properties and climatic conditions. With respect to this, a new method for the evaluation of two useful hazard indicators (TOW and Ncy) was elaborated. This method is based on the measurements of the PM DRH and CRH that were applied to accurately calculate both TOW and Ncy in combination with climatic data.

The new method was applied to the case study of the urban area of Milan (Po Valley). DRH and CRH of PM samples collected within this area were experimentally measured in an Aerosol Exposure Chamber (*Ferrero et al., 2013, 2014*). The experimental DRH and CRH values were used to accurately calculate both TOW and Ncy in Milan during the last decade (2003–2013). In this way, situ-predominant and seasonal-predominant hazards for stone substrates were identified. A comparison with the simplified methods reported in literature was also performed, and it allowed estimation of the bias that the absence of an accurate knowledge of the hysteresis loop introduce in the calculation of the hazard indicators. With a similar approach the impact of climate and pollution changes in materials conservation can be evaluated. The derived information could be also useful in the decision-making process during restoration activities: for example, if a site is subject to high percentage of TOW applying hydrophobic protective products on its exposed surfaces may be appropriate; otherwise the use of inorganic products might be more proper. Finally, the obtained results can be used to design artificial aging methods that may mimic the phase transitions and wetting behaviours of exposed surfaces with a more realistic approach.

Concerning the sampling of the correct dimensional

fraction of atmospheric PM used for this application, it must be considered that the deposition of PM on monuments and building facades is an extremely troubled issue. Several mechanisms may contribute: Brownian diffusion, impaction and interception due to the turbulent motions, gravitational sedimentation, thermophoresis, diffusiophoresis, electrostatic attraction (*Maro et al., 2014*). The results of such a complex interaction of competitors mechanisms is that the deposition features are extremely vary, even considering a single façade (*Camuffo et al. 1982*). $PM_{2.5}$ was chosen as it represents an important fraction in the deposition mechanism occurring on vertical surfaces (*Nava et al. 2010*). Concerning dry deposition on vertical surfaces, the sedimentation is expected to be negligible, since it occurs mainly for the coarse fraction (i.e., $PM_{2.5–10}$), and the turbulent diffusion is assumed as the main mechanism (*Maro et al. 2014*). Moreover, fine particles have a longer residence time in the atmosphere. Thus, they are able to reach higher altitudes than coarse particles even within the mixing layer itself, as PM vertical profiles in the Po Valley demonstrated (*Ferrero et al. 2010 and 2012*). Furthermore, the longer residence time of $PM_{2.5}$ results in a smaller influence of short-range emission sources than coarse fraction. Thus, the choice of $PM_{2.5}$ is more representative for the PM pollution overall the whole urban area of Milan.

Finally, water soluble compounds (i.e., sulphates), are generally abundant in fine PM and, because of this, $PM_{2.5}$ is a large fraction of PM_{10} in urban areas. In this respect, the average $PM_{2.5}/PM_{10}$ ratio measured at Milan during the last decade was 81 ± 7% (*Casati et al. 2015*).

2.2   Material and Methods

The experimental approach first required the collection of PM samples, whose DRH and CRH values were measured in a specifically-designed Aerosol Exposure Chamber (AEC). The chemical composition of PM was also analysed to interpret the seasonal variations of both DRH and CRH. Finally, meteorological data, coupled with PM DRH and CRH measures, allowed the calculation of TOW and Ncy and their seasonal behaviour over the last decade in Milan.

2.2.1   *Sampling Activity*

$PM_{2.5}$ samples were collected in Milan at Torre Sarca, that is the U36 building of the University of Milano Bicocca (45°31′19″N, 9°12′46″E). A FAI-Hydra dual channel Low-Volume-Sampler was used. All the samples were collected using the same sampling specifications, according to UNI-EN-14907:

sampling flux = 2.3 m³/h,
sampling time = 24 hours,
sampling filters = PTFE Pall Corp. 47 mm, 2.0 µm.

The site has been used since 2005 by the atmospheric chemistry research group as an atmospheric monitoring station (*Ferrero et al. 2010 and 2011; Perrone et al. 2012 and 2013; Sangiorgi et al. 2011*). The long-time series of $PM_{2.5}$ samples collected at Torre Sarca is found to be particularly useful in the case of the following application in which DRH and CRH of Milan's atmospheric PM was used for the estimations of TOW and Ncy over the last decade.

After collection, the PM samples were dried out and stored in the Filter Bank of the University of Milano-Bicocca (temperature –20°C in darkness), which was specifically designed for the storage of PM samples. In order to obtain a dataset that could be representative of the Milan PM's properties during the last decade, forty $PM_{2.5}$ samples were taken from the Filter Bank to be used this study. They were chosen uniformly distributed according to the seasons and spanning a time range from 2006 to 2013. Prior to the chemical analysis, the PM filters were cut into two halves: one half was analyzed in the AEC, while the other half was extracted to determine the chemical composition of the ionic fraction. The uniformity of PM samples on filters was examined in a previous work *(Owoade et al. 2006).*

2.2.2 *Experimental measurements of DRH and CRH in the AEC*

Aerosol's deliquescence and crystallization were investigated using an innovative electrical conductance method. A similar method, based on impedance measurements, was previously proposed by Yang et al. (2006) and applied only for the case of simple salts mixtures. The experimental method for the determination of aerosol's DRH and CRH develop by the atmospheric chemistry research group takes advantage of a custom-made Aerosol Exposure Chamber named AEC (figure 2.1). This is a 1 m^3 environmental-controlled chamber in which it is possible to vary the relative humidity (RH) by introducing water vapour (humidification) or dry air (dehumidification). The inlet of the water vapour was realized by means of an evaporation system in which a pure dry air flow (grade ZERO air, Sapio Srl.) goes through a flask filled with pure water (Milli-Q water, Millipore Corp.) kept at high temperature. In this way, the air-flow became saturated with water-vapour and then comes into the AEC through a nozzle. The dry air inlet was realized simply connect the pure air flow to the AEC. The control of the dry and humid air takes place by means of on/off switches that can be manually-activated. A schematic representation of the air control system is reported in figure. 2.1. A fan ensure uniform conditions inside the AEC.

Temperature and RH in the AEC were constantly monitored by means of a DMA 572.1 thermo-hygrometric sensor connected to an ELO 008 M-LOG data-logger (LSI Lastem s.r.l.). The DMA 572.1 sensor has an accuracy of ±0.2°C and a resolution of 0.035 °C in terms of temperature, while the accuracy in terms of RH is ±1.5% in the range 5 ÷ 95 % and ± 2 % in the range < 5 % > 95 %, the resolution is 0.25 % and the response time is 10 s. In the AEC it is possible to achieve up to 0.5 % sensitivity in terms of RH variation while temperature was set to room conditions.
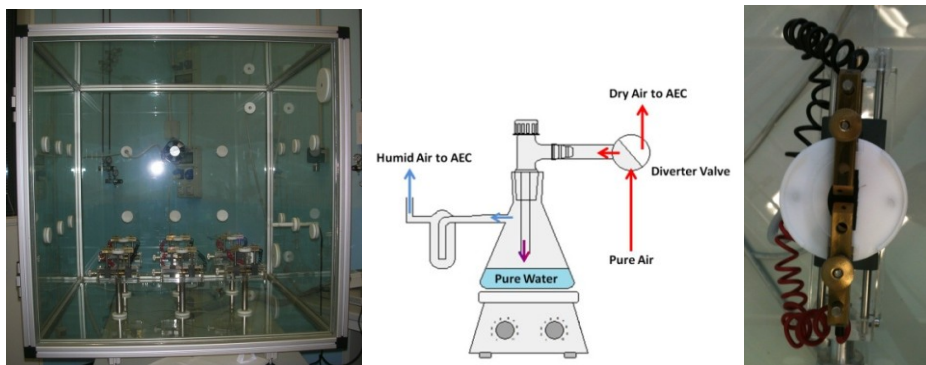
Figure 2.1: image of the AEC with the scheme of the air control system and the particular of one of the measuring conductance cell

Electrical conductance of PM samples can be measured in custom-built conductance cells (figure 2.1). These are made by two electrodes, positioned at calibrated distance,

and a filter-holder made by PTFE. Up to six conductance cells can be housed in the AEC, in order to perform several simultaneous conductance measurements. Conductance measurements were performed with an Agilent 34411A 6 ½ digital multimeter, connected to the cells by means of an Agilent L4421A 40-channels armature multiplexer.

The measuring protocol for the determination of PM's DRH and CRH provides the execution of a complete humidification-dehumidification cycle from 30% to 90% and vice-versa. The cycle is performed with 1.0% RH steps and five conductance measurements for each samples were acquired and averaged at each RH step. Before carrying out the conductance measurements a 5 minutes equilibration time were waited.

The output of the described process is a plot in which the conductance is plotted against the RH. In figure 2.2, a typical conductance curve is presented. Observing the plot it is possible to observe the behaviour of PM during the hygrometric variations. When the particles are in a completely dry or completely wet status, the conductance values measured during the humidification and the dehumidification steps are comparable. If the particles on the filter are dry, conductance values are null or close to the multimeter detection limit (0.0007 µS). In such a situation a little variation of RH doesn't involve significant changes in

conductance. If the particles are in a wet status, conductance values are relatively high and the RH variation led to a quite-linear growth in terms of measured conductance. On the other hand, during the phase transitions the two curves differ significantly, thus revealing the hysteresis loop. According to Ferrero et al. (2014), observing the conductance curves registered during the humidification and dehumidification steps, it is possible to identify both a DRH and a CRH region.

The DRH region occurs when a strong increase of conductance led to the wet condition. The maximum gradient of the conductance increase corresponds to the midpoint of the DRH region. For the purpose of this application, where it is important to identify the RH threshold above which liquid water is present, DRH_{end} point was taken in account looking at the last measured point before the wet zone. Similarly, a CRH region is identifiable in the dehumidification curve. Consequently, the CRH_{end} point was taken as the last measured point before the dry zone, when the conductance comes back to the starting values. The proposed method is in agreement with Schindelholz et al. (2014), who performed similar measures on pure salt samples.
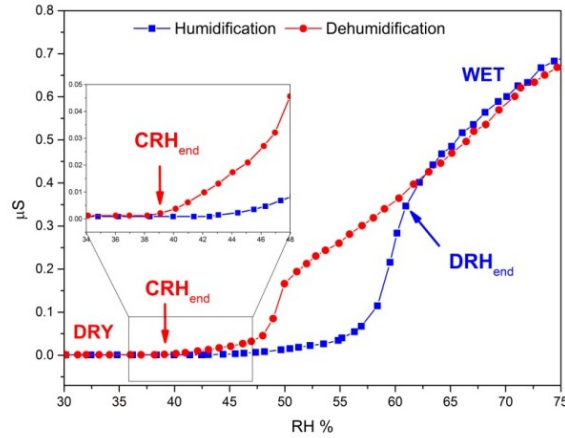
Figure 2.2: Typical conductance Vs RH curve for a generic PM sample. From the plot it is possible to assess DRH$_{end}$ and CRH$_{end}$ points

The measurements protocol was optimized by evaluating the uniformity of conditions in terms of temperature and RH inside the AEC, and also to assess the optimum equilibration time. Concerning the data-processing and the method used to determine DRH and CRH a detailed comparison between experimental data, obtained with the presented procedure, and DRH and CRH values predicted by theoretical models was performed and reported in Ferrero et al. (2014).

2.2.3   *Computation Algorithm for TOW and Ncy*

The computation algorithm used for the computation of TOW and Ncy combines meteorological data with PM's DRH and CRH values. DRH$_{end}$ and CRH$_{end}$ were determined for each of the forty analyzed PM$_{2.5}$ samples. DRH$_{end}$ and CRH$_{end}$ average values were calculated for each seasonal period:

winter, summer, and spring + fall. Meteorological data for the years 2003–2013 were acquired from all the meteorological stations of ARPA Lombardy placed in Milan, whose location in shown in figure 2.3:

Lambrate: 45.49N; 9.26E   **Brera**: 45.47N; 9.19E
Juvara: 45.47N; 9.22E   **Zavattari**: 45.47N; 9.14E
V.le Marche: 45.49N; 9.19E

Figure 2.3: Location of the monitoring stations of the environmental protection agency of Lombardy in Milan.

By averaging the acquired data, hourly mean values of ambient T and RH representative for the overall urban area of Milan were derived.

Comparing DRH_{end} and CRH_{end} seasonal values with hourly ambient RH, three different situations were identified for the state of hydration of ambient PM:

- when RH < CRH_{end}, particles were "dry";
- when RH > DRH_{end}, particles were "wet";
- when DRH_{end} > RH > CRH_{end}, particles were "dry" or "wet" depending on the RH trend: if RH was decreasing

from an above-DRH$_{end}$ value, particles were still "wet" until the CRH$_{end}$ was reached. Otherwise, if RH was increasing from an under-CRH$_{end}$ value, particles were still "dry" until DRH$_{end}$ was reached.

In this way, TOW and Ncy were calculated. A cycle was counted when RH was lower than CRH$_{end}$ value and RH trend was decreasing from a condition in which particles were in a "wet" status (RH previously higher than DRH$_{end}$). TOW was determined by adding up the hours in which particles were wet: RH > DRH$_{end}$ plus the hours in which RH was decreasing from DRH$_{end}$ to CRH$_{end}$. TOW was expressed as a percentage of hours in the considered period. A graphical example of the computational algorithm is shown in figure 2.4.
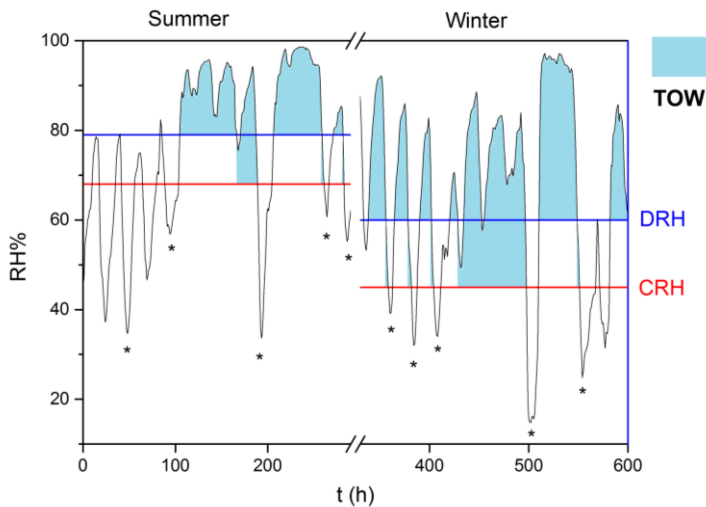
Figure 2.4: graphical example of the computation algorithm used for the determination of TOW and Ncy. TOW is highlighted in blue, while the crystallization events are marked with an asterisk

2.2.4   *Chemical composition of the water-soluble fraction of PM*

The water-soluble inorganic fraction of the PM samples was analyzed by ion chromatography (IC) coupled to conductivity detection. PM filters were extracted in 3 mL of Milli-Q® water (18.2 MΩ) by using an ultrasonic bath (20 minutes, SONICA®, SOLTEC). The extract was filtered with a syringe filter (0.45 µm PTFE) to remove the water insoluble fraction. Cations (Na^+, NH_4^+, K^+, Mg^{2+}, Ca^{2+}) and anions (F^-, Cl^-, NO_3^-, SO_4^{2-}) were analyzed using two coupled ionic chromatography systems (Dionex ICS-90 and ICS-2000). Cations were determined using a Dionex IonPac CS12A-5 analytical column (isocratic elution with 20 mM methanesulfonic acid flow rate of 0.5 mL/min). The eluent signal was suppressed using a Dionex CMMSIII 4 mm MicroMembrane chemical suppressor. Anions were analyzed using a Dionex Ion Pac AS14A-5 analytical column, a solution of $Na_2CO_3/NaHCO_3$ (8.0 mM/1.0 mM, Dionex056937) was employed as eluent (flow rate 1 mL/min). The eluent signal was suppressed by means of a Dionex AMMSIII 2 mm MicroMembrane chemical suppressor. Quantification was achieved by means of the external standard method. Standard solutions were made starting from solutions of each single ion (1000 mg/L).

2.3 Results and Discussion

2.3.1 *Seasonal values of DRH$_{end}$ and CRH$_{end}$ of the PM of Milan*

Winter samples showed the lowest values of both DRH$_{end}$ and CRH$_{end}$: 60 ± 4% and 39 ± 6%, respectively. Conversely, summer samples showed the highest values of both DRH$_{end}$ and CRH$_{end}$: 73 ± 1% and 52 ± 6%, respectively. Fall and spring samples showed values that were very close to winter ones: DRH$_{end}$ was 61 ± 3% while CRH$_{end}$ was 42 ± 4%. The values of DRH$_{end}$ and CRH$_{end}$ of the single samples used to obtain the seasonal averages are listed in table 2.1.

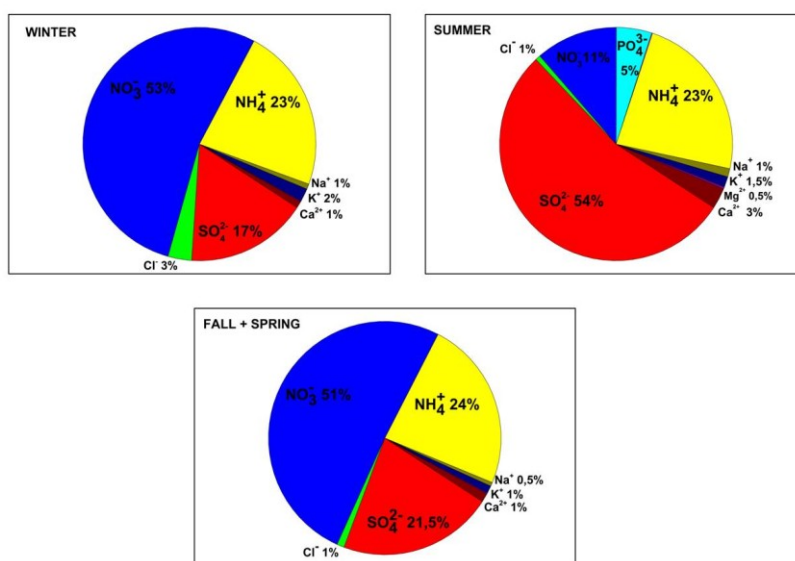**Table 2.1: DRH and CRH of the PM samples used in this work**

WINTER		DRH	CRH	FALL/SPRING		DRH	CRH	SUMMER		DRH	CRH
B384	22/12/2006	65,2	35,3	B322	08/10/2006	59,2	43,4	AT31	30/06/2013	71,2	53,8
B08-255	11/09/2008	65,2	50,1	B08-281	07/10/2008	57,2	35,1	AT26	08/07/2013	74,1	47,1
B381	19/12/2006	65,2	40,2	B08-283	09/10/2008	67,2	51,0	AT36	20/07/2013	74,9	56,0
B382	20/12/2006	60,0	25,2	B340	01/11/2006	60,1	41,1	AT51	16/07/2013	72,6	41,9
B07-012	12/01/2007	60,0	34,9	B2	17/11/2005	55,4	36,7	AT52	18/07/2013	72,6	53,5
B390	28/12/2006	60,1	41,1	B08-284	10/10/2008	57,2	41,1	AT57	02/08/2013	71,1	50,2
B09-054	23/02/2009	59,1	41,5	B08-285	11/10/2008	62,5	43,1	AT62	08/08/2013	72,0	61,9
B52	07/01/2006	61,2	36,7	B08-100	09/04/2008	59,9	40,9	AT64	10/08/2013	72,9	52,1
B09-052	21/02/2009	54,3	40,3	B08-092	01/04/2008	67,2	43,0	AT65	12/08/2013	73,1	55,2
B09-055	24/02/2009	58,3	35,1	B07-089	30/03/2007	60,1	41,1	AT68	22/08/2013	73,1	52,1
B09-073	14/03/2009	56,6	46,2	B07-095	05/04/2007	61,2	41,1	AT69	24/08/2013	73,1	48,2
B09-057	26/02/2009	55,2	40,5	B07-083	24/03/2007	59,5	38,2	AT71	28/08/2013	70,2	57,8
B40	27/12/2005	58,4	44,4	B07-87	15/03/2009	59,9	46,0	AT72	30/08/2013	72,6	44,2
				B193	14/03/2009	62,3	46,4				
	Winter	60	39		Fall/Spring	61	42		Summer	73	52
	dev.st	4	6		dev.st	3	4		dev.st	1	6
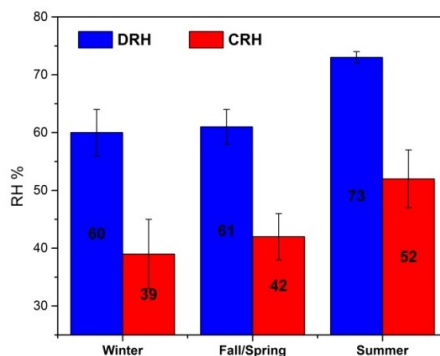
Figure 2.5: Seasonal mean values of DRH$_{end}$ and CRH$_{end}$

The different values of DRH and CRH of winter and summer samples (figure 2.5) and the good agreement between winter and spring/fall samples, can be explained considering the seasonally chemical composition of the PM. The average composition of the ionic fraction of the forty PM samples is reported in Figure 2.6. The ionic fraction accounted for 35 ± 12% of the total PM mass, this value is almost constant during all the seasons. The chemical composition of the ionic fraction changed according to the season. A nitrate-predominance (53 ± 12% of the total inorganic ions) occurs in the winter samples, while a sulphate-predominance (54 ± 17% of the total inorganic ions) was found for the PM samples collected during summer. NH_4^+ was the main cation and its mass fraction remained quite constant both in winter and summer (23 ± 1%). The ionic fraction of spring and fall PM samples showed a

chemical composition very close to winter one. The PM chemical compositional data are in agreement with the other previous studies performed in Milan (*Perrone et al. 2012*).

Figure 2.6: seasonal average chemical composition of the ionic fraction of the PM samples used in this study

The knowledge of PM's DRHend and CRHend could be very important to assess the potential impact of particles for heritage substrates conservation. Low DRH_{end} values suggest a high tendency for the adsorption of water. In the other hand, high CRH_{end} values suggest a tendency to crystallize even at high relative humidity. Depending on the climatic conditions, DRH_{end} and CRH_{end} values can lead to a high TOW or to a high frequency of crystallization events. Another

relevant feature is the width of the hysteresis loop, which is computed as the difference between DRH_{end} and CRH_{end}. The average hysteresis loop for the samples analyzed in this work was of 20 ± 6%. The magnitude of the hysteresis loop can affect TOW an Ncy. Considering the same RH conditions, a smaller hysteresis loop led to lower TOW and higher Ncy. This is a crucial point since most of the computation approach for TOW and Ncy reported in the literature do not consider the hysteresis loop (*Brimblecombe et al. 2006; Bonazza et al. 2009*).

2.3.2   *Seasonal profiles of TOW and Ncy*

TOW and Ncy were computed over the period 2003–2013 in Milan. Average experimental DRH_{end} and CRH_{end} points were assigned for every season based on figure2.5. The same DRH_{end} and CRH_{end} were assigned for spring and fall. The output of the computation algorithm (section 2.2.3) provides TOW and Ncy for each month over the period, TOW is expressed as percentage of hours while Ncy is express as the absolute number of dissolution/crystallization cycles. Results of the last decade were reworked in table 2.1 were the seasonal statistics of TOW and Ncy are shown.

**Table 2.2: descriptive statistic of TOW and Ncy computed along the last decade**

Ncy (± SD)		TOW (± SD)	
Total N_{cy} (2003–2013)	1221	Yearly Hours of Wetness	5518 ± 350
Yearly Average N_{cy}	111 ± 17	Yearly Average TOW	63% ± 5%
Winter N_{cy} Monthly Avg	3 ± 3	Winter TOW	89% ± 11%
Summer N_{cy} Monthly Avg	11 ± 5	Summer TOW	20% ± 13%
Fall N_{cy} Monthly Avg	8 ± 6	Fall TOW	83% ± 15%
Spring N_{cy} Monthly Avg	14 ± 5	Spring TOW	61% ± 16%

In winter a very high TOW (89 ± 11%) was obtained, on the other hand Ncy reached the lowest annual values in winter, and only 8% of the total number of transitions occurred in this season. Minimum values of TOW (20 ± 137%) were reached in summer when Ncy was relatively high, in fact 30% of total transitions in a year occurred in summer. During spring TOW showed intermediate values (61 ± 16%) and 38% of total transitions in a year occurred in this season. Concerning fall, TOW was quite high (83 ± 15%) and 22% of total transitions occurred in this season.

The monthly average values of TOW and Ncy were reported in figure 2.7. The figures show the trend of the two parameters in the same graph. In this way it is possible to highlight the potential monthly-predominant hazards that could interests heritage stone surfaces. In the red bars Ncy is showed, while TOW is represented with the blue line. The

variability of the parameters is indicated by the standard deviation of the monthly average that is represented with the error bars in the case of Ncy and with the blue area in the case of TOW.
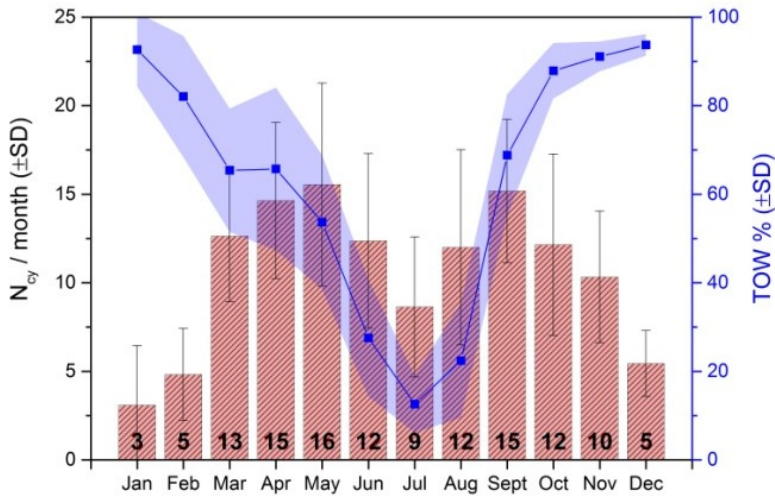
Figure 2.7: monthly average trend of TOW and Ncy computed along the last decade in Milan

Results showed that three main conditions can be identified in the case of the environmental situation of Milan. A first condition occurs in winter, that is characterized by a very high TOW. This led to a high hazard of "chemical" stress and this is due to both the low DRH_{end} values and the high RH conditions. The low winter Ncy resulted in a low hazard of "mechanical" degradation instead. Such a situation can be considered particularly dangerous, for example, in the case

of carbonate substrates, as they are more susceptible to acid and karst attacks (*Cardell-Fernández et al. 2002*). A second condition occurs in summer, when "mechanical" hazard prevailed. This is the result of the low RH conditions coupled with the high DRH_{end} values. Therefore, high values of Ncy were obtained in summer when TOW reached its annual minimum value. The dangerousness of this condition may depends on the porosity and mechanical properties of the materials. The third condition involved the intermediate seasons, spring and fall, which showed the highest level of hazard for exposed materials. In fact they were characterized by relatively high values of both TOW and Ncy. Looking closely at the obtained results, it can be stated that fall has a winter-like situation, with high TOW, while spring has a situation more similar to summer.

The aforementioned results highlighted how the proposed method considers the specific characteristics emerging by the synergy between the PM properties and the climate at the investigated site. Even thought the results here shown are site-specific, the method used for their determination is of general application. Thus, it can be used as an efficient tool for the hazard assessment of exposed surfaces in a heritage climatology perspective.

2.3.3 *Comparison with other literature approaches*

A comparison between the computational algorithm described in section 2.2.3 and other literature approaches was performed.
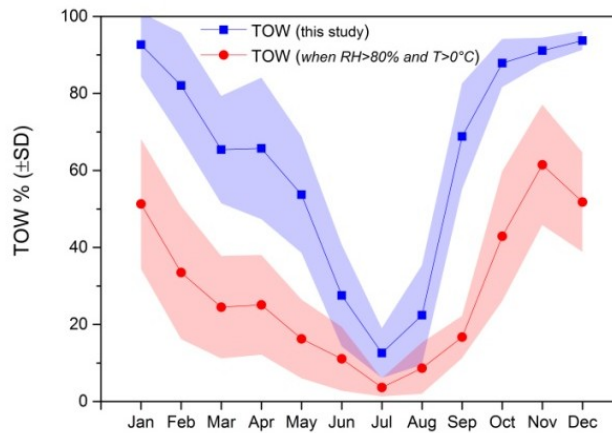
Figure 2.8: Comparison between the TOW calculated with the algorithm described in this work and with the common transformation which count TOW when RH>80% and T>0°C

The TOW derived in this work was compared with the TOW calculated by assuming that the surfaces' wetting occurs just when RH > 80% and T > 0°C. This transformation is commonly used in cultural heritage studies (*Brimblecombe et al. 2006; Bonazza et al. 2009*). Figure 2.8 reports the comparison, and it can be noticed that the shape of the trend obtained with the computation algorithm of this work (blue line) is similar to the trend

obtained with the literature's approach (red line). This finding indicates that the wetting behaviour of surfaces is strongly related to climatic conditions. Looking at the values of TOW, it can be stated that the use of experimental values of both DRH_{end} and CRH_{end} led to higher values of TOW compared to those obtained by the previous literature method. This tendency seems to emerge more clearly during winter.

From the comparison shows in figure 2.8, the role of PM and its hysteresis loop in moisture absorbing processes can be highlighted. In fact, considering an hypothetical stone surface covered by a PM deposit, the wetting can occurs both when RH > DRH_{end} (instead that RH > 80%) and when CRH_{end} < RH < DRH_{end}.

In figure 2.9 is reported the comparison between different computation algorithm used for Ncy computation. As stated in section 2.1, a common literature's approach for Ncy determination used only one critical values of RH to assess the phase transition events. The RH_{eq} of simple salts is commonly used as critical values, thus such a kind of approach does not consider any hysteresis loop. For making a proper comparison between the different computation approaches, results obtained in this study (which considers the hysteresis loop of PM) were compared with the results obtained using only one critical values of RH (avoiding the

hysteresis loop). DRH was chose as critical values for make the comparison, and in this way it is possible to assess the bias caused by not taking into account the hysteresis loop.
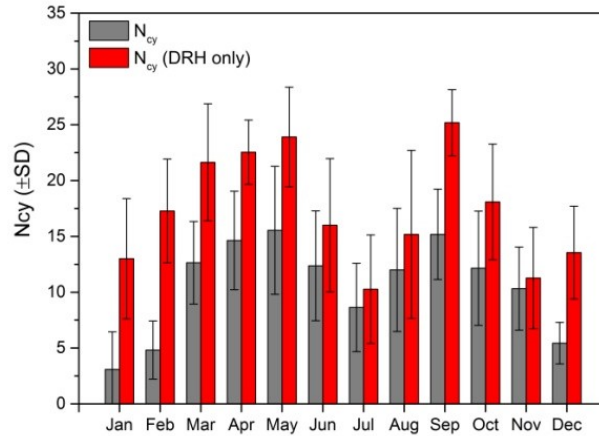
Figure 2.9: comparison between the results of different computation algorithm for Ncy determination. The grey bars refers to the algorithm used in this work while the red bars refers to the more common approach which involve the use of only one critical value of RH.

The red bars refer to the Ncy derived considering only the DRH_{end} as critical RH threshold (60% for winter; 73% for summer and 61% for spring and fall). In this situation crystallization events were counted each time the RH decreased under DRH. The grey bars were instead computed considering the hysteresis loop. The figure 2.9 shows that

without a proper knowledge of the hysteresis loop, a significant overestimation of Ncy can occurs: about 64% more cycles/years were calculated when the hysteresis loop was neglected. The differences between the results of the two different approaches appeared more evident during winter.

2.3.4   *Relationship between TOW, Ncy and monthly RH averages*

To extend the applicability of the approach described in this study to sites where hourly data are not available, or to take advantage of future-climate models, a functional approach it is to study the relationship between Ncy and the RH monthly mean values (*Grossi et al. 2011*). Monthly RH mean values are more frequently available indeed.

TOW and Ncy calculated within this work were related to the RH monthly average values. TOW values are plotted against an x-variable that was calculated, according to equation 2.1, as the difference between the monthly averaged RH (RH_{mm}) and the midpoint between DRH_{end} and CRH_{end}. The x-variable was named Transition Distance (TD) and describes the "distance" of the environment condition (RH) from the aerosol properties in terms of deliquescence and crystallization (DRH_{end}-CRH_{end}). Negative values of TD are associated to dry ambient conditions with low RH_{mm}, far from promoting aerosol hydration. The opposite happens

with high positive values.

$$TD = RH_{mm} - \frac{DRH_{end} + CRH_{end}}{2} \quad (Eq.\,2.1)$$

Equation 2.1: equation for the determination of the Transition Distance.
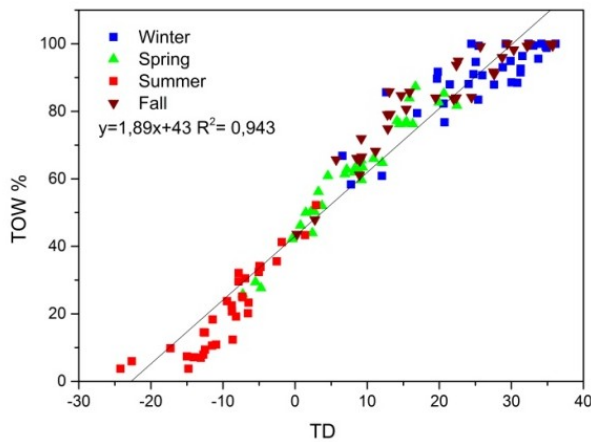
Figure 2.10: Correlation between TOW and TD

The correlation between TOW and Ncy is shown in figure 2.10. A clear tendency to a linear correlation was found indicating that the wetting behaviour of particles depends strongly on climatic conditions. In fact, the greater is the difference between RH_{mm} and the average between DRH_{end} and CRH_{end}, the greater is the TOW. Another result of this study is that along with the linear trend it is possible to observe a seasonal pattern. Points associated to summer

months are in the lower-part of the graph, with negative TD values and low TOW. On the other hand, winter points lie in the upper-part of the graphs with positive TD and high TOW. Spring points tend to arrange in the central part of the graph, while fall points are very close to winter ones. This is a further confirm of the fact that, concerning the situation of Milan, in fall there is a winter-like situation by the point of view of TOW (see section 2.3.2).

The same correlation study is shown in fig.2.11 concerning the Ncy versus TD. In this case no linear trend was found.
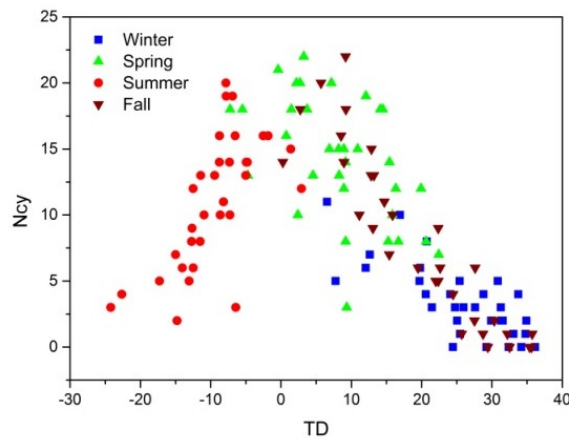
Figure 2.11: Correlation between Ncy and TD

Some information can be derived from figure 2.11. Ncy seems to be greater in the months in which the TD is close to zero. When TD has high and positive or high and negative values, Ncy seem to have low values. It can be assumed that,

when TD is closer to zero, RH_{mm} lies at the midpoint between DRH_{end} and CRH_{end}. As a result, diurnal variations of RH around the monthly mean value promote high frequency variations across DRH_{end} and CRH_{end}, resulting in a large number of Ncy. Also in the case of Ncy, a seasonal pattern can be identified in figure 2.11. Spring and some fall points lie in the central part of the graph with TD close to zero and high Ncy. Summer, winter and some fall points are spread in the side part of the graph where the TD reaches the highest values in the case of winter and the lowest in the case of summer.

The above-stated results allow a better understanding of the annual trend of figure 2.7. Looking at the figure, both TOW and Ncy are decreasing shifting from May to July, while the two parameters are increasing going from July to September. Conversely, from September to April the two parameters are anti-related. Considering results reported in figures 2.10 and 2.11 it can be stated that this behaviour is the result of the different kind of relationship between both TOW and Ncy with TD.

2.3.5 *TOW and Ncy variability along the last decade*

The variability of the two hazard indicators, TOW and Ncy, during the period 2003–2013 was also analyzed. Annual values of TOW, Ncy, temperature and RH for the four seasons are shown in figure 2.12. This kind of study allows to identify possible trends along the years, or to highlight if anomalous season by the point of climatic conditions (T and RH) are associated to unusual values of TOW or Ncy.
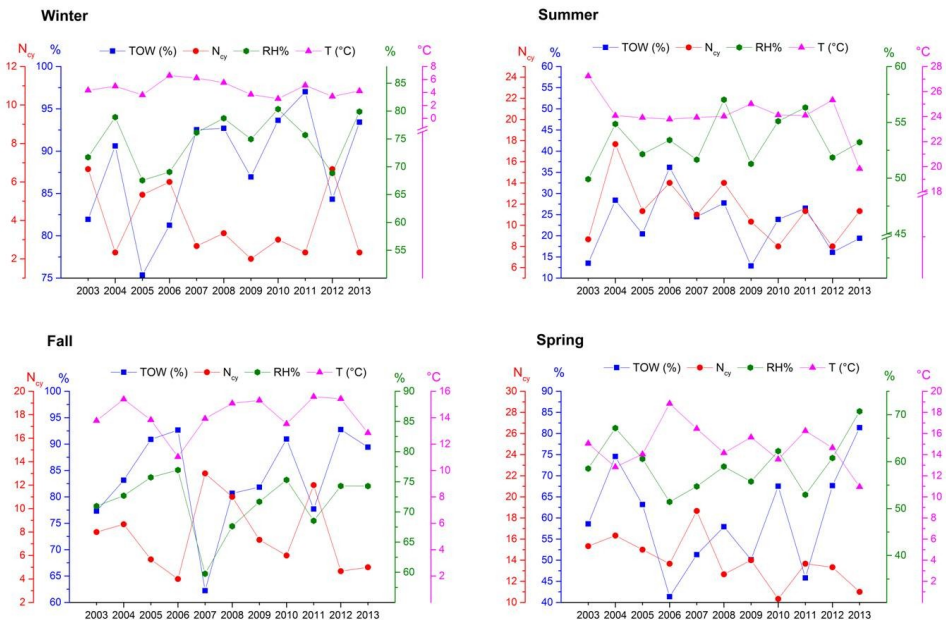
Figure 2.12: TOW and Ncy variability along the last decade. Results were shown in comparison seasonal values of relative humidity and temperature.

No trends are clearly identifiable in the graphs. Despite this, in figure 2.12 it is possible to observe the relations between TOW, Ncy and the climatic characteristics of each single year that are expressed through the RH and temperature seasonal average. Concerning winter, figure 2.12 shows that the years with low TOW (2003, 2005, 2006, and 2012) corresponded to years with high Ncy. This situation is also associated to relatively low values of RH. An opposite behaviour was observed in years with high values of RH. Such evidence confirmed the fact that Ncy and TOW were anti-related in winter. For the summer season, it can be seen that years with high RH led to both high Ncy and TOW (2004, 2006, 2008). On the other hand, years with low RH led to low Ncy and TOW (2003, 2005, 2009, 2012). Such evidence suggests that, contrary to winter, the behaviour of the two parameters (Ncy and TOW) shows a positive correlation in summer. Concerning spring it is possible to noticed that two years with low TOW (2006, 2011) presented intermediate values of Ncy. Average values in terms of RH and TOW for year 2007 corresponded a high Ncy value. This suggests that in spring a clear behaviour is less evident if compared to the results observed for winter and summer. Such tendency could be due to the wide climatic variability of the season. Finally, during fall TOW and Ncy showed an anti-related behaviour: years with high TOW (2006, 2010,

and 2012) corresponded to years with low-Ncy and vice-versa. From the point of view of the hazard for exposed stones, this can be considered as a further evidence of the fact that fall presents a winter-like behaviour in Milan.

2.4 Concluding Remarks

An innovative method was develop and employed to evaluate the decay hazard for heritage stone substrates exposed to the deposition of PM. The method couples experimental measurements of PM deliquescence and crystallization relative humidity with climatic data. Two well-known hazard indicators for stone materials were determined: the time of wetness and the number of dissolution and crystallization cycles. This indicators were associated to different type of hazards. A "chemical" hazard is related to high time of wetness and a "mechanical" hazard is related to high number of cycles. The new method can be considered as an advance for the recently-introduced concept of heritage climatology.

The method was applied to the case-study of Milan. PM's DRH_{end} and CRH_{end} in Milan showed seasonal variations that reflected the seasonal variations of the chemical composition. Observing the seasonal trend of TOW and Ncy the seasonal-predominant hazard for stone surfaces was identified. In

winter a chemical hazard prevails due to the high time of wetness and the low number of dissolution and crystallization cycles. In summer the chemical stress reached the minimum value, since the season is associated to low time of wetness, while the mechanical stress increased. In spring and fall, both the time of wetness and the number of dissolution and crystallization cycles were relatively high. These can be associated to a greatest hazard for stone surfaces.

Differences among seasons in DRH_{end}, CRH_{end}, chemical composition, time of wetness and number of dissolution and crystallization cycles suggested that different PM chemical compositions can lead to different hazard for exposed materials. The proposed method provides a tool to make nowadays hazard-assessment, but it is also exploitable for evaluating future situations.

CHAPTER 3

Study of Particulate Matter Dry Deposition on Stone Materials and Surrogate Surfaces with a New Exposure Method: the "Deposition Box"

3.1 Theoretical background

Airborne particulate matter (PM) can be removed from the atmosphere by wet and dry deposition processes. The deposition of atmospheric particles and pollutants related thereto, can impact the terrestrial and aquatic ecosystems (*Balestrini et al., 2000; Inomata et al., 2009; Baker et al., 2010*) and also the outdoor-exposed materials causing corrosion and decay (*Ferm et al., 2006; Rampazzi et al., 2011; Sabbioni, 1995*). In particular, dry deposition is less well understood because of the difficulty to make affordable measures of dry deposition fluxes (*Huang et al., 2012*). In

dry depositions, fluxes can strongly depend not only on the atmospheric factors (winds, sampling height, temperature) but also on the sampling method. With regard to this, several studies highlight that relevant difference in the estimated deposition fluxes can rise as a function of the sampler geometry and the sampling surface characteristics (*Shannigrahi et al., 2005; Huang et al., 2011; López-García et al., 2013*). The problem of sampling dry depositions is even more troublesome in the field of conservation science. In fact, to perform a proper study about the decay of typical heritage substrates (stones, metals, glasses etc.) it is fundamental to carry out surface chemical analysis and microscopic observation. Thus, PM must be sampled directly deposited on the surface of interest and the deposits must be repeatable, in terms of mass, and homogeneous by the point of view of the coating grade. Another open issue is to assess the capacity of different materials to restrain PM and amass soiling, in order to study the dirtying of the surfaces or the re-dirtying after conservation treatments.

Since PM is one of the most relevant hazardous factors for the exposed artefacts, several literature works deal with the problem of PM dry deposition in conservation science. These works exploit different approaches, including modelling (*Monforti et al 2004; Maro et al 2014*), laboratory

experiment (*Pesava et al. 1999*) and in-field exposure tests (*Ferm el al 2006; Realini et al 1995; Zappia et al 1998; Urosevic et al 2012, Butlin et al 1992*). Concerning the aforementioned exposure tests, several exposure methods were proposed and employed, making even more clear the difficulties related to the dry deposition sampling. Just for this, there is still not a standard exposure method for the exposure tests of stone or other heritage materials.

3.2   Materials and Methods

In this chapter is described a new exposure method for the evaluation of the decay of materials exposed to the atmospheric depositions. The method involves the use of a new device named "deposition box", henceforth named depbox, that has the aim to collect PM directly deposited on any kind of substrates, including not-filter substrates like stone or metallic specimens. The device was specifically designed to study the effect of dry deposition on typical heritage materials. The design specification of the device allows to mime the dry deposition and it has low construction and operating costs. After a careful phase of design and test (section 3.2.1 and 3.2.2), several exposure campaigns were performed with the aim to measure the deposition rates in the city of Milan (section 3.2.4). Stone

materials and surrogate surfaces were exposed inside the depbox allowing the evaluation of deposition rates on different material and the potential decay processes triggered by the presence of PM deposits. A special attention was given to the characterization of deposited PM in term of dimensional distribution and uniformity of deposition (3.2.5). Chemical analysis (3.2.7; 3.2.8) allows to better understand the deposition rates of some chemical species that may be of interest from the conservative and environmental point of view.

3.2.1   Design and construction of the "Deposition Box"

The Depbox is made by a 50x50x20cm box covered by a pitched roof. The overall dimension of depbox is 70x70x55 cm. The scheme of the device is reported in figure 3.1. A punctured steel exposure floor is placed inside the box for the accommodation of the specimens. On the bottom of the box, a fan is housed with the aim of standardizing the air exchange ratio through the exposure floor. The fan (figure 3.1) is a Sunon DR MagLev DC fan 17x17x8 mm, maximum current 160mA, supply voltage 5 V dc and 20000 rpm with and air flow of 1,5 m^3 h^{-1}. The fan is connected to a power adapter to provide current at 220 V. With the given fan specifications the calculated air exchange ratio is 7 min^{-1}.

The distance between the exposure floor and the bottom of the box is 150 mm. The Depbox rests on 4 pins of 20 mm in height, which ensure the correct operation space for the fan discharge.
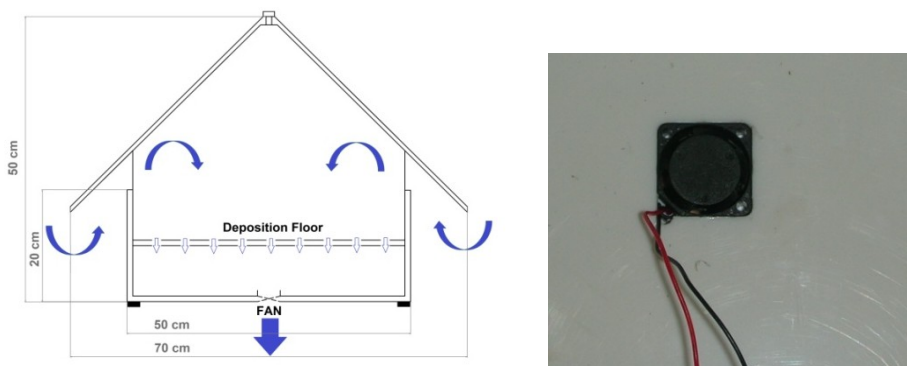
Figure 3.1: scheme of Deposition Box and particular of the fan placed in the bottom of the box.

The external structure of depbox is made of white polypropylene (PP) (figure 3.2). This polymer was chosen because it is supposed to be inert at environmental conditions and the white feature is useful to avoid an overheating within the structure in conditions of high temperature or high solar radiation. The roof is secured by a threaded fastener, so it can be easily removed allowing the inspection and substitution of the specimens housed on the exposure floor. Samples can be housed in depbox directly on the exposure floor, this is the case of stone, metal or polymeric specimens. In the case of filters used as surrogate surfaces, Quartz, PTFE or Polycarbonate filters can be used

for this purpose, and they can be inserted in special sampler holder.

The basic concept of the depbox is to expose samples of different materials to the dry deposition of atmospheric particles. Dry deposition is affected by many variables (see section 3.1), depbox standardizes some of these variables, such as wind speed, since the air exchange ratio inside the box is fixed. In addition to this, also the surface temperature of the specimens it is uniform as possible, since the roof fully protects the specimens from the solar radiation. Another characteristic of the depbox is that the good protection guaranteed by the pitched roof, avoids potential problem of wetting or overturning of the samples during extreme meteorological events


Figure 3.2: On the left, the external feature of the "deposition box". On the right, the inside of the box, with some samples arranged on the exposure floor.

3.2.2 Test of the deposition box with Optical Particles Counters

With the aim of verifying that the chosen manufacturing specifications, in terms of dimension and air fluxes, do not create dimensional artefact in the particles size distribution inside the depbox, the size distribution of atmospheric PM inside and outside the depbox was measured with Optical Particles Counter (OPC). Portable Aerosol Spectrometer Grimm model 107G was used to perform the measures. Measurements were performed in Milan, at Torre Sarca (45°31′19″N, 9°12′46″E) on a sunny day (18/06/2013) with stable atmospheric conditions (T = 33.5 ± 0.5 °C). During the test, the average $PM_{2.5}$ concentration measured by OPC was 23 ± 6 μgm^{-3}. This value is in agreement with the data declared by the local environmental protection agency ARPA Lombardy (www2.arpalombardia.it) for the day: 23 μgm^{-3} at the station of "Senato street" and 26 μgm^{-3} at the station of "Pascal Città Studi".

A three-hours sampling (from 15:00 to 18:00), with 1 minute time resolution, using two identical Grimm 107G OPC was performed. One instrument was put inside the exposure box while the other one was put outside the box. Results of this comparison activity show a quite-identical (R^2 = 0.993) size distribution of the PM when the two instruments were placed inside and outside the depbox

(figure 3.3). Such an experimental evidence allows to state that the manufacturing specifications of the depbox are suitable to mime the dry deposition process, since the PM dimensional characteristics are identical inside and outside the box.
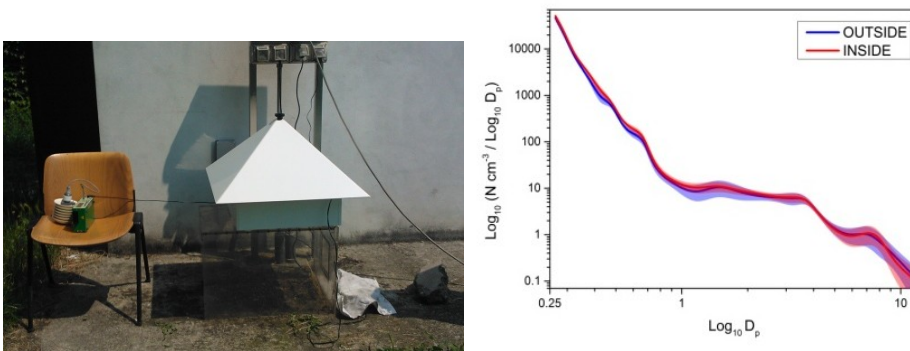
Figure 3.3: Parallel OPC measurements inside and outside depbox and graph of the dimensional distribution of the particles inside and outside the exposure chamber

3.2.3   Specimens Preparation

As stated in section 3.2.1, any kind of materials could be placed inside the depbox. In this work it was chosen to expose some "surrogate surfaces" for which an inert behaviour respect to the deposited PM is assumed. From this point of view, the typical substrates for the PM sampling were employed as ideal surrogate surfaces. The chosen substrates are:

Millipore® 47mm Quartz fibre filters (**Qz**)

PTFE - PALL® 47mm 2.0 μm PTFE filters (**PTFE**)

Aluminium 47 mm discs (**Alu**)

Aluminium   Quartz   PTFE
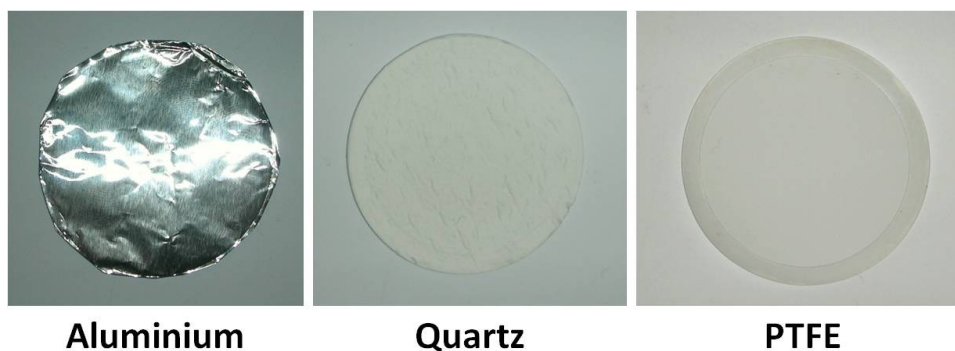
Figure 3.4: photo of the surrogate surfaces before the exposure in the depbox.

Different substrates were chosen because, albeit they are supposed to be inert, they have different properties in terms of surface roughness and porosity. Alu discs were punched from aluminium foils and before the exposure they were washed in MilliQ® water and acetone. Qz filters were baked at 600°C for 3 hours in a muffle-furnace to burn organics impurities. PTFE filters do not require treatments before the exposure instead. The mass of the Qz, PTFE and Alu was determined with a Sartorius SE2 balance (Capacity 2 g; Uncertainty 0.1 μg) after 24 hours drying in desiccator. During the exposure, Qz, PTFE and Al, were placed in suitable filter-older rings, thus giving an effective deposition

area of 11.94 cm². The filter-older rings were housed and fixed to a PTFE plate to make easy the transport and to avoid accidental overthrow.
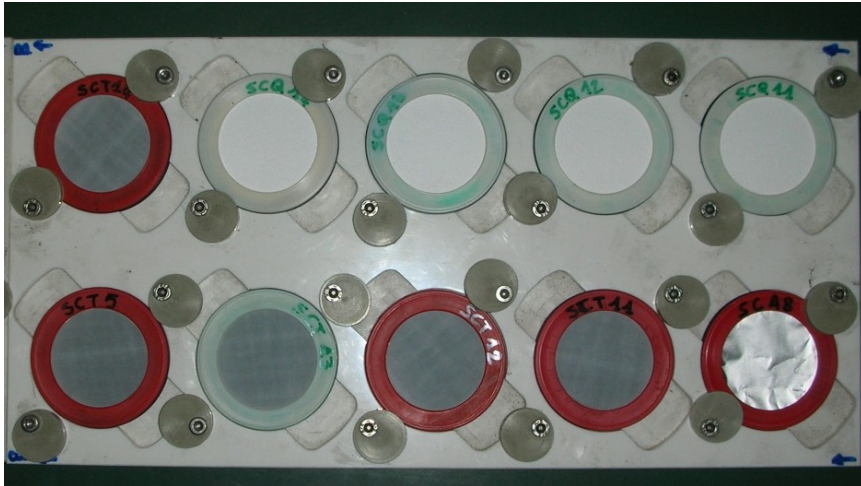
Figure 3.5: Surrogate surfaces placed in the filter-older ring and housed in the PTFE plate

Together with surrogate surfaces, some stone specimens were exposed inside the depbox. Several lithotypes were chosen: Carrara Marble, Noto calcarenite, Botticino limestone, and Montorfano Granite. The selected stone materials have different characteristics in terms of chemical compositions, physical and mechanical properties.

Carrara Marble is a metamorphic stone basically made by calcium carbonate (> 98%) with a saccaroid crystalline structures. Crystals size is between 100-800 μm and the

open porosity is around 2% (*Poli et al. 2004)*. The terms "Carrara Marble" it is used to identify a wide product category, the characteristics of which can hugely vary not only by an aesthetic point of view. The quarries of Carrara Marble are placed in the north of Tuscany, in the mountain range of Apuan Alps. Carrara Marble is one of the most famous variety of statuary stone, and it is one of the most used stone materials for buildings and decorations from the ancient Rome to nowadays.

Botticino limestone is a compact sedimentary rock mainly made by calcium carbonate. Botticino limestone has a typical pinkish colour, due to the presence of iron compounds, and it can have stylolites and clear spots. The more spots-reach variety is named "Flowery Botticino". It is commonly used the name "Botticino Marble" referred to this lithotype even if this is not a correct name since the stone extract in the quarries near the city of Botticino (North of Italy, Brescia, Lombardy) is not a metamorphic stone. The calcite cement has a microcrystalline structures with a calcite dimension of 1-5 μm. Also dolomite crystals (100-200 μm) may be present. The integral open porosity is 0.4 ± 0.2 % (*Fermo et al. 2014*). Botticino limestone is an appreciated building stone, which use is well-documented both in Italy (Bergamo's cathedral, Altare della Patria in Rome) and worldwide (Statue of Liberty, White House).

Noto calcarenite is a limestone extracted from the quarries that are placed near the city of Noto, near Syracuse, in Sicily. Noto calcarenite is mainly made by calcium carbonate, clay minerals are present in trace. From a micro-structural point of view, Noto calcarenite has a mud-supported texture with about 70% of mud. Allo-chemical components consist of various small bioclasts, including echinoids, foraminifera, bryozoa and plankton, extensively reworked by tube worms represented by skolithos (*La Russa et al 2011*). The open porosity is very high, from 30% to 40%. The pores size is between 0.08 and 1.6 mm with a quite homogeneous distribution. Noto calcarenite is one of the most common stones used in the Sicilian Baroque.

Montorfano Granite is a white medium-grained biotite granite, rarely horneblende bearing (*Boriani et al., 1988*) comes from quarries located in the southern foothills of the little Montorfano pluton (*Dino & Cavallo, 2014*). Montorfano granite is the white variety of the granites extracted in the Verbano-Cusio-Ossola area (Piedmont, NW Italy), which is one of the most important Italian quarrying districts. These granites have quartz, K-feldspar (orthoclase), plagioclase and biotite as main minerals, with smaller amount of horneblende and chlorite. The white Montorfano sometimes contains a lot of mafic xenoliths and disseminated

arsenopyrite that adversely affect the quality of the stone (*Dino & Cavallo, 2014*). The Montorfano quarries are one of the oldest exploited quarries in the area, since 15th century, and the "Cavadonna" quarry is one of the most important historical quarries that is still active (*Dino & Cavallo, 2014*). White Montorfano Granite is commonly employed in Piedmont region, also in some historical building, for example in the city of Turin (*Borghi et al. 2013*).

5 x 3 x 1 cm stone specimens were cut from new-extracted quarries blocks. The area suitable for the deposition is 15,00 cm^2. Stone specimens were prepared according to UNI10921 (figure 3.6).

Figure 3.6: stone specimens before the exposure in depbox

The surfaces were polished with FEPA 180 (82 µm) sandpaper with the aid of a polishing machine. Any soluble substances were removed by a threefold 20 minutes total immersion in MilliQ® water. After water immersion, stone

specimens were dried in a convection oven at 60 °C. The mass of the stone specimens, before and after the exposure, was determined by using a laboratory analytical balance (Uncertainty = 0.1 mg). The steady weight of the stone specimens was reached when the difference between the weights at 24 hours away was under the 0.01%. Between the weighting procedures, stone specimens were placed in a desiccator. As in the case of surrogate surfaces, also stone specimens were placed in a suitable sampler holder for the exposure in the depbox.

Figure 3.7: Stone specimens placed in the sampler-older for the exposure in the depbox

3.2.4   Sampling Campaigns

Several sampling campaigns were carried out, involving the exposure of both surrogate surfaces (Qz, PTFE and Alu) and stone specimens. Two sites in the urban area of Milan were chosen for the campaigns (figure 3.8):

- TS - Torre Sarca (45°31′19″N, 9°12′46″E)
- VN - Villa Necchi Campiglio (45°28'08"N, 9°12'08"E)

Figure 3.8: Milan's map with the location of the sampling sites

Torre Sarca can be considered as a traffic site since it is placed in the middle of a big business area, in correspondence of one of the busiest ways of access to the city centre. The sampling site (figure 3.9) is near Sarca avenue, that is one of the most busy street of the district. Torre Sarca has been active until 2005 as air-quality monitoring site managed by the atmospheric chemistry research group. This allows the interpretation of the results

of this study considering the long and detailed knowledge of the aerosol properties and chemical composition at the site (see chapter 2).

Figure 3.9: location of the two depbox at the sampling sites Torre sacra (left) and Villa Necchi (right). (*www.google.it/maps*)

Villa Necchi-Campiglio is an heritage site property of FAI (Fondo Ambiente Italiano; *www.visitfai.it/villanecchi/*). The site is placed inside the Low Emission Zone of Milan, named "Area C" (*www.areac.it*). The closest street to Villa Necchi, Mozart street, is interested by little vehicular traffic. The depbox was placed in the garden of the manor (figure 3.9), far from the tourist trail. Nevertheless, a signboard was placed near the depbox to inform the visitors about the aims and scope of the research project.

A summary scheme of the several sampling campaigns carried out at Villa Necchi and Torre Sarca is reported in table 3.1. A minimum of 3 , for each type of specimens or surrogate surfaces, were exposed in each sampling

campaigns. Three parallel campaigns were performed at the two sites: one in winter (**win14**), one in summer (**sum14**) and one of 16-moths long (**16m**). At Torre Sarca a sampling campaign in summer 2013 (**sum13**) and a 22-months campaign (**22m**) were also performed.

Table 3.1: Summary of the sampling campaigns performed at Torre Sarca and Villa Necchi.

Torre Sarca					Villa Neccchi Campiglio				
ID	start	end	surrogate surface	stones	ID	start	end	surrogate surface	stones
Sum13	03/07/2013	01/10/2013	Al, PTFE, Qz						
Win14	23/12/2013	26/03/2014	Al, PTFE, Qz	Carrara	Win14	23/12/2013	26/03/2014	Al, PTFE, Qz	Carrara
Sum14	30/05/2014	01/10/2014	Al, PTFE, Qz	Carrara	Sum14	30/05/2014	01/10/2014	Al, PTFE, Qz	Carrara
16m	23/12/2013	05/05/2015	Al, PTFE, Qz	Carrara	16m	23/12/2013	05/05/2015	Al, PTFE, Qz	Carrara
22m	03/07/2013	05/05/2015	Al, PTFE, Qz	Carrara, Noto, Botticino, Granite					

3.2.5   Determination of the size-distribution of the deposited PM

The determination of size distribution of particles deposited on Alu was performed through the acquisition of Variable Pressure Scanning Electron Microscopy (VP-SEM) images and processing them with the freeware software ImageJ™. Specifically, several different SEM images were acquired at different magnification (from 100x to 5000x) and with different detector modes (QBSD and VPSE)

according to a mapping path, in order to represent the whole sample. Alu is the optimal support for this kind of analysis. Two samples of Alu were exposed in Torre Sarca during sum14 and win14 respectively, while two samples were exposed in Villa Necchi in the same period in order to investigate the seasonal deposition pattern at both sites. In order to make a proper comparison, specifically homogeneous areas were selected for SEM/EDS analysis on all considered filters SEM images were obtained using a SEM Zeiss EP EVO 50 (working in low vacuum mode, with 20 kV as accelerating voltage and 7-9 mm as working distance). Therefore, ImageJ software allows to separate particles deposited from the matrix below by means of a threshold value (Figure 3.10a-b) and then through the use of "*Analyze particle*" plug-in to count them as a function of their area (Figure 3.10c).
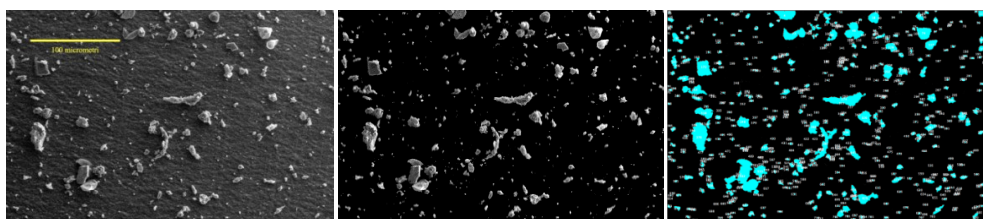
Figure 3.10: Original SEM image of exposed Alu filter (left); particles are separated from the matrix by means of a threshold value (centre); "*Analyze particle*" plugin counts particles as a function of their area (right).

3.2.6   *Cross Section observation of the exposed stone specimens*

Exposed stone specimens were observed in cross section with the aim to detect any decay phenomena affecting the surfaces. Only the carbonaceous stones, Botticino limestone, Noto calcarenite and Carrara marble were observed. A sample of Botticino and one of Noto exposed for 22m at Torre Sarca were observed. As regards Carrara marble, three samples were investigated, two of them exposed at Torre Sarca in the 22m and 16m campaigns respectively, while the other one exposed at Villa Necchi in 16m campaign. A portion of the samples was incorporated in a double-component epoxy resin (EpoFix Struers®). The samples were crosswise cut with a cut-off machine, and the cross sections were polished with a semi-automatic polishing machine. The cross sections were observed with a scanning electron microscope JEOL 5910 LV, with a tungsten filament source. Images were acquired in back-scattered electron (BSE) at low-vacuum mode and the surface of the cross sections was made electrically conductive by means of a graphite tape. For each lithotypes, one not-exposed sample was also observed as a reference.

3.2.7 Analysis of the water-soluble fraction by ion chromatography

The water-soluble inorganic fraction of collected deposits was analyzed by Ion Chromatography (IC). Concerning the analysis of the deposits collected on Quartz-fibre and PTFE filters, each filter was cut into half and half-filter was extracted in 3 mL of Milli-Q® water (18.2 MΩ) by using an ultrasonic bath (20 min, SONICA®, SOLTEC). In the case of 5 x 3 cm Stone specimens, the whole specimen was dipped into 50 mL Milli-Q® water and extracted with the ultrasonic bath. Aqueous extracts were filtered with a syringe filter (0.45 μm PTFE) to remove the water insoluble fraction. Cations (Na^+, NH_4^+, K^+, Mg^{2+}, Ca^{2+}) and anions (F^-, Cl^-, NO_3^-, SO_4^{2-}, formate HCO_2^-, acetate $C_2H_3O_2^-$, propionate $C_3H_5O_2^-$, piruvate $C_3H_3O_3^-$, oxalate $C_2O_4^{2-}$) were analyzed using two coupled ion chromatography systems (Dionex ICS-90 and ICS-2000). Cations were determined using ICS-90 equipped with a Dionex IonPac CS12A-5 analytical column: an isocratic elution was performed with 20 mM methanesulfonic acid (flow rate of 0.5 mL/min). The eluent signal was suppressed using a Dionex CMMSIII 4 mm MicroMembrane chemical suppressor. Anions were analysed using ICS-2000 equipped with a Dionex Ion Pac AS11 4x250 mm Analytical column. An EGC II KOH Eluent Generation Cartridge was used to perform a gradient

elution with a 0.8 mL/min flux and a KOH concentration ranging from 0.10 to 6.50 mM. The column temperature was set at 30°C. Quantification was achieved by means of the external standard method. Standard solutions were made starting from solutions of each single ion (1000 mg/L). Together with the exposed samples, three non exposed samples for each substrate were water-extracted and analyzed too. For each determined ion, the mean content of the non exposed samples was used as "blank" value and it was subtracted to the values obtained for the exposed samples. In this way, the ions content due to the particles deposition was obtained.

A detailed study of the stability of some analytes while performing the analysis was conducted. A multi-component standard containing acetate, formate, propionate, piruvate and oxalate at 1.5 pmm and nitrate at 2.5 ppm, was analyzed for seven times in succession, for a total time of about 6.30 hours. This experiment was repeated taking the vials under different temperature conditions:

-       Ambient: the vials were simply housed in the sampler holder of the auto-sampler as long as necessary for the execution of the seven chromatographic runs. This experiment simulates what normally happens when a sequence of samples is analyzed (laboratory temperature about 20 °C)

- Refrigerated: the vials were stored in a refrigerator at 4 °C in the time elapsed between the analyses. The vials were removed from the refrigerator just before the injection.

- Ice Bath: the vials were stored in a custom-made ice bath during the execution of the analyses. The ice bath was realized by modifying the sampler holder of the auto-sampler to make it suitable to contain the melting ice.

Figure 3.11 shows the trend of the chromatogram's area of some analytes in function of the time during the execution of the analyses. The area of each replica was divided by the maximum detected area. This study highlights that some of the analyzed ions are significantly thermolabile. By observing the results obtained at ambient temperature, a decreasing trend can be clearly seen in the case of acetate, formate, piruvate and nitrate. Concerning the test conducted in refrigerated conditions, the decreasing trend is less evident, even if in the case of piruvate data shows a wide variability. The results obtained with the ice bath are very similar to "refrigerated" ones. This evidence suggests that the use of the ice bath would be recommended for a proper evaluation of these analytes. The results obtained in this test are in agreement with the study of Tsai et al. (2008), which have conducted similar study on low

molecular weight di-carboxylic acids. The maximum area reduction is observed in the case of formate, which shows a reduction of 80% after 6 hours at ambient temperature. In the case of acetate the reduction is of 44%, while nitrates show a decreasing of 30%. Piruvate shows a wide variability of the data but no decreasing trend seems to be evident. The same considerations are also true in the case of oxalate, in agreement with Tsai et. al., (2008).
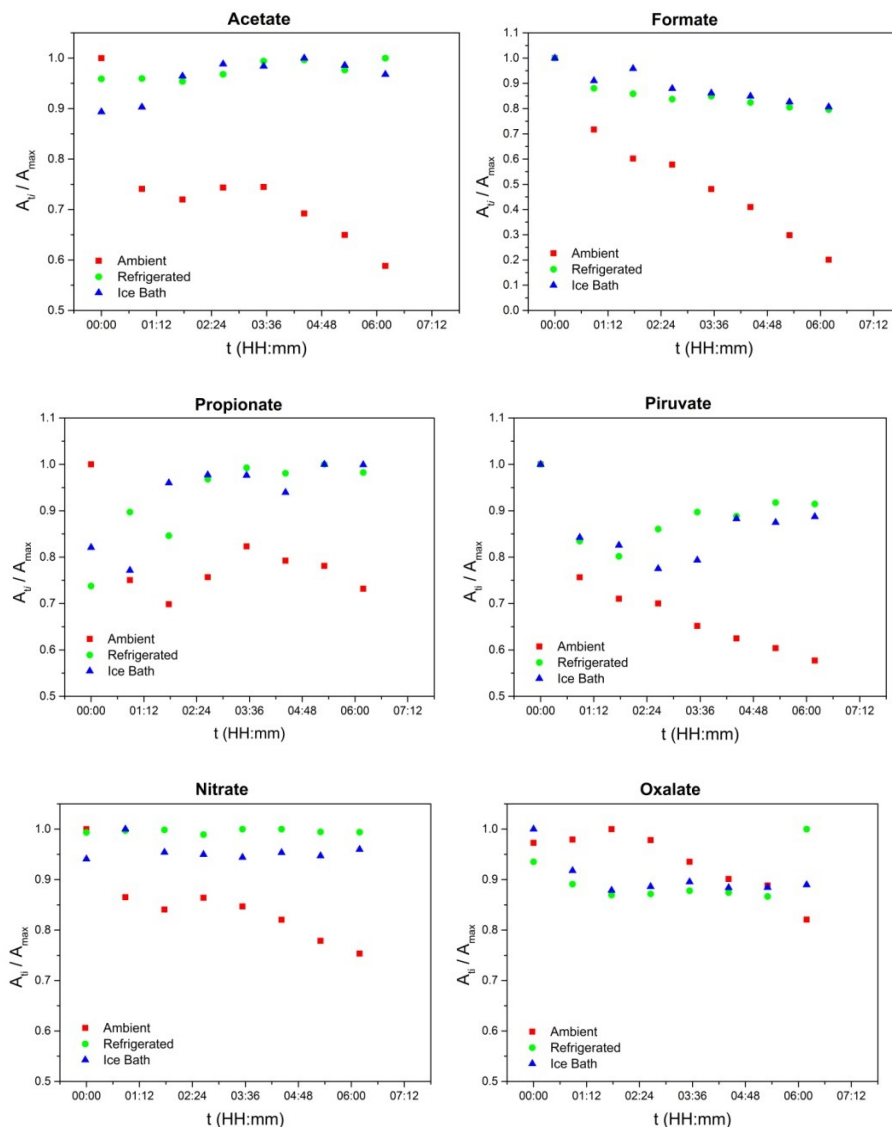
Figure 3.11: Ratio between the Area, A_{ti} ($\mu S \cdot min$), and the maximum area, A_{max} of some analytes in function of time. Ambient = ambient T; Refrigerated = vials were stored at 4 °C in elapsed time between the analyses; Ice Bath = vials were stored in a custom-made ice bath during the analyses.

3.2.8 *Analyses of polycyclic aromatic hydrocarbons and alkanes by GC-MS*

The presence of polycyclic aromatic hydrocarbons (PAHs) (Table 3.2) and *n*-alkanes (homologues series from C18 to C32) inside PM deposits collected with the depbox were investigated by means of gas chromatography-mass spectrometry. Qz and PTFE exposed filters were extracted in 1.5 mL of dichloromethane (≥99.9% Sigma-Aldrich). For 20 minutes in an ultrasonic bath (Sonica®, Soltec, Italy). The extract was then filtered with PTFE syringe filters (MS® pore size = 0.22 μm), evaporated under N_2 and dissolved in 200 μL of isooctane for GC-analysis (Panreac). In the case of stone specimens, the PM deposit was first removed from the specimens by means of a scalpel, the removed powder was analyzed according to same procedure used for Qz and PTFE.

The samples were analyzed with a Agilent 6850 GC system equipped with a Agilent 5973 Network Mass Selective detector and a Agilent 7683 Series injector (injection volume 2 μL, splitless mode). A Zebron phase ZB-XLB column (L = 60 m, I.D. = 0.25 mm, df = 0.25 μm) was used. PAHs were analyzed by a temperature ramp starting from 80 °C and ending at 330 °C with a total analysis time of about 52 minutes. Alkanes were analyzed with a temperature ramp from 60 °C to 300 °C, with a total

analysis time of 50 minutes. The transfer line was kept at 305 °C for both programs.

The analytes output from the column were ionized by a 70 eV electron impact, the mass selector was used in single ion monitoring for the analyses of PAHs (table 3.2) while the sum of 57, 71 and 85 m/z ratio was used for the quantification of n-alkanes. Quantification of the analytes was achieved by calibration curves while the recovery rates of the samples were evaluated using deuterated internal standards.

Not-exposed stone specimens and filters were also analyzed as "blank" references, and the mean signal of all analyzed blank samples of each type (stone specimens, Qz or PTFE filters) were subtracted to the amounts measured on exposed samples in order to assess the amount of deposited PAHs and alkanes. The blank of the stone specimens was prepared by scraping the surface of blank specimens with a scalpel, according to the same procedure used for the exposed specimens.

Table 3.2: list of analyzed PAHs

NAME	ABBREVIATION	MOLECULAR MASS	MONITORED m/z
NAPHTALENE	NAPH	128	128
ACENAPHTHYLENE	ACTY	152	152
ACENAPHTHENE	ACT	154	154
FLUORENE	FLN	166	166
PHENANTHRENE	PHE	178	178
ANTHRACENE	ANT	178	178
FLUORANTHENE	FLNT	202	202
PYRENE	PYR	202	202
BENZO[A]ANTRACENE	BAA	228	228
CICLOPENTA[C,D]PYRENE	CPCDP	226	226
CHRYSENE	CHR	228	228
BENZO[B,J]FLUORANTHENE	BBJF	252	252
BENZO[K]FLUORANTHENE	BKF	252	252
BENZO[A]PYRENE	BAP	252	252
BENZO[E]PYRENE	BEP	252	252
DIBENZO[A,H]ANTHRACENE	DBAHP	278	278
INDENO[1,2,3 C,D]PYRENE	I123CDP	276	276
BENZO[G,H,I]PERYLENE	BGHIP	276	276

3.2.9   X-Ray Diffraction of the collected deposits

The collected deposits were also analyzed by X-ray diffraction in order to identify the main crystalline phases that compose the deposits. A Panalytical X'pert PRO diffractometer was used, equipped with a X'celerator PW3015/20 detector. XRD spectra were recorder between 3° to 75° degrees (2θ), using a Cu K_α radiation (40 kV, 20 mA). XRD analyses had involved in particular the marble specimens. The specimens were directly inserted inside the samples-holder clamp of the diffractometer. In this way, the analysis can be considered as non-destructive towards the exposed specimens, which are then available for other subsequent analyses. In order to obtain an optimal signal-to-noise ratio, it was chosen a relatively long-time method of analysis (Scan speed 0.1 deg. s^{-1}). A not-exposed marble specimen was also analyzed in order to better distinguish the crystalline phases attributable to the deposited PM.

3.3 Results and Discussion

3.3.1 Deposition Rates

After the exposure, stone specimens and surrogate surfaces were covered by a particles deposit. Deposited mass (m_{dep}) is given by the difference between the mass of samples before and after the exposure. The deposited mass increases with the exposure time (table 3.3). This behaviour is due to the design of the depbox, which has the goal to mime the dry deposition process but any possible particles removal mechanism is avoided. On real exposed surfaces, several mechanisms take part in the deposition, with either a positive (i.e. impaction and interception due to the turbulent motions, brownian diffusion, gravitational sedimentation, diffusiophoresis, electrostatic attraction, thermophoresis) (*Maro et al. 2014*) or a negative (i.e. high wind speed, extreme meteorological events) contribution. The result of such a complex scenario is that very different depositional contexts can occur even in a single façade or artefact (*Camuffo et al. 1982*). Considering this, the depbox method was designed to obtain repeatable samples in terms of deposited mass and to study the deposition with a seasonal time scale. With respect to the latter point, in the short-terms campaigns (win14 and sum14) about 2 mg of particles were collected, and this amount is enough in order to carry out chemical analyses.

Starting from the deposited mass, the deposition rates were determined according to equation 3.1.

$$D = \frac{m_{dep} \cdot 1000}{A \cdot dy} \cdot 30 \quad \left[\frac{\mu g}{cm^2 month} \right]$$

(*Eq. 3.1*)

D = deposition rate
m_{dep} = deposited mass [mg]
A = deposition area
dy = days of exposure

The deposition rates measured on surrogate surfaces and Carrara Marble at Torre Sarca and Villa Necchi are reported in table 3.2. Considering the surrogate surfaces, deposition rates ranged from a minimum of 30.5 ± 4.5 µg cm^{-2} month^{-1} for Alu exposed at Villa Necchi in win14, to a maximum of 94.1 ± 28.0 µg cm^{-2} month^{-1} for Qz exposed at Villa Necchi for 16m. As an order of magnitude, these values are in good agreement with a similar study performed by Ferm et al. (2006) who simply exposed surrogate surfaces to air in sheltered conditions. Therefore, it can be stated that the deposition rates measured with depbox are good proxies of the deposition rates that may occur on real surfaces, especially as regards well-sheltered horizontal surfaces. With respect to surrogate surfaces, deposition rates measured during the short-term campaigns (fall13; win14 and sum14) allow the observation of a different behaviour between the surfaces: Qz has a tendency to collect greater

quantities of particles compared to PTFE and Alu (Figure 3.12). This result could be due to the greater surface roughness of Qz than PTFE and Alu, thus Qz collects more particles. A similar trend was not found in the case of the long-term campaigns (16m and 22m), in which the differences of the deposition rates measured on surrogate surfaces do not appear to be statistically significant. This is probably due to the fact that once covered by a quite uniform particles deposit, all surfaces have similar characteristics in terms of surface roughness. Thus the deposition rates became similar at long-time scale. Carrara Marble specimens show deposition rates ranging from 33 ± 10 µg cm^{-2} month^{-1} at Villa Necchi in win14, to 69 ± 8 µg cm^{-2} month^{-1} at Villa Necchi in sum14. These values are more similar to Qz.
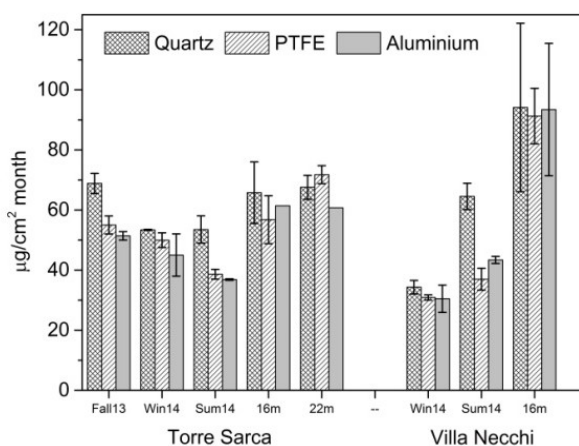

Figure 3.12: deposition rates of the total deposited mass measured at Torre Sarca and Villa Necchi.

Some differences between the two exposure sites can be highlighted. In win14 campaign, Torre Sarca shows greater deposition rates if compared to Villa Necchi. The average of the deposition rates measured on the different surfaces is 49 ± 8 µg cm^{-2} month^{-1} at Torre Sarca and 32 ± 4 µg cm^{-2} month^{-1} at Villa Necchi. An opposite situation occurs in sum14, when the average rate of Villa Necchi is 53 ± 3 µg cm^{-2} month^{-1}, greater than for the specimens exposed at Torre Sarca (42 ± 3 µg cm^{-2} month^{-1}). This difference is attributable to the presence of a *Tilia* tree near the depbox placed at Villa Necchi. This tree can be considered as an emission source that is particularly active during the growing season in connection with the inflorescence and pollination processes. The presence of ultra-coarse particles related to the presence of the tree is confirmed through optical microscope observation (see section 3.2) and they can strongly affect the deposited mass. Similar considerations can explain the high deposition rates and the high data-spread observed for the 16m campaign at Villa Necchi. These ultra-coarse particles have a short residence time in atmosphere, so their deposition is limited to the surfaces next to the emission source. The presence of these particles suggests that the characteristics of the deposits occurring on surfaces can strongly depend on extremely local factors. Even with an exposure method that

standardizes some variables, like air exchange rate, the influence of local emission sources can clearly emerge. Despite this, the significant seasonal differences in the deposition rates measured at the two sites highlight the importance of developing methods to study the deposition process with a seasonal timescale.

Some differences in the deposition rates measured on different lithotypes exposed at Torre Sarca (22m) were detected. Noto limestone amasses a greater amount of deposit if compared to the other lithotypes (Figure 3.13). This can be due to its surface characteristics in terms of roughness and microcavities (see section 3.2). The deposition flux measured on Noto calcarenite is 104 ± 7 μg cm^{-2} $month^{-1}$, whereas other lithotypes show significant lower values: 56 ± 3 μg cm^{-2} $month^{-1}$ for Carrara Marble, while 47 ± 1 μg cm^{-2} $month^{-1}$ and 46 ± 1 μg cm^{-2} $month^{-1}$ were found for Granite and Botticino respectively.
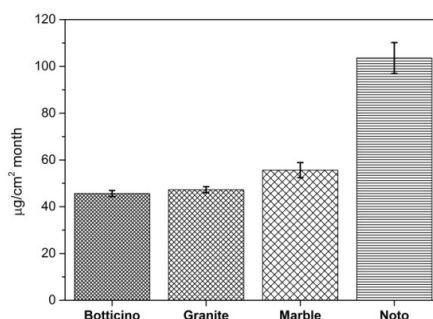
**Figure 3.13: Deposition rates measured on different stone substrates at Torre Sarca 22 months of exposure**

Table 3.3: Deposited mass and deposition fluxes measured at Torre Sarca and Villa Necchi Campiglio

| Torre Sarca	Qz		PTFE		Alu		Carrara	
	mg	σ	mg	σ	mg	σ	mg	σ
Fall13	2,4117	0,1171	1,9315	0,0777	1,7996	0,0495		
win14	1,9761	0,0068	1,8493	0,0907	1,6656	0,2603	2,3	0,2
sum14	2,5770	0,2192	1,8607	0,0783	1,7747	0,0123	2,5	0,4
16m	12,8742	1,0071	11,1182	0,7850	16,3588		11,8	1,2
22m	17,7980	1,1600	18,9100	0,7560	16,0030		18,4	1,1
	µg·cm² month⁻¹	σ	µg·cm² month⁻¹	σ	µg·cm² month⁻¹	σ	µg·cm² month⁻¹	σ
Fall13	68,9	3,3	55,0	3,0	51,4	1,4		
win14	53,4	0,2	50,0	2,5	45,0	7,0	49	5
sum14	53,5	4,6	38,6	1,6	36,9	0,3	41	6
16m	65,7	10,2	56,8	8,0	61,4		48	5
22m	67,6	4,0	71,8	3,0	60,7		56	3
Villa Necchi	Qz		PTFE		Alu		Carrara	
	mg	σ	mg	σ	mg	σ	mg	σ
win14	1,2702	0,0836	1,1433	0,0317	1,1280	0,1677	1,5	0,5
sum14	3,1076	0,2103	1,7807	0,1754	2,0890	0,0571	4,2	1,3
16m	18,4273	2,7583	17,8671	0,9070	18,2937	2,1675	13,0	1,1
	µg·cm² month⁻¹		µg·cm² month⁻¹		µg·cm² month⁻¹		µg·cm² month⁻¹	σ
win14	34,3	2,3	30,9	0,9	30,5	4,5	33	10
sum14	64,5	4,4	37,0	3,6	43,4	1,2	69	8
16m	94,1	28,0	91,2	9,2	93,4	22,0	53	4

3.3.2   *Optical Microscope Observations*

Some differences between the morphology of the deposits collected at the two sites can be determined by observing them with optical microscope. Looking at the deposits with stereo-microscope, it can be seen that Villa Necchi's deposits seem to be less dense and more heterogeneous compared to the Torre Sarca ones. Figure 3.14 refers to the deposits of the 16m campaign, and shows that Villa Necchi's deposits are characterized by the presence of some ultra-coarse particles, which have irregular or filamentous shape. These ultra-coarse particles are due to the *Tilia* tree and they are common on Villa Necchi's deposits collected during the sum14 and 16m campaigns, while they are not present in the samples exposed during the win14 campaign.
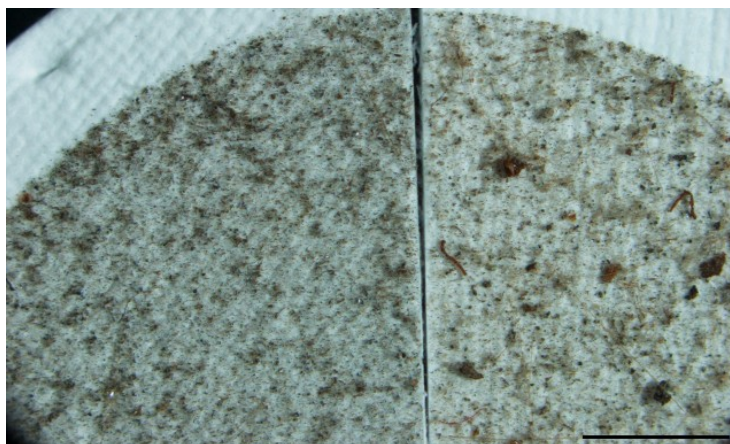

Figure 3.14: Stereomicroscope image (stick = 0.5 cm) of the particles deposited after 16 months on quartz-fibre filters. Torre Sarca, Left; Villa Necchi, Right.

Another interesting result concerns the behaviour of different lithotypes exposed at Torre Sarca for 22 months. From a macroscopic point of view, the most compact lithotypes (Botticino, Granite and Carrara Marble) have a similar pattern of deposit (Figure 3.15A, 3.15B and 3.15D). Conversely, the surface of Noto calcarenite is characterized by microcavities in which particles tend to slide into (Figure 3.15C), and consequently the deposition pattern obtained on Noto calcarenite is different from the other lithotypes. Some of the microcavities of Noto calcarenite have a clear biogenic origin, and the presence of dark particles inside these microcavities highlights shape of fossil (Figure 3.16).
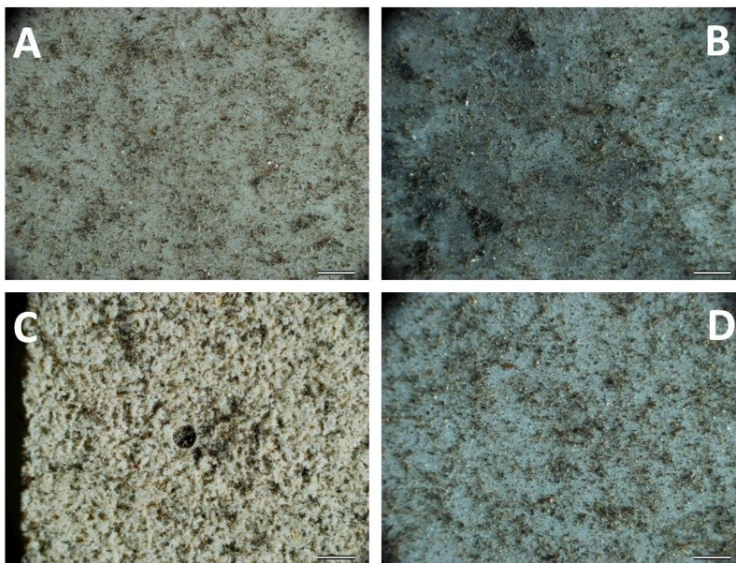
Figure 3.15: Stereomicroscope images (sticks = 1 mm) of the deposits collected at Torre Sarca in 22 months on different lithotypes: A) Botticino B) Montorfano Granite C) Noto D) Carrara Marble.
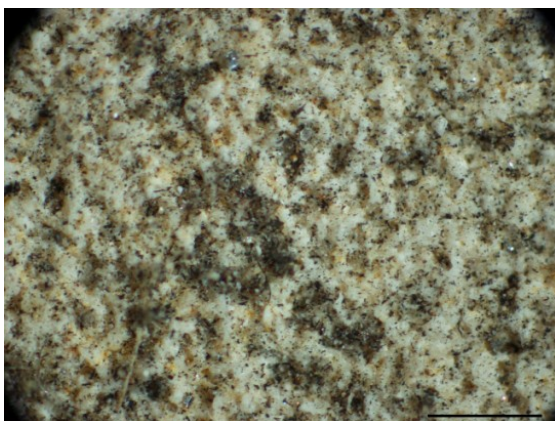
Figure 3.16: Detail of the deposit collected on Noto calcarenite (stick = 1mm). It can be seen that the particles tends to putting into the microcavities of the surfaces.

3.3.3 Characterization of the dimensional distribution of the deposited PM

A first result of SEM characterization is the identification of fine particles on exposed samples. The smallest identified particle has an area of 0.4 μm^2 hence also fine particles may deposit through the depbox. The biggest observed particle was found in Torre Sarca sample exposed during sum14, and it has an area of 1080.0 μm^2. It has to be considered that only homogeneous areas were selected to be observed with SEM. For example, the areas of Villa Necchi samples which present ultra-coarse particles, coming from *Tilia* tree, were avoided. Thus, SEM characterization allows

to achieve a good evaluation of the fine particles that composed the deposits. The smallest and biggest value of particles area and the total number of particles found on each Alu sample are reported in Table 3.4 Moreover, Table 3.4 shows also the density (number of particles for mm^2) on the Alu surfaces.

Table 3.4: Dimension (µm^2) of the smallest and biggest particles, total number of particles and density of the deposits (Num/mm^2) detected on Alu samples in win14 and sum14 campaigns at Villa Necchi and Torre Sarca.

	Villa Necchi		Torre Sarca	
	win14	sum14	win14	sum14
Smallest Particle (µm^2)	4E-01	4E-01	4E-01	4E-01
Biggest Particle (µm^2)	1E+06	1E+06	6E+05	1E+06
Total Number of Particles	364	452	515	380
Density (Num/mm^2)	4150	5150	5870	4330

The size distribution observed on Alu samples is represented in Figure 3.17. All the samples present a common trend of dimensional distribution of particles, and this is an interesting result in order to validate the depbox as an alternative exposure method. 0.4 – 5.0 µm^2 is the predominant class for all the samples, and also the number of big particles (area over 200.0 µm^2) is almost the same.

Probably, the differences between the sampling campaigns are not so large because of the choice of homogeneous areas for the SEM images acquisition. However, the fact that the most represented dimensional class is 0.4 - 5.0 μm^2, suggests that fine PM fractions could significantly deposit also in the conditions of the depbox. In addition to this, even if the total deposited mass seems to be variable in the different exposure campaigns (table 3.3), the number and the dimensional distribution of the particles observable with SEM seem to be similar. This results suggests that the total deposited mass is not the only parameter to take into account for a proper study of PM-induced decay.
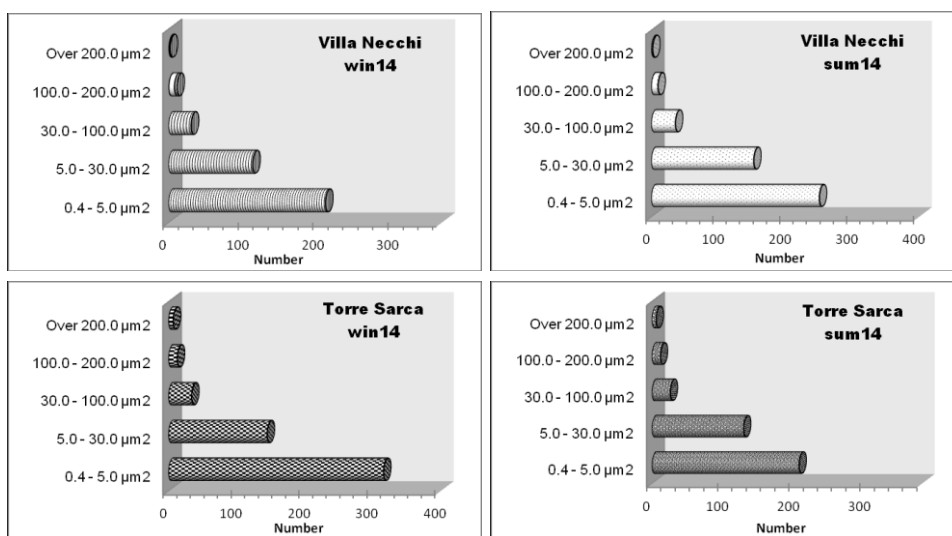
**Figure 3.17: Dimensional distribution of particles in Alu filters.**

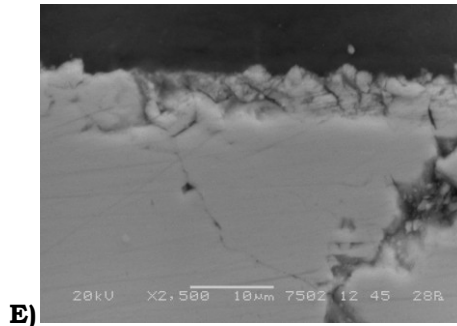### 3.3.4 Observation of the cross section of exposed stone specimens

SEM images of the not-exposed marble specimen show a compact and quite homogeneous structure. Looking at the image at 200x magnification (Figure 3.18A) the surface seems to be quite smooth, while observing the images at higher magnifications (Figure 3.18B, C and D) it appear irregular owing to the presence of grooves, probably due to the smoothing procedure. In some points of the surface's front the grooves are more evident (figure 3.18C) while in other points they are less evident (figure 3.18B).
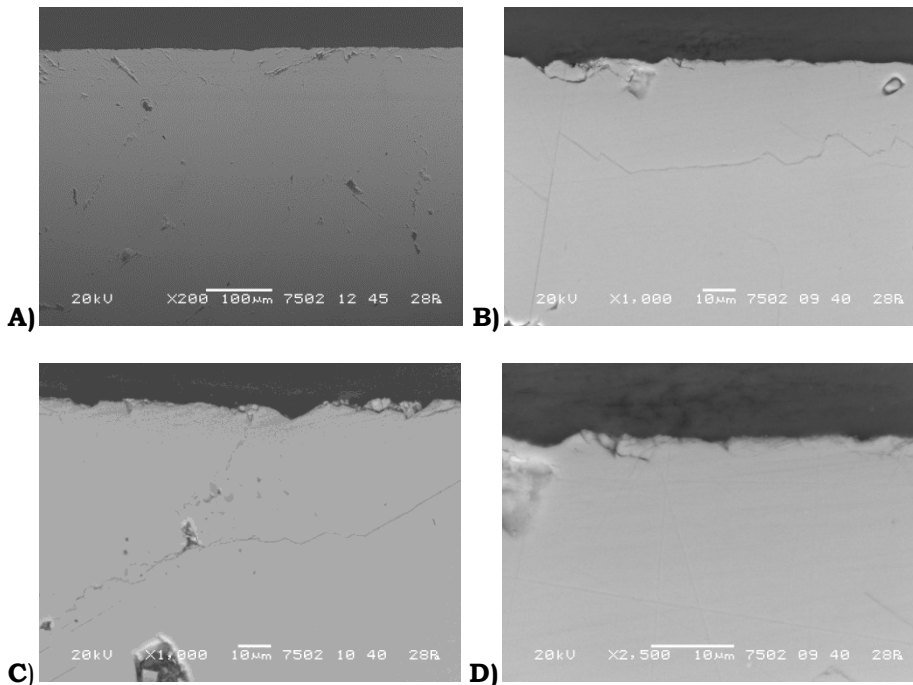
Figure 3.18: SEM images of the cross section of a non-exposed marble specimen at different magnifications.

In the marble specimen exposed at Villa Necchi (16m campaign), it is possible to notice the presence of some PM particles deposited on the exposed surface. The images at lower magnification (Figure 3.19A and B) show that, after the exposure, the marble seems to be still compact while it can be observed some slight marked inter-crystalline discontinuity (Figure 3.19A and B), that indicates an incipient decay process. At high magnifications the crystals on the section profile (figure 3.19C, D and E) are characterized by a network of microfractures.
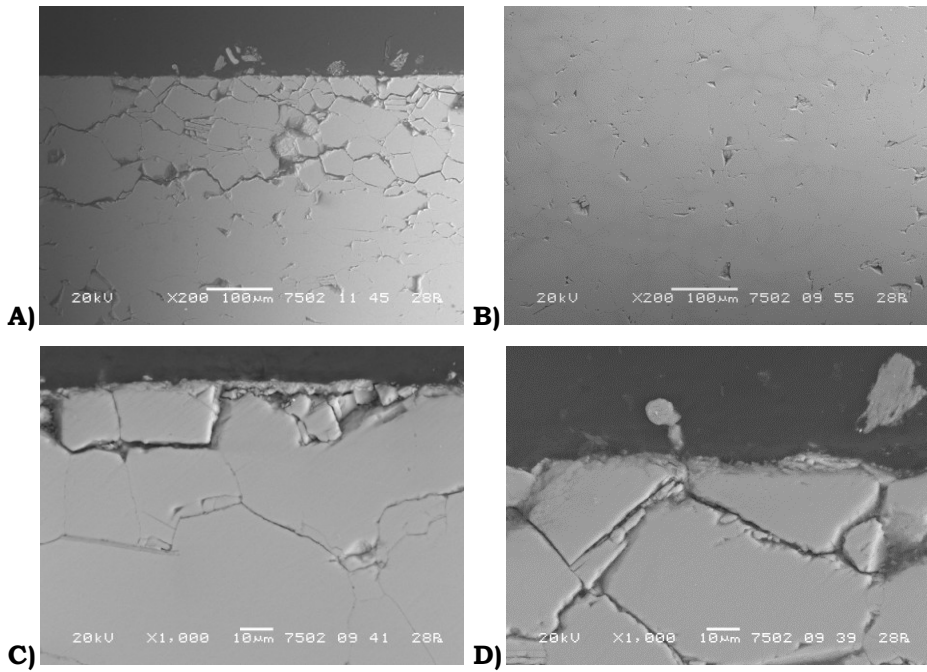
E)
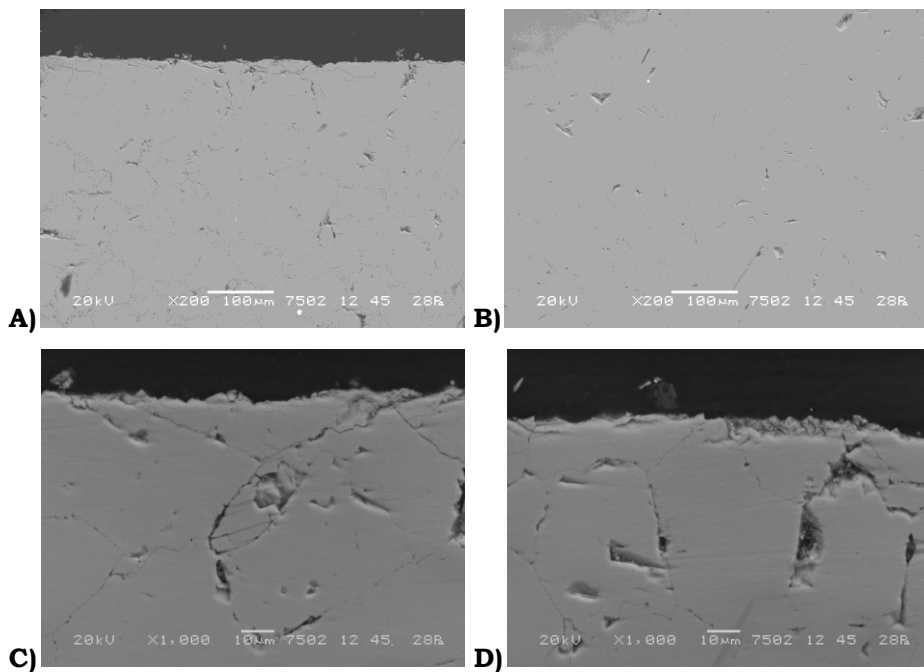
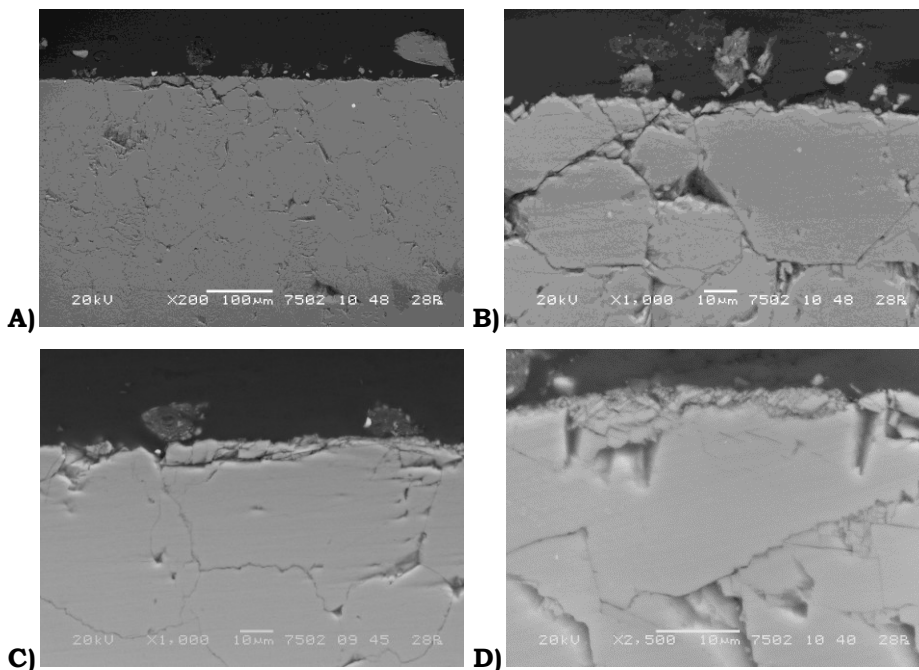**Figure 3.19: SEM images of the cross section of a marble specimens exposed at Villa Necchi for 16m.**

The marble specimen exposed at Torre Sarca (16m campaign) shows the presence of PM particles on the exposed face. Intergranular microfractures in the upper part of the section are also visible. These fractures are evident even at low magnification (figure 3.20A) and they can be attributable to an advanced mechanical decay. It is uncertain if such a kind of advanced decay is due to the exposure or to accidental mechanical stress occurring during the preparation of the polished cross section. Deeper inside, the material seems to be compact with micro-cavities ascribable to a good stone. Observing more in detail the surface (figure 3.20C and D) the calcite grains are characterized by intra and inter-crystalline discontinuity system. As well as in the case of the specimen exposed at Villa Necchi, the exposed site of the grains show signs of erosion decay phenomena.
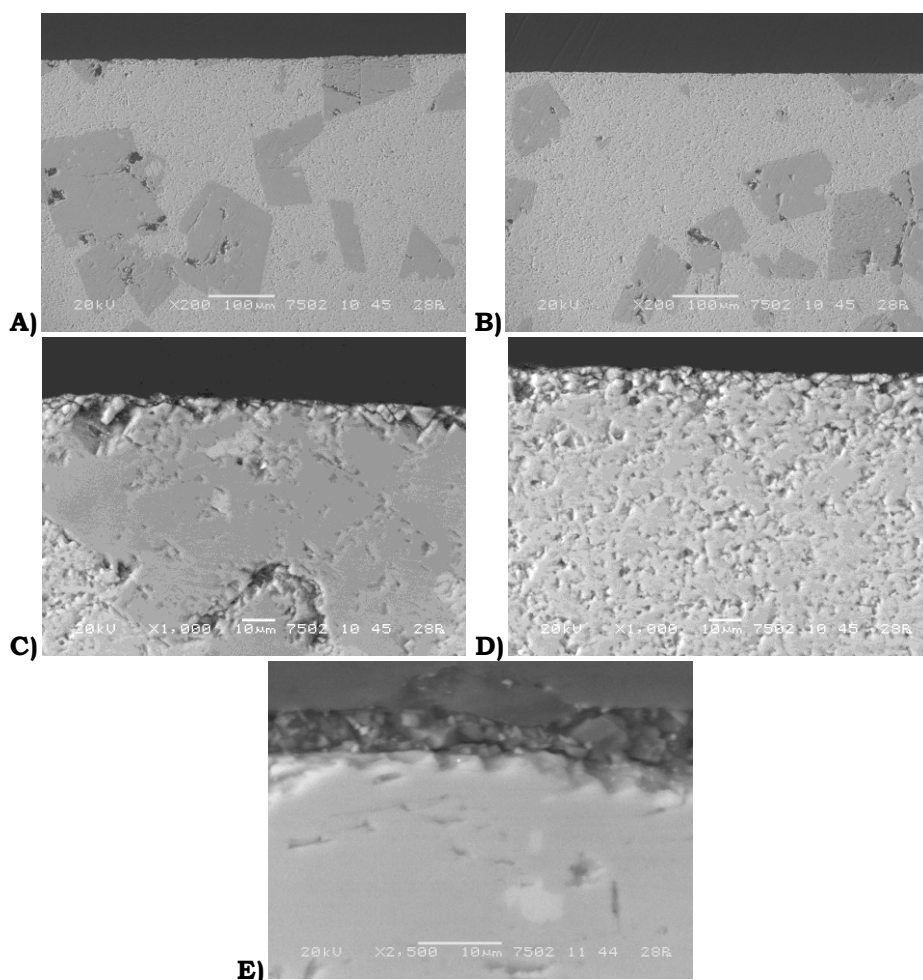
Figure 3.20: SEM images of the cross section of a marble specimen exposed at Torre Sacra for 16m.

The marble specimen exposed at Torre Sarca (22m campaign) shows some intergranular discontinuity in the upper part of the sample (figure 3.21A), although they seems to be less deep compared to those observed in the samples exposed in the shortest (16m) campaign (figure 3.20A). Looking at the images at higher magnifications (figure 3.21B, C and D), it can be seen how the intergranular microfractures seems to be more evident in some points (figure 3.21B) and less evident in some other points (figure 3.21C). As well as in the other exposed specimens, the outer face of the calcite crystals seems to be interested by an erosion phenomenon.

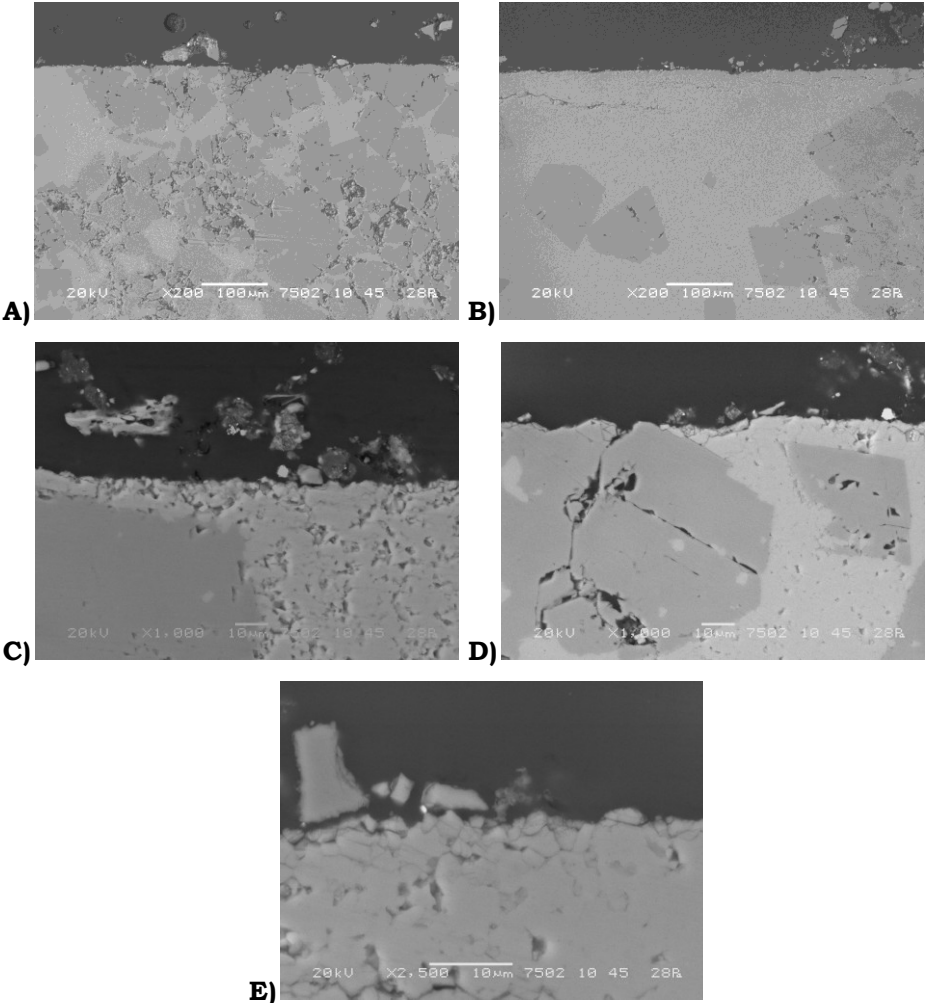**Figure 3.21: SEM images of the cross section of a marble specimen exposed at Torre Sarca for 22m.**

The cross section of the not-exposed Botticino specimen revealed a very compact and homogeneous calcareous matrix (figure 3.22A and B). Looking at higher magnifications, the marks left by polishing processes are detectable.
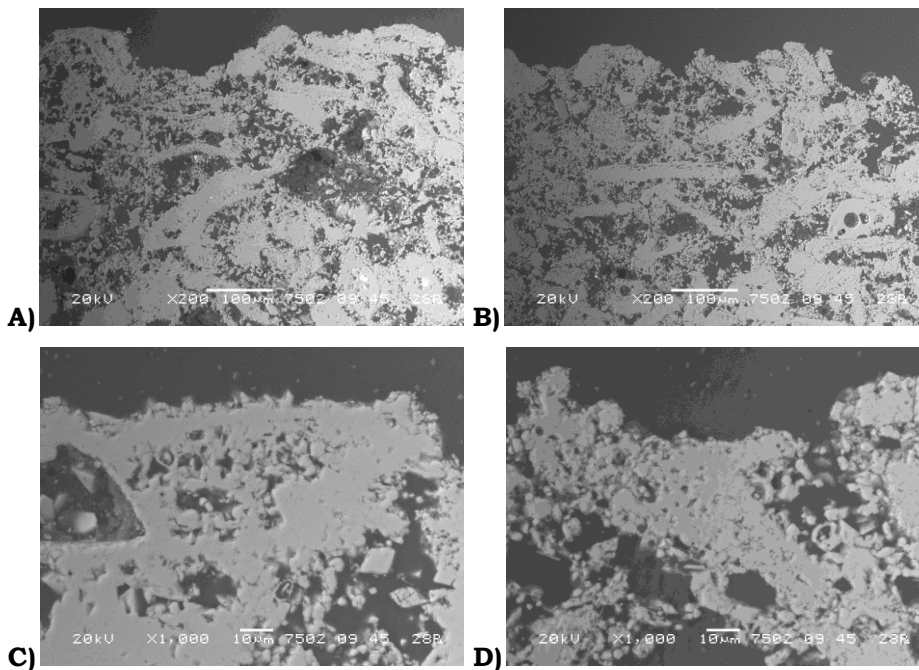

Figure 3.22: SEM images of the cross section of a non exposed Botticino specimen.

The Botticino specimen exposed at Torre Sarca in 22m campaign seems to be compact, both in the upper part of the specimen and deeper inside the material, thus no significant differences between the exposed and not-exposed samples are detectable at low magnification (figure 3.23A). Only rarely some fractures, parallel to the surface, are observable in the upper part of the specimen (figure 3.23B). Looking at higher magnifications, some slight decay marks are distinguishable. The surface appears less smooth (figure 3.23C and D) if compared to the not-exposed specimen (figure 3.22C and D). In the case of dolomitic domains, marks of discontinuity arise between the dolomitic clasts and micritic calcite (figure 3.23D). In some of the surface dolomitic clasts a 5-7 μm deep network of microfractures is present (figure 3.23E). On the contrary, micritic calcite areas appear very similar to those of the not exposed specimen. Botticino limestone shows very different decay effects compared to those observed on Carrara marble sample (figure 3.21). This is obviously due to the different minero-petrographic characteristics of the two lithotypes investigate, and the depbox exposure method has allowed to observe their different behaviour.

Figure 3.23: SEM images of the cross section of a Botticino specimen exposed at Torre Sarca for 22m

Noto stone is a fossiliferous and highly porous calcarenite (figure 3.24A and B). The surface profile is very rough, and a lot of cavities appear evident both on the surface and within the material. Looking at higher magnifications (figure 3.24C and D), it can be observed the presence of a lot of grains and bioclast and the highly porosity of the cement.

Figure 3.24: SEM images of the cross section of a non exposed Noto specimen.

The complex structure of the Noto calcarenite does not allow observing differences between the exposed (figure 3.25A) and not-exposed specimen and the presence of the PM deposit, always observed on Botticino and Carrara specimens profile (figures 3.23, 3.21, 3.20 and 3.19). In some points it seems observable that the particles tend to arrange inside the surface microcavities (figure 3.25B). Also at higher magnifications, no differences between exposed and not-exposed samples can be observed (figure 3.25C and D).
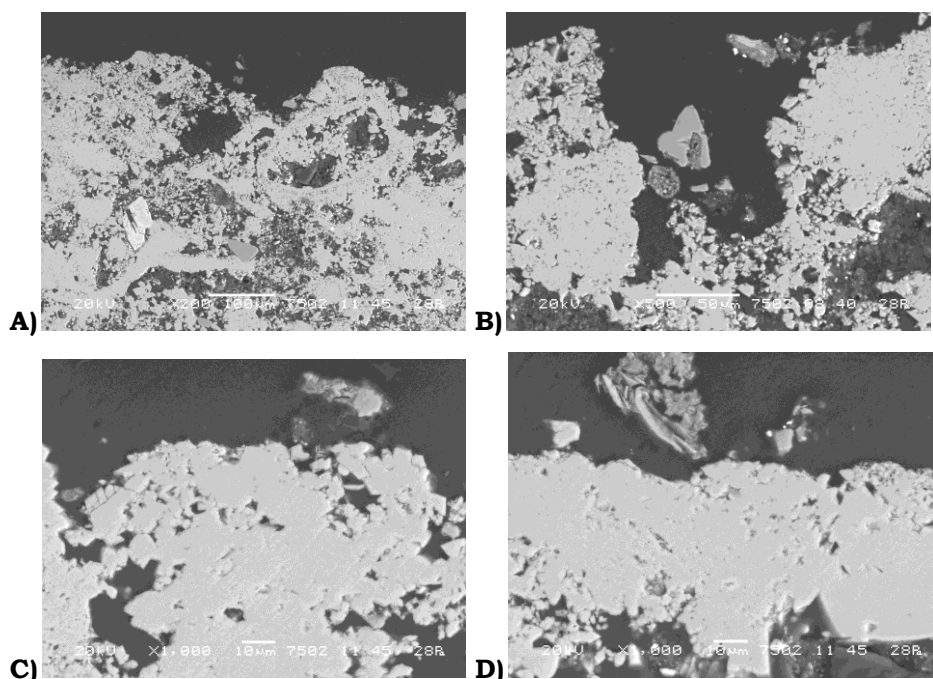
Figure 3.25: SEM images of a cross section of a Noto specimen exposed at Torre Sarca for 22m.

The scanning electron microscope observation of the polished cross sections of exposed and not-exposed specimens, allowed to better understand the capacity of the depbox exposure method. After 22 months of exposure, Carrara marble and Botticino limestone shows evidences of deterioration. The morphologies of these signs depend on the lithotypes. Noto calcarenite does not shows decay marks, but this is probably due to the intrinsic proprieties of this lithotype. Thus, from this point of view, it can be stated that the depbox exposure method allows to observe the lithotype-specific decay morphologies. Comparing the marble specimens exposed with different time horizon (16 and 22 months) and in different exposure sites (Torre Sarca and Villa Necchi) results are not clearly interpretable. The specimen exposed at Villa Necchi highlight slight decay effects compared to the specimen exposed at Torre Sarca. However, it must be point out that the specimen exposed at Torre Sarca for 16 months seems to be the most decayed, even more that those exposed for 22 months in the same exposure site. This latter results confirm that the decay of a single stone artefact can be strongly influenced by several variables which depends on the artefact itself, like i.e. heterogeneities or features due to the manufacturing process, thus making difficult to perform a proper comparison regarding the decay rate of stone materials,

even in the case of stone specimens coming from the same quarry.

3.3.5   Composition of the water-soluble fraction of the deposits.

In all exposed samples a significant increase of the water-soluble species, compared to the not-exposed samples, was observed. This evidence confirms that the atmospheric deposition can represent a considerable source of soluble species for the exposed surfaces. The analyzed water-soluble content represents on average the 6% of the total deposited mass even if this value showed a wide variability. For the surrogate surfaces, a maximum of 18% of water-soluble content in the case of Qz exposed at Villa Necchi in win14 and a minimum of 2% in the case of PTFE exposed at Torre Sarca for 22m was found. The ions deposition rate and the water-soluble content seemed to be greater in the case of the short-terms campaigns, since it is the 9% on average considering the surrogate surfaces exposed at the two sites in win14 and sum14 campaigns while it is the 4% on average considering 16m and 22m campaigns. Similar considerations were also true in the case of stone specimens. This result can be explained considering that, especially regarding log-term exposure, several processes

can act on exposed substrates (i.e. partition the gas-phase, deep migration in the porosity of the material, formation of insoluble species) decreasing the water-soluble species detectable by ion chromatography. These results confirm the importance of performing short-term study for a proper evaluation of the impact of atmospheric deposition in materials decay phenomena.

The total mass of deposited ions seems to be not correlated with the total deposited mass (R^2 = 0.24, figure 3.26). This evidence could be explained considering that the most of the ions can be found in the fine fraction of PM while, in the case of the deposits collected in this study, the total deposited mass can be strongly influenced by the biggest particles. This evidence allows to state that, also in the case of materials decay studies, a special attention should be paid to fine PM fractions.
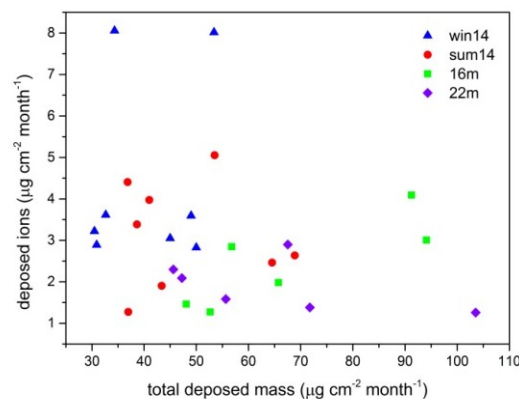
Figure 3.26: correlation between the total deposited mass and the deposited ions (µg cm^{-2} month^{-1})

Even if fine PM is supposed to have a low sedimentation rate, fine PM can represent an important fraction concerning deposition occurring in special conditions, like vertical surfaces (*Nava et al. 2010*), where sedimentation is expected to be negligible and the turbulent diffusion is assumed as the main deposition mechanism (*Maro et al. 2014*). Data obtained with the depbox show that, even in the case of horizontal surfaces in conditions of low air flow speed, fine PM fraction can significantly deposit. In addition to this, some important chemical components, such as water soluble compounds and elemental carbon, are generally abundant in the fine fraction of PM (*Perrone et al. 2012*). These components are particularly harmful for the surfaces on which they are deposited on, since they are directly related to specific decay mechanisms like salts weathering or blackening (*Bonazza et al 2005*). The ions deposition rates (table 3.4) seemed to be similar in the two sites in the case of win14 campaign, while they seemed to be greater at Torre Sarca if compared to Villa Necchi in the case of sum14 and 16m campaigns. Only PTFE in 16m campaign seemed to be an exception to this latter evidence. Considering that ions are more present in the fine PM fraction, the difference between the ions deposition rates could be explained with the different characteristics of the two sampling sites. Torre Sarca is an high-traffic site in which the influence of local

fine PM emission sources can result in a higher ions deposition. A different situation occurs at Villa Necchi that is inside the Low Emission Zone of Milan next to low traffic roads. As stated, this difference clearly emerges in summertime. This is another evidence of the fact that, concerning materials-decay studies, the total deposited mass determined through a long-period exposure campaign is not a correct parameter to take into account for a proper evaluation of the decay-hazard for the surfaces. Contrariwise, a proper knowledge of the chemical composition of deposits, their dimensional distribution and seasonal variation related thereto, has to be achieved.

Another interesting result regards the deposition of sulphates and nitrates on different materials. The ratio between sulphates and nitrates, calculated according to Equation 3.2 (*Potukuchi and Wexler, 1995*), seemed to be greater on marble specimens rather than surrogate surfaces.

$$R_{sulphates/nitrates} = \frac{m_{SO_4^{2-}}}{m_{SO_4^{2-}} + m_{NO_3^-}} \quad (Eq.\,3.2)$$

$m_{SO_4^{2-}}$ = mass of deposited sulphate [µg]
$m_{NO_3^-}$ = mass of deposited nitrates [µg]

The sulphates/nitrates ratio is on average 0.43 ± 0.09 on PTFE; 0.51 ± 0.13 on Qz and 0.76 ± 0.15 on marble specimens. These results could be explained assuming an

incipient sulphatation phenomenon acting on marble surfaces. This phenomenon involves the transformation of carbonate substrates in gypsum (calcium sulphate dihydrate), by the work of acid substances (i.e. H_2SO_4) that could be present on the deposited particles, but also by the work of acid gas substances (i.e. SO_3). The heterogeneous phase reaction (solid-gas) between marble surface and acid gases can be catalyzed by the presence of some specific components of the PM deposit (*Rodriguez-Navarro & Sebastian, 1996*) and by the presence of liquid water. Concerning the presence of liquid water, the PM deposit can promote water-adsorption process (*Casati et al. 2015*). However, the different behaviour between the substrates (surrogate and marble) confirms the fact that the study of dry depositions is a complex issue and in the estimated deposition fluxes significant differences can rise depending on the exposure substrates (*Ferm et al. 2006*) and exposure methods (*Huang et al. 2011*).

**Table 3.4: Composition of the ionic fraction of the deposits collected at Torre Sarca and Villa Necchi.**

	F %	Cl⁻ %	NO₃⁻ %	SO₄²⁻ %	C₂O₄²⁻ %	Σacids %	PO₄³⁻ %	Na⁺ %	K⁺ %	Ca²⁺ %	Mg²⁺ %	Σionsdep µg cm⁻² m⁻¹	%ions
Marble													
TSwin14	1,4 ±0,1	4,4 ±1,3	15,0 ±1,9	31,4 ±0,7	9,4 ±3,2	14,5 ±1,7	0,4 ±0,3	7,6 ±2,3	1,5 ±1,1	9,0 ±0,5	5,5 ±1,3	3,37	7,2%
VNwin14	1,4 ±0,5	6,0 ±2,0	13,8 ±3,4	33,7 ±2,8	10,4 ±1,3	11,0 ±3,2	0,3 ±0,2	6,1 ±1,9	1,6 ±0,6	10,7 ±2,3	5,2 ±2,0	3,32	11,1%
TSsum14	1,2 ±0,1	1,5 ±0,7	12,1 ±4,1	39,6 ±7,2	8,4 ±0,9	1,1 ±0,8	4,4 ±0,2	1,7 ±0,8	0,6 ±0,2	25,5 ±0,7	3,9 ±0,1	3,97	10,1%
VNsum14	1,7 ±0,5	2,5 ±0,6	18,6 ±3,2	20,9 ±0,1	7,7 ±0,7	4,9 ±1,3	7,8 ±0,1	5,9 ±0,3	1,1 ±0,3	22,8 ±1,8	6,2 ±0,1	2,63	3,1%
TS16M	0,8 ±0,5	1,1 ±0,7	2,8 ±0,6	54,5 ±35,0	20,0 ±12,6	4,0 ±1,0	0,5 ±0,1	2,9 ±0,0	0,9 ±0,0	12,5 ±11,9	0,1 ±0,1	1,46	3,4%
VN16M	0,8 ±0,6	1,7 ±0,2	3,9 ±0,9	64,2 ±3,5	13,6 ±4,4	4,0 ±1,3	0,8 ±0,2	3,9 ±0,5	1,5 ±0,2	5,2 ±1,9	0,4 ±0,1	1,27	2,5%
TS22M	1,2 ±0,2	3,6 ±0,6	9,9 ±0,8	36,6 ±2,2	30,8 ±7,8	4,5 ±0,9	0,7 ±0,2	6,3 ±0,6	1,9 ±0,2	4,1 ±3,4	0,5 ±0,1	1,58	2,9%
Quartz													
TSwin14	0,4 ±0,1	3,9 ±0,3	13,1 ±0,7	28,3 ±2,2	2,6 ±0,3	4,8 ±0,7		28,5 ±1,4	2,2 ±0,3	14,9 ±1,7	1,3 ±0,1	6,32	18,1%
VNwin14	0,4 ±0,1	3,8 ±0,2	11,2 ±0,0	27,1 ±0,1	3,1 ±0,7	3,4 ±1,4		27,9 ±1,3	2,6 ±0,2	18,5 ±2,2	1,2 ±0,1	6,36	11,9%
TSsum14	0,2 ±0,1	2,7 ±1,8	30,6 ±8,1	20,6 ±3,6	8,5 ±3,9	0,7 ±0,3	1,5 ±0,7	5,4 ±2,0	1,2 ±0,7	25,5 ±6,0	3,1 ±1,2	5,05	9,2%
VNsum14	0,2 ±0,1	2,7 ±0,3	27,3 ±2,0	17,7 ±1,8	10,4 ±3,8	1,0 ±1,0	2,4 ±0,4	8,6 ±2,3	1,4 ±0,1	23,8 ±4,1	4,5 ±0,2	2,46	3,2%
TS16M	0,1 ±0,1	8,7 ±1,2	27,7 ±5,1	21,3 ±4,6	6,4 ±0,7	1,5 ±0,8	1,9 ±0,4	13,4 ±1,0	2,5 ±0,9	14,7 ±2,3	1,6 ±0,3	3,00	4,6%
VN16M	0,2 ±0,1	6,5 ±1,3	21,8 ±4,0	26,3 ±6,3	5,9 ±1,3	1,2 ±0,6	5,3 ±1,2	14,8 ±2,6	3,7 ±0,7	12,5 ±3,3	1,8 ±0,5	1,98	2,1%
TS22M	0,2 ±0,1	8,0 ±2,4	29,8 ±7,3	22,7 ±5,8	5,1 ±1,2	1,4 ±0,8	1,5 ±0,7	11,4 ±3,3	1,9 ±0,5	16,3 ±3,3	1,6 ±0,5	2,90	4,6%
PTFE													
TSwin14	0,6	6,9	19,3	19,8	2,8	6,8	1,4	4,9	4,5	31,7	1,3	2,83	9,4%
VNwin14	0,7	6,9	23,7	18,2	2,4	7,9	1,7	6,4	2,4	28,2	1,4	2,89	6,0%
TSsum14	0,4 ±0,1	2,5 ±0,3	29,0 ±4,6	11,5 ±1,7	2,4 ±0,8	1,9 ±1,8	1,5 ±0,5	4,1 ±0,6	0,9 ±0,1	43,6 ±17,3	2,2 ±0,1	3,38	8,8%
VNsum14	0,8 ±0,1	3,2 ±0,3	22,0 ±3,0	11,3 ±0,8	3,2 ±0,1	1,5 ±0,3	3,2 ±0,2	5,4 ±0,1	0,9 ±0,1	44,8 ±8,8	3,6 ±0,0	1,27	3,4%
TS16M	0,6 ±0,1	10,4 ±1,6	28,4 ±5,4	22,5 ±3,1	4,5 ±0,5	2,0 ±0,6	0,3 ±0,1	8,3 ±1,3	2,2 ±0,3	19,1 ±3,3	1,6 ±0,3	2,84	5,0%
VN16M	0,7 ±0,5	9,7 ±5,0	18,0 ±0,8	22,5 ±8,6	7,1 ±2,0	3,1 ±1,5	0,8 ±0,3	8,0 ±4,7	3,3 ±0,2	24,8 ±16,0	2,1 ±0,6	3,20	3,5%
TS22M	0,5 ±0,2	4,4 ±2,6	13,4 ±6,6	12,7 ±6,1	14,3 ±12,7	1,1 ±0,8	0,8 ±0,3	13,3 ±11,6	4,0 ±2,1	32,3 ±26,3	3,1 ±2,1	1,38	1,9%

3.3.6   Deposited organics: PAHs and Alkanes

PAHs and Alkanes were analyzed on Torre Sarca and Villa Necchi stone specimens and surrogate surfaces in the case of sum15, 16m and 22m campaigns. A significant increase in the content of PAHs and alkanes was observed in the exposed stone specimens and surrogate surfaces, compared to the not exposed "blanks". Thus the PM deposits collected with the depbox contain both PAHs and alkanes.

PAHs have an environmental significance since they are markers of combustion, traffic being an important source in urban area. There are many sources of PAHs in vehicle exhaust, including unburned fuel, lubrificating oil and pyrosynthesis. The study of these compounds can help to figure out which PM sources impact on the surface. Results obtained on surrogate surfaces (PTFE and Qz) (figure 3.27) shows that there is no a significant difference in the PAHs content between Torre Sarca and Villa Necchi. An interesting issue arise from the comparison between the results obtain in the long-term campaigns (figure 3.27) and the sum14 campaign (figure 3.28). The PAHs pattern of the long-term campaigns shows a greater abundance of PAHs with high molecular weight, while this evidence does not occur in the case of sum14 campaign. These results can be attributable to the fact that low-molecular weight PAHs are

semi-volatile, they can therefore transfer to the gas phase and this effect is more evident at long-time scale. However, the different pattern between short-time and long-time exposure points out that even in the case of PAHs seasonal study are fundamental for a proper assessment of the deposition pathways.
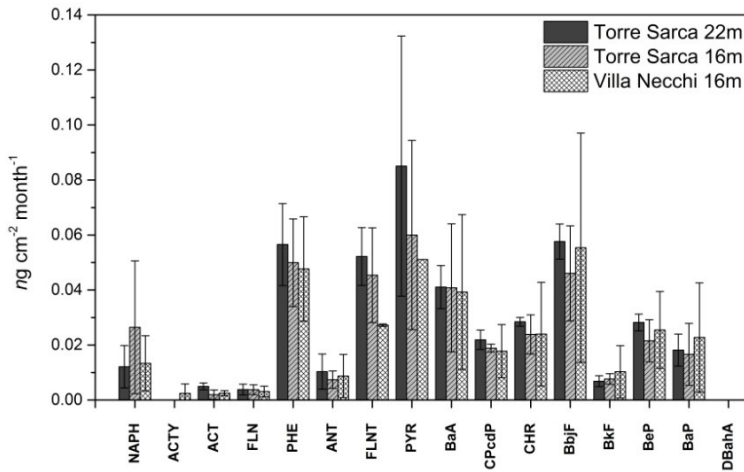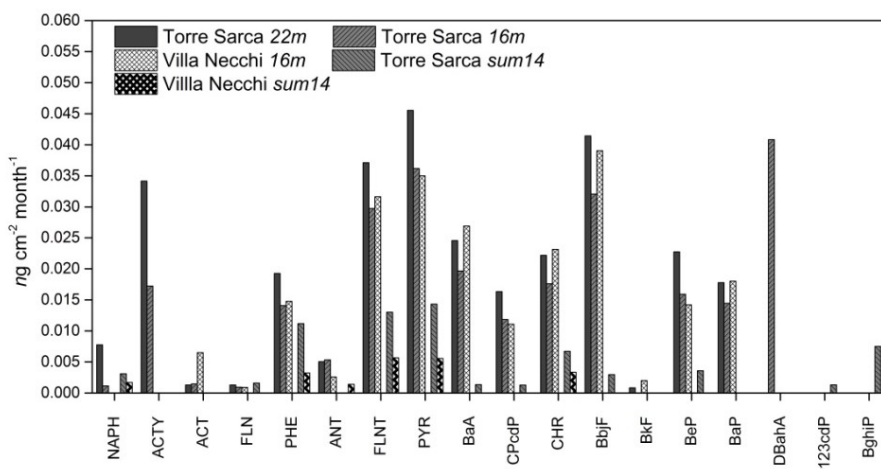

Figure 3.27: deposition rates (ng cm^{-2} month^{-1}) of PHAs detected on surrogate surfaces (Qz and PTFE) on 22m and 16m campaigns
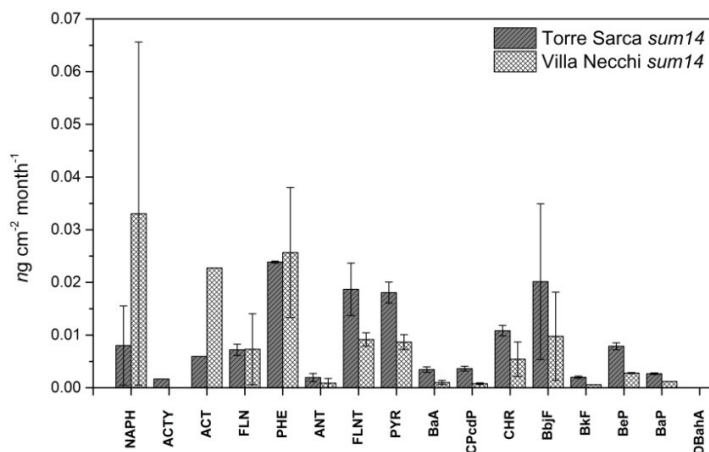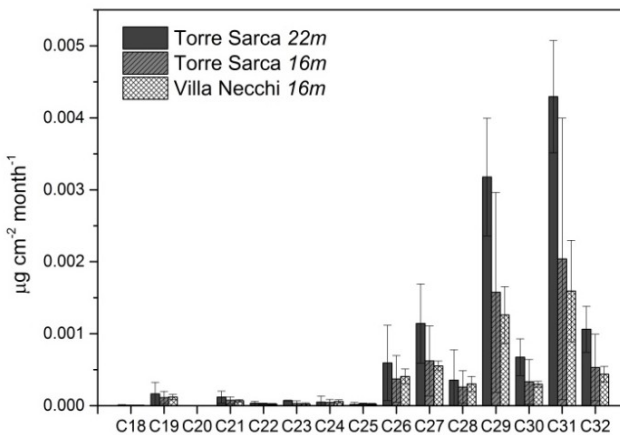
Figure 3.28: deposition rates (ng cm^{-2} month^{-1}) of PHAs detected on surrogate surfaces (Qz and PTFE) on sum14 campaign.
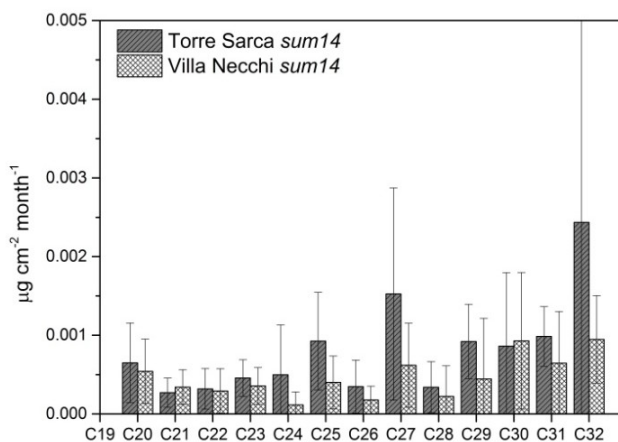

Figure 3.29: deposition rates (ng cm^{-2} month^{-1}) of PHAs detected on Marble specimens.

Homologous series of n-alkanes which are present in the atmospheric PM can originate from various sources, including anthropic and biogenic sources. The abundance distribution of the odd/even terms in the series is a key

diagnostic parameter in tracking the biogenic and anthropogenic nature of n-alkanes sources. In particular, anthropogenic emissions from utilization of fossil fuel generate a random distribution of odd versus even term; on the other hand, alkanes originated from terrestrial plant material (plant debris) show a predominance of odd-numbered terms. Also in the case of alkanes it is possible to observe a difference between long-term and short-term campaigns, with high-molecular weight alkanes that are more abundant in the case of long-term campaigns. Considering the long-term campaigns, the most abundant alkanes are C_{29} and C_{31}. This results is in agreement with Saiz-Jimenez (*1993*) which analyzed the content of alkanes in black crusts present on monuments of different European locations.

Figure 3.30: deposition rates (μg cm^{-2} month^{-1}) of Alkanes detected on surrogate surfaces (Qz and PTFE) on 22m and 16m campaigns

Figure 3.31: deposition rates (μg cm^{-2} month^{-1}) of Alkanes detected on surrogate surfaces (Qz and PTFE) on sum14 campaign.
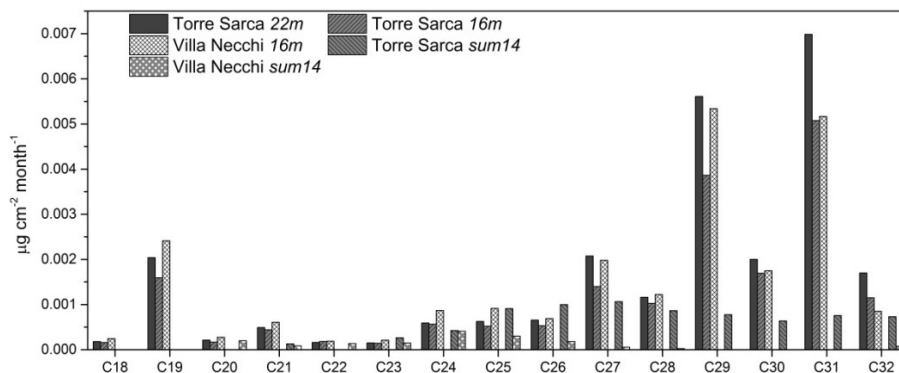
Figure 3.32: deposition rates (μg cm^{-2} month^{-1}) of Alkanes detected on Marble specimen.

3.3.7   *Main deposited crystalline phases*

XRD pattern of the non-exposed marble specimen shows the main presence of calcite, but also the presence of dolomite and magnesium calcite was detected. This result indicates an impure Carrara marble, as a matter of fact, with the commercial name "Carrara marble" a wide variety of Apuan marble are identified and in this case the Carrara marble specimens used in this study may contain dolomitic impurities.

Four exposed marble specimens were analyzed, two of the sum14 campaign, one exposed at Torre Sarca and the other one exposed at Villa Necchi. The other two analyzed specimens were exposed in the 16m campaign at the two site. Results of the analyses are reported in table 3.5. In addition to the phases related to the stone substrate (calcite and dolomite), in all the exposed specimen other phases were detected. These phases are attributable to terrigenous material i.e. quartz, mica (muscovite, phlogopite) chlorite, plagioclase and feldspar. Such an abundance of terrigenous minerals revealed by XRD, confirm that a large part of the deposited mass is attributable to the coarse fraction which has an high sedimentation rate. Three samples also show the presence of gypsum. The origin of the gypsum can be related to the deposition of terrigenous PM, but it can be also attributable to a incipient sulphatation of the marble

surfaces. In any case, the presence of gypsum is to be consider as an hazardous factor for the marble surfaces, since it is involved in the formation of black crusts.

Table 3.5: interpretation of the XRD spectra.

Sample	Mineralogical Phases *(in order of score)*
TS sum14	calcite, dolomite, quartz, gypsum, muscovite.
VN sum14	calcite, dolomite, quartz, muscovite, chlorite, plagioclase.
TS 16m	calcite, quartz, dolomite, gypsum, albite, phlogopite.
VN 16m	calcite, quartz, dolomite, gypsum, muscovite, plagioclase, chlorite.

3.4 Conclusions

A new exposure method was developed. The method involves the use of a device, named "deposition box" that is able to mime the dry deposition. Every kind of material can be housed inside the "deposition box". The new exposure method is designed to standardize some variables underlying the dry deposition process, like the air exchange rate across the exposure floor, where the specimens are placed. Several exposure campaigns were performed, some with a seasonal timescale, other over a longer period. The new exposure method allows to obtain repeatable measurements of seasonal deposition rates, highlighting significant differences in the deposition rates measured during winter and summer at the two exposure sites, Torre Sarca and Villa Necchi Campiglio. Differences between the deposition rates measured on different substrates were also detected, both in the case of surrogate surfaces (quartz, PTFE and aluminium) and stones (Carrara marble, Noto calcarenite, Botticino limestone and Granite). In the case of surrogate surfaces the differences became less evident in the case of long-term campaigns. Similar differences between seasonal and long-term campaigns were detected in the case of amounts and chemical composition of the water-soluble fraction of the deposits. Particularly, the ions deposition rates were similar in the two sites during winter, while they were greater at

Torre Sarca during summer and in the long-period exposure. These evidence point out the importance of performing seasonal studies about the decay effects of atmospheric deposition on materials. The dimensional distribution of the collected deposits, evaluated with a specially developed method based on SEM images, shows that the dimensional distribution of the deposited particles is quite similar both in winter and summer at the two sites, and a very significant presence of fine particles (area $0.4 - 5$ μm^2) was detected. This result is in agreement with the fact that the deposition rate of the ionic fraction (driven by the fine PM fraction) seems to be not correlate with the total deposited mass ($R^2 =$ 0.24), pointing out that the fine PM fraction can play a potentially crucial role as regards the decay of materials. This latter result is of particular interest considering that in conservation field, only PTS or PM_{10} are considered as relevant PM fraction inducing surface blackening and materials decay (see section 1.2).

CHAPTER 4

Study of potential decay-effects on stone substrates of each size fractions of atmospheric PM and single-salts PM.

4.1   Theoretical Background

The study of decay effects of particulate matter on materials is a very complex issue (*see section 1.1 and references therein*). In this regards, a first challenge concerns how to deposit PM on the surfaces of interest, in order to study the interactions between PM and surface. A brief overview of the literature provides several different approaches. In the field of cultural heritage, it is usual to make simple outdoor-exposure of specimens which can be made by stone or other materials of interest. With the aim of highlight the effect of PM, the specimens can be exposed in sheltered conditions (*Ferm et al., 2006; Maro et al., 2014; Realini et al., 1995; Zappia et al., 1998*). Another fruitful

approach is to use an exposure method which is able to standardize some variables related to the dry deposition process in order to obtain more repeatable samples (*see section 3 and Casati et al., 2015b, Nobili et al., 2015*). In any case, these methods are time-consuming, it takes months or years to obtain suitable samples.

Looking at other fields, the problem of corrosion due to PM is widely study related to corrosion prevention in data centres (*Ferrero et al.*, 2013 and 2014). In this field, only water-soluble fraction is often considered, and the specimens were soaked with a salt solution by means of spin coating technique (*Sandroff et al., 1992*) or by simple droplet deposition (*Singh et al., 2015; Verdingovas et al., 2015*). Considering the whole PM, some authors (*Song et al., 2013*) exploit the guidelines of the American Society of Heating Refrigerating and Air-Conditioning Engineers (*ASHRAE, 2011*) which recommend to collect dust in the environment of interest, and distributed it on the surface of the specimens by means of a brush. Even in this case, another helpful approach is to expose the specimens inside the studied environments for a certain time, which is of weeks or months (*Ding et al., 2015*).

Considering the state of the art in this topic, a new device was designed by the atmospheric chemistry research group with the aim of collecting atmospheric particles directly

deposited on any kind of substrates of interest, like i.e. stone, metallic or polymeric specimens, printed circuit boards, interdigitated arrays etc. This device exploits the principle of the sampling by impact (*Marple & Willeke, 1976*), based on the following relation:

$$S_{tk50} = \frac{d_p^2\, \rho_p\, C_p\, U}{9\eta W} \quad (Eq.\,4.\,1)$$

Were:

S_{tk50} = Stokes number of a particle having 50% of probability of impacting the sampling stage
d_p = geometrical diameter of a particle having a 50% probability of impacting
ρ_p = particle density (g cm^{-3})
C_p = Cunninghan slip correction factor (*Hinds, 1982*)
U = average velocity of the jetstream (cm s^{-1})
η = dynamic viscosity of the air (g cm^{-1} s^{-1})
W = impactor's nozzle width (cm)

Briefly, a stream of air is forced to pass through a nozzle, downstream of which is placed an impaction plate (figure 4.1). Considering the equation (4.1), the particles that are too small to impact follow the air stream while the other particles impacted the impaction plate. A full description of a prototype of the sampler will be provided in the next section (4.2).
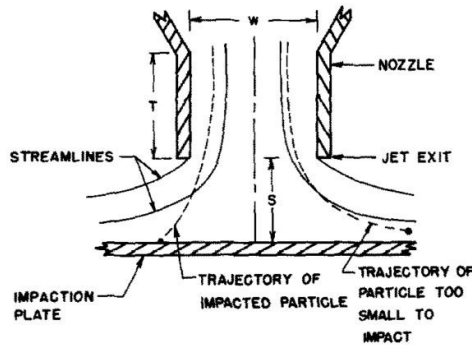
**Figure 4.1: Streamlines and particles trajectories for a typical impactor (*Marple& Willeke 1976*)**

4.2 Project and construction of a prototype of rotating cascade impactor

A prototype of a new sampling device was develop starting from the "personal cascade impactor" proposed by Misra et al. (2002). It has 4 impaction stages, on which the following size-classes of PM are selected, according to the equivalent aerodynamic diameter (d_{ae}) :

Stage A: $d_{ae} > 2.5$ μm
Stage B: 2.5 μm $> d_{ae} > 1.0$ μm
Stage C: 1.0 μm $> d_{ae} > 0.5$ μm
Stage D: 0.5 μm $> d_{ae} > 0.25$ μm

After the impaction stages it is placed a backup filter, to collect the particles with $d_{ae} < 0.25$ μm and to protect the pump. The airflow is set to 10 L min^{-1} by means of a

vacuum pump. A block diagram of the sampler is shown in figure 4.2.
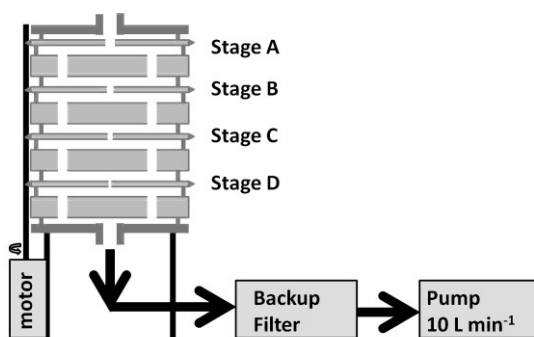
Figure 4.2: scheme of the prototype of the rotating cascade impactor

Two main characteristics make the sampler highly innovative. First of all, the sampling nozzles, which have variable width according to the impaction stage and 2 cm of length, can be set into rotation by means of an adjustable mechanism with a rotating velocity ranging from 2.8 to 13.4 minutes per rotation. In addition to this, the impaction plates made by PTFE, can accommodate any kind of specimens with a maximum dimension of 5 x 5 x 1 cm (figure 4.3), which is a dimension compatible with the Italian and international standards (*UNI 10921; UNI 10859*) regarding the evaluation of materials and products in the field of conservation. Any other smaller specimen or artefact can be accommodated thanks to PTFE adapters. The

sampling device is suitable for both indoor and outdoor use. The prototype of the sampler is shown in figure 4.4.
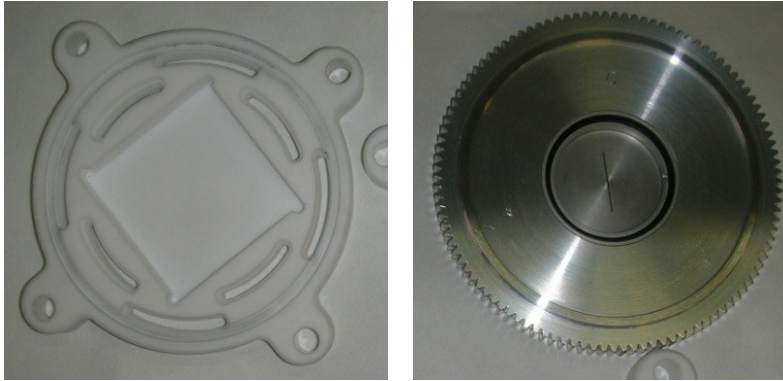

Figure 4.3: photo of stage of impact (left), made by PTFE. The 5 x 5 x 1 cm hole, made for the housing of the specimens, is visible. On the right a nozzle stage is shown.

Figure 4.4: Prototype of the rotating cascade impactor. On the left, the assembled prototype is shown. The external structure is shown in the centre. On the left, the head cap removed allows to better see the assembling of the stages.

Thanks to its innovative features, with this sampler it is possible to obtain round deposition spots, with a diameter of 2 cm, figure 4.5.
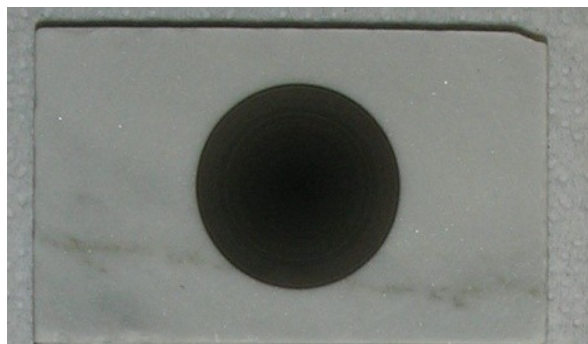
Figure 4.5: example of deposition spot (stage D) obtained with the prototype of rotating cascade impactor.

4.3 Test of the prototype of the new sampling device

A sampling test was performed with the aim of verifying the goodness of operation of the prototype. The test was carried out by performing three different 48 hours sampling, 4 PTFE filters were placed on the impaction stages while a quartz fibre filter was placed on the backup. In parallel to the sampling with the rotating cascade impactor, a monitoring of the number size distribution was also performed using an Optical Particles Counters (Grimm model 107G); PM_{10} and $PM_{2.5}$ atmospheric concentrations declared by the Lombardy environmental protection agency

were also acquired (*www2.arpalombardia.it*). The sampling activity was carried out on the roof a building of the University of Milano Bicocca. In table 4.1, the 48-hours average atmospheric concentration of PM, declared for the city of Milan is reported in comparison with the apparent concentration resulting from the sum of the mass deposited on the four impaction stages and in the backup filter of the rotating cascade impactor, divided by the nominal sampled volume (PM_{rot} in table 4.1).

Table 4.1: Mean atmospheric concentration declared by the local environmental protection agency and apparent concentration obtained from rotating cascade impactor during the sampling test.

# sampling	PM_{10}	$PM_{2.5}$	PM_{rot}
	$\mu g\ m^{-3}$	$\mu g\ m^{-3}$	$\mu g\ m^{-3}$
S1	36 ± 4	27 ± 4	15
S2	59 ± 13	51 ± 12	26
S3	63 ± 10	45 ± 9	30

Results of the test showed that the rotating cascade impactor estimates far lower concentration (-42% on average) if compared to the data declared by the local environmental protection agency. To explain this high discrepancy of the data, it has to be taken into account that the sampling site, where the test was performed, is

considered to be an urban background site. In addition to this, a vacuum pump with 10 L min^{-1} nominal flux was used, but the chosen pump did not have an accurate flux-control. Since it is a prototype, the pump was selected with the aim of ensuring the continuous operation of the device, avoiding problems of interruption of the sampling flux in case of obstruction of the backup filter or of the backup stages. This choice is justified by the fact that the new device was projected for sampling both environmental PM (section 4.4) and generated aerosol (section 4.5). In the future versions of the device this aspect will be evaluated more carefully. Anyhow, the main purpose of the new device is to collect the single size fractions of PM on different kind of materials. In figure 4.6 it is reported the numerical size distribution, as measured by optical particles counter, during the three sampling test. Since the numerical size distribution is very similar in all the tests, an unique line is visible in the graph (figure 4.6, left).
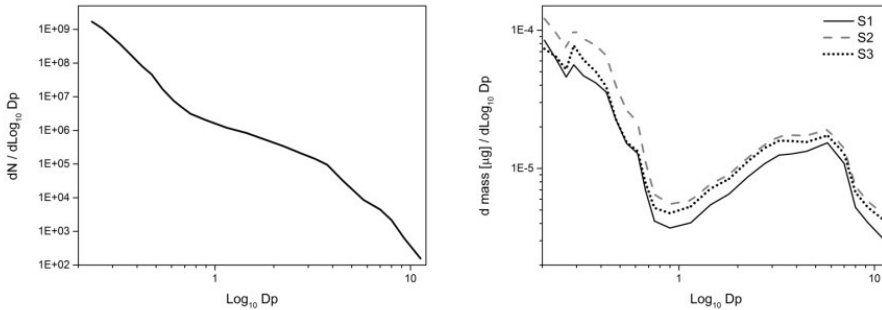
Figure 4.6: Left: mean numerical size distribution measured by OPC during the sampling tests, Right: mass size distribution computed starting from OPC data assuming an aerosol density of 1.7 g cm^{-3}.

Starting from numerical size distribution, a mass distribution was hypothesized, considering the volume distribution and assuming a 1.7 g cm^{-3} aerosol density. In this latter distribution, slight differences between the three sampling tests were identified (figure 4.6). By observing these distributions, it can be noticed that the more represented size class is the one of the finest particles, which corresponds to the stage D of the rotating cascade impactor.

By observing the masses deposited on the different stages during the three sampling tests (figure 4.7), the higher mass deposition occurred at the D stage, even if there seems to be a different distribution between S1 and the other two samplings.
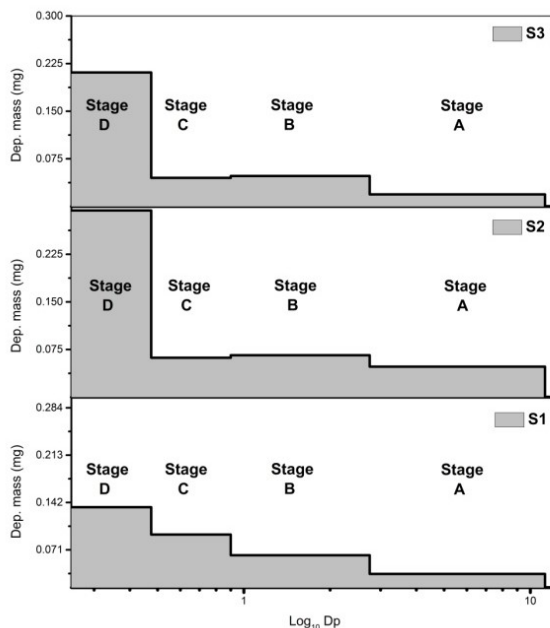
Figure 4.7: mass (mg) measured on the four impaction stages during the three sampling tests.

Sampling tests allowed to check the functioning of the prototype. These tests revealed the need of a more accurate control of the air flux in order to achieve an accordance with the standardized sampling methods. Despite this, most of the mass is sampled on the D stage, and this is in accordance with the size distribution measured by optical particles counters. This latter evidence suggests a good ability in the selection of the dimensional classes, allowing the use of the prototype to perform a size-dependent study about the PM decay impact on different materials.

4.4 Study of the potential decay-impact of the single size fractions of atmospheric particulate matter

With the aim of studying the potential decay-impact of the single dimensional fractions of PM, a sampling on Carrara marble specimens was performed (section 4.4.1). The prototype of the new rotating cascade impactor was used. Four single size fractions spots, deposited on marble specimens were thus obtained. These Carrara Marble specimens, soaked with the PM deposit, were investigated with the Aerosol Exposure Chamber method (section 4.4.2). This method was chosen since it allowed to evaluate the potential impact of PM towards the decay of a surfaces (see chapter 2) and it can help to understand how particles with different sizes behave during the environmental hygrometric variations.
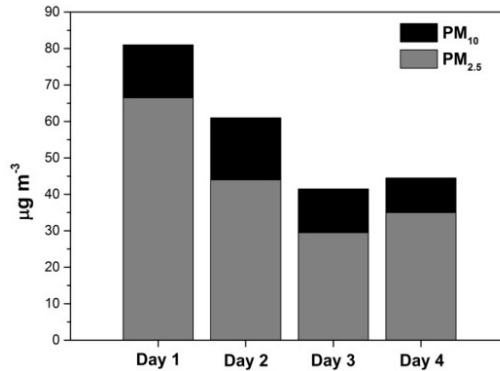
4.4.1   Sampling on Carrara Marble specimens

Four 5 x 3 x 1 cm Carrara Marble specimens were used for the test. The specimens were prepared according to UNI10921 (see section 3.2.3). The marble specimens were housed in the impaction stages thanks to suitable PTFE adapters (figure 4.8)

Figure 4.8: housing of the Carrara marble specimens inside of one of the four impaction stages.

The sampling was performed in the "U1" building of the University of Milano Bicocca (p.zza della Scienza 1, Milano, 45°30'47.4"N; 9°12'42.6"E) at an approximate height of 15 m, for a total of 63 hours of sampling spread over 4 days of sampling. The rotation velocity of the nozzles was set to the minimum velocity of 13.4 minutes per rotation. The average concentration of PM_{10} and $PM_{2.5}$ in Milan during the sampling period was provided from the local environmental protection agency and it is shown in figure 4.9. During the first day of sampling, the PM atmospheric concentration was very high (81 µg m^{-3} as regards PM_{10}), while it is decreasing during the following days.

Figure 4.9: atmospheric concentration of PM₁₀ and PM₂.₅ during the period of the sampling, declared from the local environmental protection agency .

After the sampling, all the Carrara marble specimens were contaminated by a dark round spot (figure 4.10). A first evidence was that the darkness of the spot seemed to be inversely proportional with the diameter of the deposited particles: the darkest spot correspond to the D-stage, which collect particles of 0.5 μm > d_{ae} > 0.25 μm.
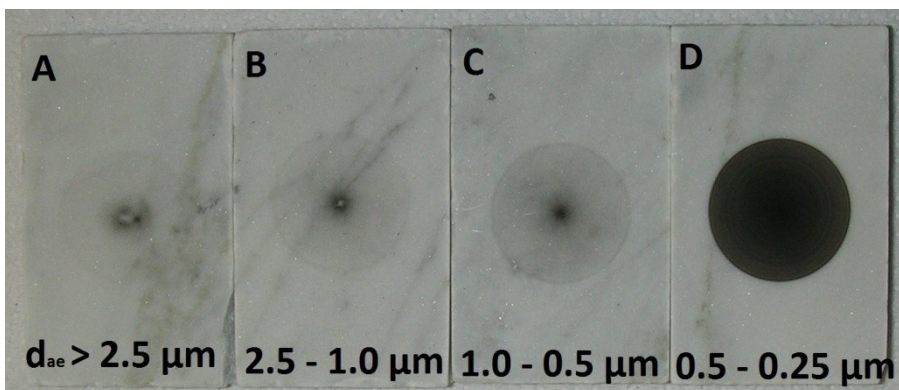

Figure 4.10: Carrara marble stone specimens after 63 hours sampling with the rotating cascade impactor.

These results are easily explained if it is taken into account that Black Carbon, which is considered to be the major factor inducing blackening of the exposed surfaces, is mainly constituted by submicrometric particles. Therefore, Black Carbon was more deposited at the lowest impaction stages, i.e. stage D. From this point of view, the rotating cascade impactor can be considered as an useful tool to study the PM-induced blackening of the surfaces.

4.4.2   Evaluation of the potential decay-impact of the single size fractions with AEC

The potential decay impact of the single size fractions of PM was evaluated by studying the PM deposits collected with the prototype of rotating cascade impactor. It was chosen to apply the Aerosol Exposure Chamber (AEC, see section 2.2.2) method. Briefly, in the AEC it is possible to vary the Relative Humidity (RH) in a controlled way. During the RH variations, the electrical conductance of PM particles collected on filtering supports can be measured. In the case of this study, the electrical conductance of the PM deposited on marble specimens was measured during a gradual RH ramp starting from 30% ending at 85% with step of about 1%. This test allows to investigate the behaviour of the PM deposits in terms of water-adsorption and solubilisation of salts. When the soluble substances,

contained in the PM deposit, switch in water-solution (deliquescence process) an increasing of the electric conductance is observed. In this way, the electrical conductance profile provides information about the content of salts and their behaviour during the RH variations. As well as the PM-contaminated marble specimens, a not-contaminated specimen was also tested in order to highlight the effects due to the presence of the PM deposit.
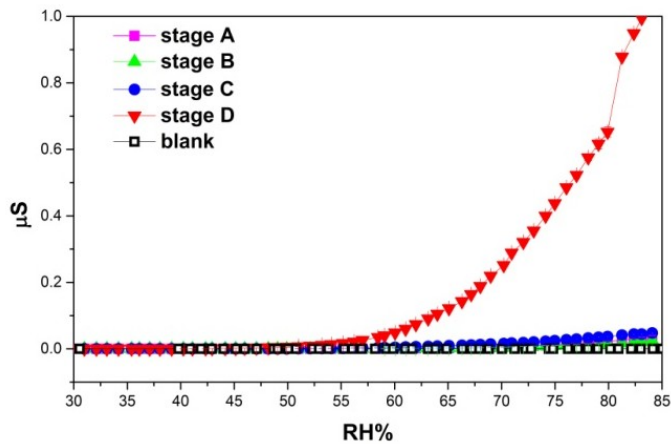
Figure 4.11: Electrical conductance of marble specimens contaminated with PM. The different colours represent the different stages of the rotating cascade impactor, therefore the different particles size fractions.

Figure 4.11 shows the conductance values in function of relative humidity detected on marble specimens contaminated with PM by means of the rotating cascade impactor. In table 4.2 the maximum conductance values and the activation RH are reported. The activation RH is the

RH values in which the first electrical signal is detected, therefore when the detection limit (0.0007 µS, see section 2.2.2) is exceed.

Table 4.2: activation RH and maximum conductance measured on marble specimens.

Stage	Activation RH [%]	Maximun Conductance [µS]
A	60	0.0404
B	59	0.0250
C	51	0.0475
D	40	1.06
blank	87	0.019

A first evidence is that the not-contaminated specimen showed higher activation RH and lowest conductance values if compared to PM-contaminated specimens. This evidence allows to highlight the role of the atmospheric deposits in promoting decay. In fact, the conductance signal, is to be placed in relation to the formation of a electrolytic solution on the marble surfaces. When the electrolytic solution is formed, salts can migrate into the porosity of the material and cause mechanical damage when they crystallize back again as consequence of a decreasing of RH.

Looking more in detail the results referred to the four stages (figure 4.12), it can be notice that the higher

conductivity was measured in the case of the stage D (0.5 μm > dae > 0.25 μm). The second highest is stage C (1.0 μm > dae > 0.5 μm) while stage B (2.5 μm > dae > 1.0 μm) and A (dae > 2.5 μm) show similar values, with stage A slightly higher after 75% RH.
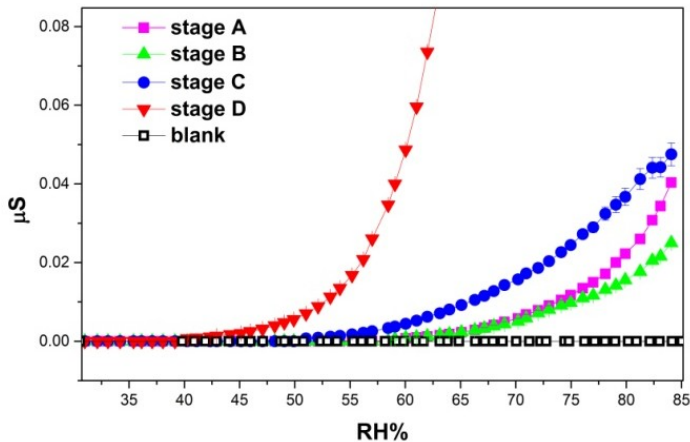
Figure 4.12: detail of the data shown in figure 4.11.

These results suggest that the finest deposited PM (stage D) is the most dangerous for stone materials since it is associated to the highest conductance values. This evidence indicates that the PM deposited on stage D has the highest content of soluble substances. In addition to the this, the fact that the specimen corresponding to stage D has a lowest activation RH suggests that this specimen has a tendency to adsorb water at lower RH values compared to the specimens referred to the other stages. This fact affects both the time of wetness and the number of dissolution crystallization cycles (see section 2.1).

4.5 Deposition of single-salts PM and study of their decay impact with AEC

4.5.1 Deposition of single-salts PM on marble specimens

Thanks to the innovative characteristics of the rotating cascade impactor it was possible to deposit single-salt particles on marble specimens. Single-salt particles were generated with a dedicated aerosol generation unit (figure 4.13). This is composed by a PTFE sack equipped with two nozzles, one for the inlet of the aerosol and the other one for the sampling line. The PTFE sack was made by welding some PTFE sheets to obtain an hermetic sack. The PTFE sack acts as a lung, balancing any differences between the inlet and outlet fluxes.

Figure 4.13: the Aerosol Generation Unit.

Different types of aerosols can be generated by connecting two different generation set up at the inlet of the

PTFE sack. When a TOPAS ATM 220 is used (figure 4.13), it is possible to generate saline aerosol through the atomization of water-solutions. A second set up can be arranged, allowing the generation of a saline-carbonaceous mixed aerosol. The carbonaceous aerosol is generated by an acetylene flame while the saline aerosol is generated with the ATM 220. The aerosols were premixed before being introduced in the PTFE sack (figure 4.14).
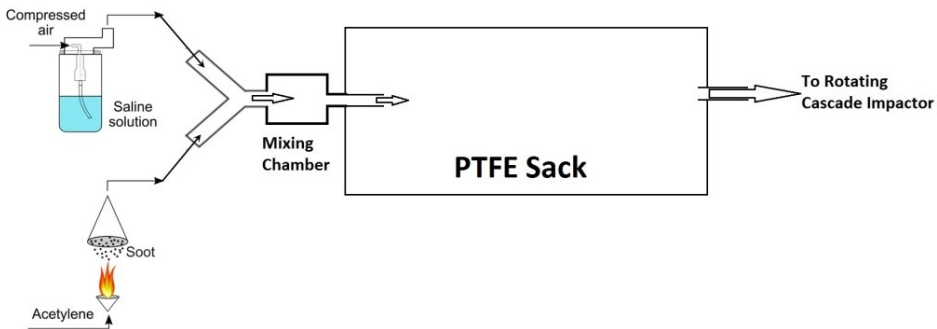
Figure 4.14: Set up of the aerosol generation unit for the generation of mixed carbonaceous-saline aerosols.

The rotating cascade impactor was connected to the aerosol generation unit settled up for the generation of saline aerosol, according to figure 4.13. In this way, it is possible to deposit any kind of salts particles on the surface of stone specimens. It was chosen to generate and deposited

three sodium salts; $NaNO_3$, $NaCl$ and Na_2SO_4 and three ammonium salts; NH_4NO_3, NH_4Cl and $(NH_4)_2SO_4$ table 4.3.

**Table 4.3: Deliquescence Relative Humidities of the salts used in this work. (*Nenes et. al. 1998*).**

Sodium series	DRH (298.15 K)	Ammonium series	DRH (298.15 K)
$NaNO_3$	0.7379	NH_4NO_3	0.6183
$NaCl$	0.7528	NH_4Cl	0.7710
Na_2SO_4	0.9300	$(NH_4)_2SO_4$	0.7997

A 25000 ppm concentrated solution of each of the salts listed in table 4.3 was prepared and put into the vessel of the ATM 220. The generation and deposition of the salts was carried out according to the following procedure:

- The PTFE sack was inflated by generating the chosen salt with ATM 220 (5 atm operating pressure; flow rate 225 l/h; 0.26 µm residual size for a 1 µm droplet; 1.3 µm residual size for a 5 µm droplet).

- When the PTFE sack was quite inflated (about 10 minutes of generation), the sampling with rotating cascade impactor started. A marble specimen was housed in the stage D, while the other impaction stages were filled with waste filters. The rotation speed was set to the maximum values of 2.8 minutes per rotation. The sampling lasted for 20 minutes. A further inflated of the sack using ATM 220 was performed if needed.

- After the generation of the salt, the PTFE sack was cleaned up with subsequent inflation and deflation with clean compressed air. The cleaning of the sack was checked counting the particles inside the sack with a portable diffusion size classifier (miniDiSC). The vessel of the ATM 220 was carefully cleaned with MilliQ water, as well as the nozzles and the impaction stages of the rotating cascade impactor.

After the sampling, all the marble specimens are subject to the presence of a white salts deposit (figure 4.15), with a 2 cm diameter circular shape.
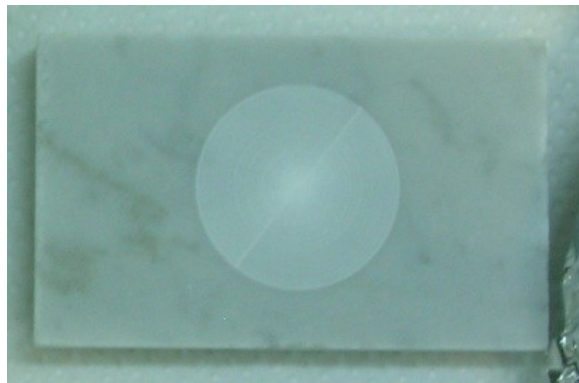
Figure 4.15: salt deposited on a marble specimen thanks to the rotating cascade impactor

4.5.2   Study of the hygroscopic behaviour of the salts-contaminated stone specimens.

The hygroscopic behaviour of the salts-contaminated stone specimens was studied with the Aerosol Exposure Chamber. The conductance of the salt-contaminated stone surfaces was measured during a progressive increasing of RH (1% steps) from 25 to 85%. The results of this study are shown in figure 4.16 concerning the sodium salts and in figure 4.17 as regards ammonium salts.
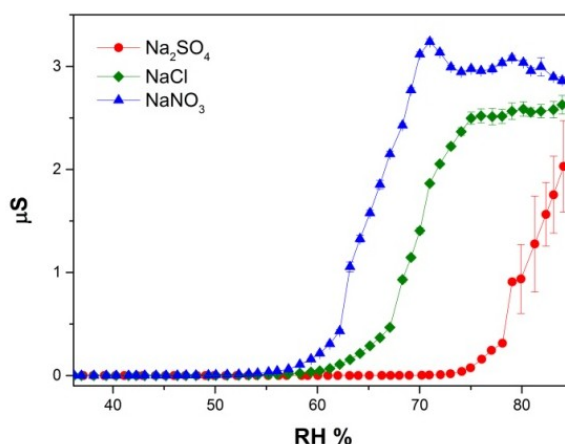
Figure 4.16: Conductance of the sodium salts deposited on marble specimen as a function of RH

Results shown in figure 4.16 pointed out that the hygroscopic behaviour of the salt-contaminated marble specimens is strongly influenced by the chemical composition of the salt. The curves are the result of several

water-adsorption mechanisms, promoted by both salt deposit and stone surface. The specimen contaminated with sodium nitrate, which is the salt with the lowest DRH (see table 4.3), has the lowest activation point and the highest maximum conductance (table 4.4). Conversely, the specimens contaminated with sodium sulphate shows instead the higher activation RH and the lowest maximum conductance. The curve of the specimen contaminated with sodium chloride lies between the curves of the nitrate and sulphate.
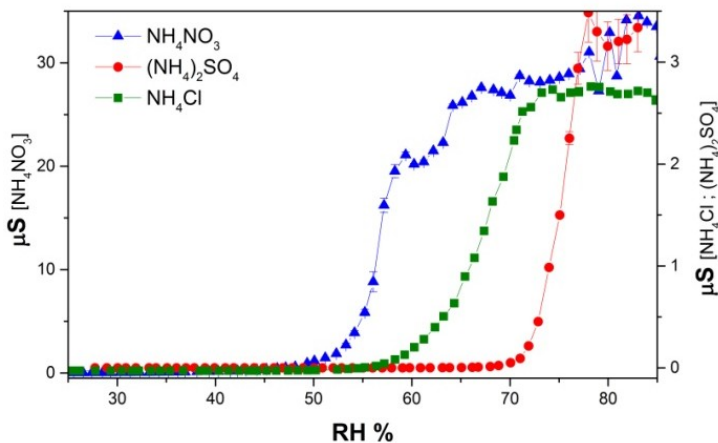
Figure 4.17: Conductance of the ammonium salts deposited on marble specimens as a function of RH.

The same consideration obtained for the case of sodium salts are also valid in the case of ammonium salts. The specimen contaminated with ammonium nitrate shows the

lower activation RH and the highest conductance values, the specimen contaminated with ammonium sulphate has the highest activation RH, while the curve referred to ammonium chloride lies between the other two.

Table 4.4: Activation RH and Maximum conductance measured on salt-contaminated stone specimen.

Salt	Activation RH [%]	Max Conductance µS	Salt	Activation RH [%]	Max Conductance µS
$NaNO_3$	43	3.23	NH_4NO_3	-	34.54
NaCl	47	2.64	NH_4Cl	44	2.66
Na_2SO_4	65	2.02	$(NH_4)_2SO_4$	59	3.33

4.6 Conclusions

A prototype of a new rotating cascade impactor was designed and built. The prototype was successfully employed to obtain PM deposits on stone surfaces. By sampling environmental PM, the single dimensional fractions were deposited. The finest PM fraction (0.25 – 0.5 µm) seems to have a greater impact both in terms of surface blackening and concerning the water-adsorption and solubilisation of water-soluble substances. These results point out that fine PM fractions have a great importance concerning both the aesthetic damage and decay of stone surfaces exposed to PM deposition. The rotating cascade impactor allowed to perform, for the first time, a study about the size-dependent potential decay impact. This issue is of fundamental importance to understand the effects of future changes in terms of atmospheric PM characteristics. Thanks to the new device it was possible to obtain a significant amount of PM deposit with a very short sampling time (63 hours) and this is another plus.

Single-salt PM deposition was performed by means of the rotating cascade impactor as well, collecting the aerosol spray that was phased into an aerosol generation unit. Thank to this experimental apparatus, it is possible to obtain deposits with known chemical composition or to study the effects of aerosols generated from specific

sources. At the best of our knowledge, this is the first time that generated synthetic aerosol were deposited on stone materials. The results related to the single-salts contaminated stone specimens, highlight that the water-adsorption of stone substrates can strongly depend on the chemical composition of the contaminants. In particular, the specimens contaminated with sodium and ammonium nitrates, which have the lowest DRH values, seem to show the water-adsorption at low RH value. On the specimens contaminated with sodium and ammonium sulphates, the water adsorption seems to be triggered at higher RH values, in accordance with the high DRH values of the salts contaminants. The specimens contaminated with sodium and ammonium chloride show the water-adsorption at intermediate RH values between nitrates and sulphates, even in this case in agreement with the DRH values of the salts. All the salts-contaminated stone specimens show extremely higher values of conductance as a function of RH, compared to not-contaminated specimens. These results allow to highlight that the presence of soluble substances can trigger decay phenomena against the materials. Such mechanisms are cyclically activated by hygrometric variations, whereas the chemical composition of the water soluble compounds can strongly influence the magnitude of the decay and the humidity safety thresholds.

CHAPTER 5

Concluding Remarks

Some issues about the interactions between particulate matter and stone substrates were studied, starting from the previous literature approaches, three main topics were investigated. These three main topics are connect not only from the point of view of the fundamental theme, but also because obtained results are related and complementary.

A first issue concerned the development of an innovative method to evaluate the stone decay hazard due to the synergic effect of PM pollution and climate, exploiting an "heritage climatology" approach. Experimental measurements of PM deliquescence and crystallization relative humidity (DRH and CRH) were coupled with climatic data to compute well-known hazard indicators for stone materials, time of wetness and number of dissolution crystallization cycles. Since DRH and CRH depends on the chemical composition, the developed method allows to evaluate how different PM chemical composition can lead to

different hazards for exposed materials. The method was applied to the case-study of Milan revealing that different hazards may prevail depending on the season. In winter, a chemical hazard prevails, due to the high time of wetness and the low number of dissolution and crystallization cycles. In summer the chemical stress reached the minimum value, since the season is associated to low time of wetness, while the mechanical stress increased. In spring and fall, both the time of wetness and the number of dissolution and crystallization cycles were relatively high. These can be associated to a greatest hazard for stone surfaces.

Since the new evaluation methods suggested a strong seasonality in the hazards which the stone surfaces are exposed on, a new method for the exposure of stone specimens was develop. The goal is to perform seasonal exposure campaigns, trying to assess the seasonal PM deposition rates and the related decay phenomena. A suitable deposition box, with a standardized air exchange rate, was designed and built. Several stone specimens and surrogate surfaces were exposed during different exposure campaigns at two Milan exposure sites: Torre Sarca and Villa Necchi Campiglio. Obtained results confirm the seasonal differences regarding both the deposition rates of the total mass and the deposition rates of the ions. A new

processing method of the scanning electron microscope images allow to evaluate the dimensional distribution of the deposited particles. These measurements showed a relevant presence of fine PM. The more abundant size fraction is that of the particles having an area between 0.4 and 5.0 μm^2. In addition to this, stone specimens that were exposed for a longer time (22 months) show slight decay signs that seemed to be differentiated according to the characteristics of the stone material. This result supports the goodness of the deposition box as exposure method for the evaluation of the decay of materials.

In order to deeper investigate the decay impact of the single size fractions of PM, a prototype of a new rotating cascade impactor was built. Thanks to this prototype, single size fractions of PM were sampled directly deposited on stone specimens, revealing that the finest PM fraction (d_{ae} = 0.25 – 0.5 μm) seem to have a greater impact, both in terms of surface blackening and concerning the water-adsorption and solubilisation of water-soluble substances. The evaluation of the water-adsorption of the PM deposited on stone surfaces was reached with an aerosol exposure chamber method developed starting from the same method used for the PM DRH and CRH determination. In addition to this, the new sampling device allowed to realized deposits of synthetic aerosol on stone specimens. In this way, the

role of the salts particles in promoting water-adsorption was studied, confirming the strong relations between the chemical composition of the deposits and the tendency to the water-adsorption.

Acknowledgment

Bibliographical Notes

6.1 Bibliography

Accardo G., Altieri A., Cacace C., Giani E., Giovagnoli A. (2002). Risk map: a project to aid decision-making in the protection, preservation and conservation of Italian cultural heritage. *Conservation Science 2002, pp 44-49.*

Accardo G., Giani E., Giovagnoli A. (2003) The risk map of italian cultural heritage. *Journal of architectural conservation, 2, pp 41-57.*

Andreae, M. O., & Gelencsér, a. (2006). Black carbon or brown carbon? The nature of light-absorbing carbonaceous aerosols. *Atmospheric Chemistry and Physics Discussions, 6(3), 3419–3463.* doi:10.5194/acpd-6-3419-2006

APAT-ICR (2006) L'impatto dell'inquinamento atmosferico sui beni di interesse storico artistico esposti all'aperto. *Quaderni Ambiente e Società. ISBN: 88-448-0170-1*

ARPA Lombardia (2014). Rapporto sulla qualità dell'aria della Città metropolitana di Milano anno 2014. *www2.arpalombardia.it*

ASHRAE, T. C. 2011 Gaseous and Particulate Contamination Guidelines For Data Centers; 2011.

Baedecker, P.A., Reddy, M.M., Reimann, K.J., Sciammarella, C.A. (1992). Effects of acidic deposition on the erosion of carbonate stone — experimental results from the U.S. National Acid Precipitation Assessment Program (NAPAP). *Atmospheric Environment Part B Urban Atmosphere, 26(2):147–58.*

Behera, S. N., Betha, R., Liu, P., & Balasubramanian, R. (2013). A study of diurnal variations of PM2.5 acidity and related chemical species using a new thermodynamic equilibrium model. *The Science of the Total Environment*, 452-453, 286–95. doi:10.1016/j.scitotenv.2013.02.062

Bonazza A., Sabbioni C., Ghedini N. (2005). Quantitative data on carbon fractions in interpretation of black crusts and soiling on European built heritage. *Atmospheric Environment 39, 2607-2618.*

Bonazza, A., Messina, P., Sabbioni, C., Grossi, C.M. and Brimblecombe, P. (2009). Mapping the Impact of climate Change on Surface Recession of Carbonate Buildings in Europe. *Sci. Total Environ.* 407: 2039–2350, doi: 10.1016/j.scitotenv.2008.10.067.

Borghi, A. and d'Atri, A. and Martire, L. and Castelli, D. and Costa, E. and Dino, G. and Favero Longo, S.E. and Ferrando, S. and Gallo, L.M. and Giardino, M. and Groppo, C. and Piervittori, R. and Rolfo, F. and Rossetti, P. and Vaggelli, G. (2014). Fragments of the Western Alpine Chain as Historic Ornamental Stones in Turin (Italy): Enhancement of Urban Geological Heritage through Geotourism. *Geoheritage, 6 (1), pp. 41-55*

Boriani, A., Caironi, V., Oddone, M., Vannucci, R., (1988). Some petrological and geochemical constrains on the genesis of the Baveno-Mottarone and Montorfano plutonic bodies. *Rendiconti della Società Italiana di Mineralogia e Petrologia vol.43-2 pp.385-394*

Brimblecombe, P., Grossi, C.M. and Harris, I. (2006). The Effect of Long-term Trends in Dampness on Historic Buildings. *Weather* 61: 278–281, doi: 10.1256/wea.267.05.

Brimblecombe, P., & Grossi, C. M. (2009). Millennium-long damage to building materials in London. *The Science of the Total Environment, 407(4), 1354–61.*

Brimblecombe, P. (2010). Heritage Climatology, In *Climate Change and Cultural Heritage*, Lefevre, R.A. and Sabbioni, C. (Eds.), Edipuglia, Bari—Italy, p. 54–57.

Brimblecombe, P., Grossi, C.M., Harris, I. (2011). Climate Change Critical to Cultural Heritage. In: *Survival and Sustainability, edited by H. Gökçekus, U. Türker and J.W. LaMoreaux. Environmental Earth Science, Springer. ISBN 978-3-540-95991-5 (online)*

Bugini, R., Laurenzi Tabasso, M., Realini, M. (2000). Rate of formation of black crust on marble. A case study. *Journal of Cultural Heritage 1, 111-116.*

Butlin, R. N., Coote, A. T., Devenish, M., Hughes, I. S. C., Hutchens, C. M., Irwin, J.G., Lloyd, G. O., Yates, T. J. S. (1992). Preliminary results from the analysis of stone tablets from the national materials exposure programme (nmep). *Atmospheric Environment 26B (2) pp. 189-198.*

Camuffo, D., Del Monte, M., Sabbioni, C. and Vittori, O. (1982). Wetting, Deterioration and Visual Features of Stone Surfaces in an Urban Area. *Atmospheric Environment* 16: 2253–2259.

Camuffo, D. (1995). Physical Weathering of Stones. *Science of the Total Environment* 167: 1–14.

Cappitelli, F., Principi, P., Pedrazzani, R., Toniolo, L., Solrlini, C. (2007). Bacterial and fungal deterioration of the Milan Cathedral marble treated with protective synthetic resins. *Science of the Total Environment 385, 172–181.*

Carbone, C., Decesari, S., Mircea, M., Giulianelli, L., Finessi, E., Rinaldi, M., Fuzzi, S., Marinoni, A., Duchi, R., Perrino, C., Sargolini, T., Vardè, M., Sprovieri, F., Gobbi, G.P., Angelini, F. and Facchini, M.C. (2010). Size-resolved Aerosol Chemical Composition over the Italian Peninsula during Typical Summer and Winter Conditions. *Atmospheric Environment* 44: 5269–5278.

Cardell-Fernández, C., Vleugels, G., Torfs, K. and Van Grieken, R. (2002). The Processes Dominating Ca Dissolution of Limestone When Exposed to Ambient Atmospheric Conditions as Determined by Comparing Dissolution Models. *Environmental Geology* 43: 160–171, doi: 10.1007/s00254-002-0640-x.

Casati, M., Rovelli, G., D'Angelo, L., Perrone, M. G., Sangiorgi, G., Bolzacchini, E., & Ferrero, L. (2015). Experimental Measurements of Particulate Matter Deliquescence and Crystallization Relative Humidity: Application in Heritage Climatology. *Aerosol and Air Quality Research* 15, 399–409. doi:10.4209/aaqr.2014.11.0289

Casati, M., Rovelli, G., D'Angelo, L., Rizzi, C., Sangiorgi, G., Perrone, G., Bolzacchini, E., Conti, C., Sansonetti, A., Bernardi, E., Nobili, L., Vassura, I., Ferrero L. (2015)b Development of a "Deposition Box" for sampling Total Suspended Particles on not-filter substrates and to perform exposure studies for decay of materials. *In EAC (European Aerosol Conference) Milano, 6-11 Settembre 2015*

Chabas, A., Jeannette, D. and Lefevre, R.A. (2000). Crystallization and Dissolution of Airborne Sea-salts on Weathered Marble in a Coastal Environment at Delos (Cyclades, Greece). *Atmospheric Environment* 34: 219–224.

Charola, A. E. (2000). Salts in the deterioration of porous materials: an overview. *Journal of American Institute for Conservation. Volume 39, Issue 3: 327-343*

Clegg, S.L., Seinfeld, J.H. and Brimblecombe, P. (2001). Thermodynamic Modelling of Aqueous Aerosols Containing Electrolytes and Dissolved Organic Compounds. *J. Aerosol Sci.* 32: 713–738, doi: 10.1016/S0021-8502 (00)00105-1.

Conti C., Brambilla L., Colombo C., Dellasega D., Gatta D., Realini M., Zerbi G. (2010). Stability and transformation mechanism of weddellite nanocrystals studied by X-ray diffraction and infrared spectroscopy. *Physical Chemistry Chemical Physics 12,14560-14566.* DOI:

10.1039/c0cp00624f.

Conti, C., Colombo, C., Dellasega, D., Matteini, M., Realini, M., & Zerbi, G. (2011). Ammonium oxalate treatment: Evaluation by µ-Raman mapping of the penetration depth in different plasters. *Journal of Cultural Heritage, 12(4), 372–379.* doi:10.1016/j.culher.2011.03.004

Conti, C., Aliatis, I., Casati, M., Colombo, C., Matteini, M., Negrotti, R., Zerbi, G. (2013). Diethyl oxalate as a new potential conservation product for decayed carbonatic substrates. *Journal of Cultural Heritage, 8–10.* doi:10.1016/j.culher.2013.08.002

Conti, C., Casati, M., Colombo, C., Realini, M., Brambilla, L., & Zerbi, G. (2014). Phase transformation of calcium oxalate dihydrate – monohydrate : Effects of relative humidity and new spectroscopic data. *Spectrochimica Acta Part A : Molecular and Biomolecular Spectroscopy 128, 413–419.*

Conti C., Casati M., Colombo C., Possenti E., Realini M., Gatta D., Merlini M., Brambilla L., Zerbi G. (2015). Synthesis of calcium oxalate trihydrate: New data by vibrational spectroscopy and synchrotron X-ray diffraction. *Spectrochimica Acta Part A: Molecular and Biomolecular Spectroscopy 150: 721–730. 2015*

Ding, K.; Xiao, K.; Dong, C.; Zou, S.; Yi, P.; Li, X. (2015). Initial Corrosion Behavior and Mechanism of PCB–HASL in Typical Outdoor Environments in China. *Journal of Electronic Materials, 44 (11), 4405–4417.*

Dino, G.A., Cavallo, A. (2014). Ornamental stones of the Verbano Cusio Ossola quarry district: characterization of materials, quarrying techniques and history and relevance to local and national heritage. *From: Pereira, D., Marker, B. R., Kramar, S., Cooper, B. J. & Schouenborg, B. E. (eds) 2015. Global Heritage Stone: Towards International Recognition of Building and Ornamental Stones. Geological Society, London, Special Publications, 407, 187–200.*

Doehne, E. (2002). Salt Weathering: A Selective Review. *Geol. Soc. Spec. Publ.* 205: 51–64.

Doherty, B., Pamplona, M., Miliani, C., Matteini, M., Sgamellotti, a., & Brunetti, B. (2007). Durability of the artificial calcium oxalate protective on two Florentine monuments. *Journal of Cultural Heritage, 8(2), 186–192.* doi:10.1016/j.culher.2006.12.002

Ferm, M., De Santis, F. and Varotsos, C. (2005). Nitric Acid Measurements in Connection with Corrosion Studies. *Atmospheric Environment* 39: 6664–6672.

Ferm, M., Watt, J., O'Hanlon, S., De Santis, F. and Varotsos, C. (2006).

Deposition Measurement of Particulate Matter in Connection with Corrosion Studies. *Anal. Bioanal. Chem.* 384: 1320–1330

Fermo, P., Gonzalez Turrion, R., Rosa, M., Omegna, A. (2014)a. A new approach to assess the chemical composition of powder deposits damaging the stone surfaces of historical monuments. *Environmental Science and Pollution Research. DOI10.1007/s11356-014-3855-y*

Fermo, P., Cappelletti, G., Cozzi, N., Padeletti, G., Kaciulis, S., Brucale, M., & Merlini, M. (2014)b. Hydrophobizing coatings for cultural heritage. A detailed study of resin/stone surface interaction. *Applied Physics A: Materials Science and Processing*, 116(1), 341–348. doi:10.1007/s00339-013-8127-z

Ferrero, L., Cappelletti, D., Moroni, B., Sangiorgi, G., Perrone, M.G., Crocchianti, S. and Bolzacchini, E. (2012). Wintertime Aerosol Dynamics and Chemical Composition across the Mixing Layer over Basin Valleys. *Atmos. Environ.* 56: 143–153.

Ferrero, L., Sangiorgi, G., Ferrini, B.S., Perrone, M.G., Moscatelli, M., D'Angelo, L., Rovelli, G., Ariatta, A., Truccolo, R. and Bolzacchini, E. (2013). Aerosol Corrosion Prevention and Energy-Saving Strategies in the Design of Green Data Centers. *Environ. Sci. Technol.* 47: 3856–3864.

Ferrero, L., D'Angelo, L., Rovelli, G., Sangiorgi, G., Perrone, M.G., Moscatelli, M., Casati, M. and Bolzacchini, E. (2014). Determination of Aerosol Deliquescence and Crystallization Relative Humidity for Energy Saving in Free-cooled Data Centers. *Int. J. Environ. Sci. Technol.* doi: 10.1007/s13762-014-0680-2.

Franzen, C. and Mirwald, P.W. (2009). Moisture Sorption Behaviour of Salt Mixtures in Porous Stone. *Chem. Erde* 69: 91–98. doi: 10.1016/j.chemer.2008.02.001.

Giavarini, C., Santarelli, M. L., Natalini, R., & Freddi, F. (2008). A non-linear model of sulphation of porous stones: Numerical simulations and preliminary laboratory assessments. *Journal of Cultural Heritage, 9(1), 14–22.* doi:10.1016/j.culher.2007.12.001

Ghedini, N., Gobbi, G., Sabbioni, C., & Zappia, G. (2000). Determination of elemental and organic carbon on damaged stone monuments. *Atmospheric Environment, 34(25), 4383–4391.* doi:10.1016/S1352-2310(00)00250-8

Ghedini, N., Ozga, I., Bonazza, A., Dilillo, M., Cachier, H. and Sabbioni, C. (2011). Atmospheric Aerosol Monitoring as a Strategy for the Preventive Conservation of Urban Monumental Heritage: The Florence Baptistery. *Atmos. Environ.* 45: 5979–5987, doi: 10.1016/j.atmosenv.2011.0 8.001.

Grossi, C.M., Esbert, R.M., Dã, F. and Alonso, F.J. (2003). Soiling of Building Stones in Urban Environments. *Buildings and Environment* 38: 147–159.

Grossi, C.M., Bonazza, A., Brimblecombe, P., Harris, I., & Sabbioni, C. (2008). Predicting twenty-first century recession of architectural limestone in European cities. *Environmental Geology, 56(3-4), 455–461. doi:10.1007/s00254-008-1442-6*

Grossi, C.M., Brimblecombe, P., Menéndez, B., Benavente, D., Harris, I. and Déqué, M. (2011). Climatology of Salt Transitions and Implications for Stone Weathering. *Sci. Total Environ.* 409: 2577–2585, doi: 10.1016/j.scitotenv. 2011.03.029.

Gualtieri, M., Franzetti, A., Longhin, E., Mantecca, P., Bestetti, G., Bolzacchini, E., Camatini M. (2011). In vitro effects of microbiologically characterized Milan particulate matter. *Procedia Environmental Sciences, 4, 192–197.* doi:10.1016/j.proenv.2011.03.023

Gulotta, D., Bertoldi, M., Bortolotto, S., Fermo, P., Piazzalunga, A., Toniolo, L. (2012). The Angera stone: a challenging conservation issue in the polluted environment of Milan (Italy). *Environmental Earth Science.* DOI 10.1007/s12665-012-2165-2

Hinds, W. C. (1982). Aerosol Technology. *Wiley, New York.*

La Russa, M. F., Barone, G., Belfiore, C. M., Mazzoleni, P., & Pezzino, A. (2010). Application of protective products to "Noto" calcarenite (south-eastern Sicily): a case study for the conservation of stone materials. *Environmental Earth Sciences,* 62(6), 1263–1272. doi:10.1007/s12665-010-0614-3

Linnow, K., Zeunert, A., & Steiger, M. (2006). Investigation of Sodium Sulfate Phase Transitions in a Porous Material Using Humidity- and Temperature-Controlled X-ray Diffraction. *Analytical Chemistry, 78, 4683–4689.*

LipfertF.W. (1989). Atmospheric damage to calcareous stones: comparison and reconciliation of recent experimental findings. *Atmospheric Environment,23:415–29.*

Livingston R.A. (1992). Graphical methods for examining the effects of acid rain and sulfur dioxide on carbonate stones. *In: Delgado Rodrigues J, Henriques F,TelmoJeremias F, editors. Proceedings of the 7th International Congress on Deterioration and Conservation of Stone p. 375–86.*

Kucera, V., Tidblad, J., Kreislov, K., Knotkova, D., Faller, M., Reiss, D. and Kobus, J. (2007). UN/ECE ICP Materials Dose-response Functions for the Multi-pollutant Situation. *Water Air Soil Pollut. Focus* 7: 249–

258, doi: 10.1007/ s11267-006-9080-z

Maro, D., Connan, O., Flori, J.P., Hébert, D., Mestayer, P., Olive, F. and Solier, L. (2014). Aerosol Dry Deposition in the Urban Environment: Assessment of Deposition Velocity on Building Facades. *J. Aerosol Sci.* 69: 113–131.

Martin, S.T. (2000) Phase Transitions of Aqueous Atmospheric Particles. *Chem. Rev.* 100: 3403–3454.

Martin, S.T., Schlenker, J.C., Malinowski, A. and Hung, H.M. (2003). Crystallization of Atmospheric Sulfate-nitrate-ammonium Particles. *Geophys. Res. Lett.* 30, doi: 10.1029/2003GL017930.

Marple, V. a., & Willeke, K. (1976). Impactor design. *Atmospheric Environment, 10(10), 891–896. doi:10.1016/ 0004-6981(76)90144-X*

McAlister, J. J., Smith, B. J., & Török, a. (2006). Element partitioning and potential mobility within surface dusts on buildings in a polluted urban environment, Budapest. *Atmospheric Environment, 40(35), 6780–6790.* doi:10.1016/j.atmosenv.2006.05.071

McAlister, J.J., Smith, B.J. and Török, A. (2008). Transition Metals and Water-soluble Ions in Deposits on a Building and Their Potential Catalysis of Stone Decay. *Atmos. Environ.* 42: 7657–7668.

Misra, C., Singh, M., Shen, S., Sioutas, C., & Hall, P. M. (2002). Development and evaluation of a personal cascade impactor sampler (PCIS). Aerosol Science, *33, 1027–1047.*

Nava, S., Becherini, F., Bernardi, A., Bonazza, A., Chiari, M., García-Orellana, I. and Vecchi, R. (2010). An Integrated Approach to Assess Air Pollution Threats to Cultural Heritage in a Semi-confined Environment: The Case Study of Michelozzo's Courtyard in Florence (Italy). *Sci. Total Environ.* 408: 1403–1413.

Nenes, A., Pandis, S. N., Pilinis, C. (1998). ISORROPIA: A New Thermodynamic Equilibrium Model for Multiphase Multicomponent Inorganic Aerosols. *Aquatic Geochemistry 4: 123-152.*

Nobili, L., Bernardi, E., Vassura, I., Raffo, S., Casati, M., Ferrero, L., Sangiorgi, G., Perrone, M.G., Bolzacchini, E. (2015). Particulate matter and decay of materials: development of a method for sem/eds analysis of atmospheric deposition sampled through "deposition box". *In XXV Congresso Divisione di Chimica Analitica Società Chimica Italiana.,Trieste 13-17 Settembre 2015*

Owoade, O.K., Olise, F.S., Obioh, I.B., Olaniyi, H.B., Bolzacchini, E., Ferrero, L. and Perrone, G. (2006). PM_{10} Sampler Deposited Air Particulates: Ascertaining Uniformity of Sample on Filter through Rotated Exposure to Radiation. *Nucl. Instrum. Methods Phys. Res.,*

Sect. A 564: 315–318.

Ozga, I., Bonazza, A., Bernardi, E., Tittarelli, F., Favoni, O., Ghedini, N. and Sabbioni, C. (2011). Diagnosis of Surface Damage Induced by Air Pollution on 20th-century Concrete Buildings. *Atmos. Environ.* 45: 4986–4995, doi: 10.1016/j.atmosenv.2011.05.072.

Pathak, R.K., Louie, P.K.K., Chan, C.K. (2004). Characteristics of aerosol acidity in Hong Kong. *Atmospheric Environment, 38(19), 2965–2974.* doi:10.1016/j.atmosenv.2004.02.044

Pedrazzani, R., Alessandri, I., Bontempi, E., Cappitelli, F., Cianci, M., Pantos, E., Toniolo, L., Depero, L.E. (2006) Study of sulphation of Candoglia marble by means of micro X-ray diffraction experiments. *Applied Physics A Materials Science & Processing 83, 689-694*

Perrone, M. G., Gualtieri, M., Ferrero, L., Lo Porto, C., Udisti, R., Bolzacchini, E., & Camatini, M. (2010). Seasonal variations in chemical composition and in vitro biological effects of fine PM from Milan. *Chemosphere, 78(11), 1368–77.* doi:10.1016/j.chemosphere.2009.12.071

Perrone, M.G., Larsen, B., Ferrero, L., Sangiorgi, G., De Gennaro, G., Udisti, R., Zangrando, R., Gambaro, A. and Bolzacchini, E. (2012). Sources of High PM2.5 Concentrations in Milan, Northern Italy: Molecular Marker Data and CMB Modelling. *Sci. Total Environ.* 414: 343–355.

Perrone, M.G., Gualtieri, M., Consonni, V., Ferrero, L., Sangiorgi, G., Longhin, E., Ballabio, D., Bolzacchini, E. and Camatini, M. (2013). Particle Size, Chemical Composition, Seasons of the Year and Urban, Rural or Remote Site Origins as Determinants of Biological Effects of Particulate Matter on Pulmonary Cells. *Environmental Pollution* 176: 215–227.

Poli, T., Toniolo, L., & Chiantore, O. (2004). The protection of different Italian marbles with two partially flourinated acrylic copolymers. *Applied Physics A: Materials Science & Processing*, 79(2), 347–351. doi:10.1007/s00339-004-2530-4

Ponziani, D., Ferrero, E., Appolonia, L. and Migliorini, S. (2012). Effects of Temperature and Humidity Excursions and Wind Exposure on the Arch of Augustus in Aosta. *J. Cult. Herit.* 13: 462–468. doi: 10.1016/j.culher.2012.01.005.

Potgieter-Vermaak, S., Horemans, B., Anaf, W., Cardell, C. and Van Grieken, R. (2012). Degradation Potential of Airborne Particulate Matter at the Alhambra monument: A Raman Spectroscopic and Electron Probe X-ray Microanalysis Study. *J. Raman Spectrosc.* 43: 1570–1577, doi: 10.1002/jrs.4052.

Potukuchi, S. and Wexler, A.S. (1995). Identifying Solid-aqueous Phase Transitions in Atmospheric Aerosols - I. Neutral-acidity Solutions. *Atmos. Environ.* 29: 1663–1676.

Potukuchi, S. and Wexler, A.S. (1995). Solid-aqueous-phase Transitions Atmospheric Aerosols - II. Acidic Solutions. *Atmos. Environ.* 29: 3357–3364.

Rampazzi, L., Giussani, B., Rizzo, B., Corti, C., Pozzi, A., & Dossi, C. (2011). Monuments as sampling surfaces of recent traffic pollution. *Environmental Science and Pollution Research International, 18(2), 184–91.* doi:10.1007/s11356-010-0363-6

Randriamiarisoa, H., Chazette, P., Couvert, P., Sanak, J. and Mégie, G. (2006) Relative Humidity Impact on Aerosol Parameters in a Paris Suburban Area. *Atmos. Chem. Phys.* 6: 1389–1407.

Realini, M., Negrotti, R., Appollonia, L. and Vaudan, D. (1995). Deposition of Particulate Matter on Stone Surfaces: An Experimental Verification on Its Effects on Carrara Marble. *Sci. Total Environ.* 167: 67–72.

Rodriguez, S., Van Dingenen, R., Putaud, J.P., Dell'Acqua, A., Pey, J., Querol, X., Alastuey, A., Chenery, S., Ho, K.F., Harrison, R., Tardivo, R., Scarnato, B. and Gemelli, V. (2007). A Study on the Relationship between Mass Concentration, Chemistry and Number Size Distribution of Urban Fine Aerosol in Milan, Barcelona and London. *Atmos. Chem. Phys.* 7: 2217–2232.

Rodriguez-Navarro, C. and, Sebastian E. (1996). Role of Particulate Matter from Vehicle Exhaust on Porous Building Stones (Limestone) Sulfation. *Sci. Total Environ.* 187: 79–91.

Sabbioni, C., Zappia, G., & Gobbi, G. (1992). Carbonaceous particles on carbonate building stones in a simulated system. *Journal of Aerosol Science, 23(1), 921–924.*

Sabbioni, C. (1995). Contribution of Atmospheric Deposition to the Formation of Damage Layers. *Sci. Total Environ.* 167: 49–55, doi: 10.1016/0048-9697(95)04568-L.

Sabbioni, C., Zappia, G., Ghedini, N., Gobbi, G., & Favoni, O. (1998). Black crusts on ancient mortars. *Atmospheric Environment, 32(2), 215–223.*

Sabbioni, C., Ghedini, N., & Bonazza, A. (2003). Organic anions in damage layers on monuments and buildings. *Atmospheric Environment, 37(9-10),* 1261–1269. doi:10.1016/S1352-2310(02)01025-7

Sabbioni C., Brimblecombe, P., Cassar, M. (2010). The Atlas of Climate Change Impact on European Cultural Heritage. *Anthem press, London. ISBN 978-92-7909800-0*

Saiz-Jimenez, C. (1993). Deposition of Airborne Organic Pollutants on Historic Buildings. *Atmos. Environ. Part B* 27: 77–85.

Sandroff, F. S.; Burnett, W. H. Reliability Qualification Test for Circuit Boards Exposed to Airborne Hygroscopic Dust. (1992). *In Electronic Components and Technology Conference, Proceedings., 42nd; IEEE, Ed.; 1992; pp 384–389.*

Sangiorgi, G., Ferrero, L., Perrone, M.G., Bolzacchini, E., Duane, M. and Larsen, B.R. (2011). Vertical Distribution of Hydrocarbons in the Low Troposphere below and above the Mixing Height: Tethered Balloon Measurements in Milan, Italy. *Environmental Pollution* 159: 3545–3552.

Schaap, M., Muller, K., Ten Brink, H.M., 2002. Constructing the European aerosol nitrate concentration field from quality analysed data. *Atmospheric Environment 36, 1323–1335.*

Screpanti, A., De Marco, A. (2009). Corrosion on cultural heritage buildings in Italy: A role foro zone?. *Environmetal Pollution 157, 1513-1520*

Schindelholz, E., Tsui, L. and Kelly, R.G. (2014). Hygroscopic Particle Behavior Studied by Interdigitated Array Microelectrode Impedance Sensors. *J. Phys. Chem. A.* 118: 167–177.

Seinfeld, J.H. and Pandis, S.N. (2006). *Atmospheric Chemistry and Physics: From Air pollution to Climate Change*, 2nd Edition. Wiley ed.

Singh, P.; Ruch, P.; Saliba, S.; Muller, C. (2015). Characterization , Prevention and Removal of Particulate Matter on Printed Circuit Boards. *In IPC APEX EXPO Conference Proceedings; 2015*

Smith, B.J., Gomez-Heras, M., McCabe, S. (2008). Understanding the decay of stone-built cultural heritage. *Progress in Physical Geography 32 (4) pp. 439-461.*

Song, B.; Azarian, M. H.; Pecht, M. G. (2013). Effect of Temperature and Relative Humidity on the Impedance Degradation of Dust-Contaminated Electronics. *Journal of the Electrochemical Society, 160 (3), C97–C105.*

Speer, R.E., Edney, E.O. and Kleindienst, T.E. (2003). Impact of Organic Compounds on the Concentrations of Liquid Water in Ambient $PM_{2.5}$. *J. Aerosol Sci.* 34: 63–77.

Stefanis, N.A., Theoulakis, P. and Pilini, C. (2009). Dry Deposition Effect of Marine Aerosol to the Building Stone of the Medieval City of Rhodes, Greece. *Build. Environ.* 44: 260–270, doi: 10.1016/j.buildenv.2008.03.001.

Steiger, M., Asmussen, S. (2008). Crystallization of sodium sulfate

phases in porous materials: The phase diagram Na2SO4–H2O and the generation of stress. *Geochimica et Cosmochimica Acta, 72(17), 4291–4306.* doi:10.1016/j.gca.2008.05.053

Steiger, M. (2005). Salts in Porous Materials: Thermodynamics of Phase Transitions, Modelling and Preventive Conservation. *Restor. Build. Monument* 11: 419–432.

Tidblad, J., Kucera V., Ferm, M., Kreisolva, K., Brüggerhoff, S., Doytchinov, S., Screpanti, A., Grøntoft, T., Yates, T., de la Fuente, D., Roots, O., Lombardo, T., Simon, S., Faller, M., Kwiatkowski, L., Kobus, J., Varostos, C., Tzanis, C., Krage, L., Schreiner, M., Melcher, M., Grancharov, I. and Karmanova, N. (2012). Review Article Effects of Air Pollution on Materials and Cultural Heritage: ICP Materials Celebrates 25 Years of Research. *International Journal of Corrosion 2012, Article ID 496321. Doi:10.1155/2012/496321*

Tidblad J, Mikhailov AA, Kucera V. (1998). Unified dose–response functions after 8 years of exposure. *Proceedings UN/ECE Workshop on Quantification of Effects of Air Pollutants on Materials. Berlin, p. 77–86.*

Tidblad J, Kucera V, Mikhailov AA, HenriksenJ, Kreislova K, Yates T, et al. (2001). UNECE ICP materials: dose–response functions on dry and wet acid deposition effects after 8 years of exposure. *Water Air Soil Pollution, 130:1457–62.*

Torfs, K. and Van Grieken, R. (1997). Chemical Relations between Atmospheric Aerosols, Deposition and Stone Decay Layers on Historic Buildings at the Mediterranean Coast. *Atmos. Environ.* 31: 2179–2192.

Tsai, Y. I., Hsieh, L.-Y., Weng, T.-H., Ma, Y.-C., & Kuo, S.-C. (2008). A novel method for determination of low molecular weight dicarboxylic acids in background atmospheric aerosol using ion chromatography. *Analytica Chimica Acta, 626(1), 78–88.* doi:10.1016/j.aca.2008.07.041

Tzanis, C., Varotsos, C., Christodoulakis, J., Tidblad, J., Ferm, M., Ionescu, A., Lefevre, R.-A., Theodorakopoulou, K., Kreislova, K. (2011). On the corrosion and soiling effects on materials by air pollution in Athens, Greece. *Atmospheric Chemistry and Physics. 11 (23) pp. 12039-12048.*

Urosevic, M., Yebra-Rodríguez, A., Sebastián-Pardo, E. and Cardell, C. (2012). Black Soiling of an Architectural Limestone during Two-year Term Exposure to Urban Air in the City of Granada (S Spain). *Sci. Total Environ.* 414: 564–575, doi: 10.1016/j.scitotenv.2011.11.028.

UNI 10921, Beni Culturali, Materiali lapidei naturali ed artificiali, Prodotti idrorepellenti Applicazione su provini e determinazione in laboratorio delle loro caratteristiche. Commissione "Beni culturali

NORMAL" February 2001.

UNI 10859, Beni Culturali, Materiali lapidei naturali ed artificiali, determinazione dell'assorbimento di acqua per capillarità. Commissione "Beni Culturali NORMAL" January 2000

Vecchi R, Chiari M, D'Alessandro A, Fermo P, Lucarelli F, Mazzei F, et al. A mass closure and PMF source apportionment study on the sub-micron sized aerosol fraction at urban sites in Italy. *Atmospheric Environment 2008;42:2240–53.*

Verdingovas, V.; Jellesen, M. S.; Ambat, R. (2015). Solder Flux Residues and Humidity-Related Failures in Electronics: Relative Effects of Weak Organic Acids Used in No-Clean Flux Systems. *Journal of Electronic Materials, 44 (4), 1116–1127*

Webb AH, Bawden RJ, Busby AK, Hopkins JN. (1992). Studies on the effects of air pollution on limestone degradation in Great Britain. *Atmospheric Environment, 26B:165–81.*

Yang, L., Pabalan, R.T. and Juckett, M.R. (2006). Deliquescence Relative Humidity Measurements Using an Electrical Conductivity Method. *J. Solution Chem.* 35: 583–604, doi: 10.1007/s10953-005-9015-8.

Zanardini, E., Abbruscato, P., Ghedini, N., Realini, M. and Sorlini, C. (2000). Influence of Atmospheric Pollutants on the Biodeterioration of Stone. *Int. Biodeterior. Biodegrad.* 45: 35–42.

Zappia, G., Sabbioni, C., Riontino, C., Gobbi, G. and Favoni, O. (1998). Exposure Tests of Building Materials in Urban Atmosphere. *Sci. Total Environ.* 224: 235–244, doi: 10.1016/S0048-9697(98)00359-3.

6.2 *Webography*

http://www2.arpalombardia.it/siti/arpalombardia/meteo/previsionimeteo/meteolombardia/Pagine/default.aspx

http://www2.arpalombardia.it/sites/QAria/_layouts/15/QAria/IDati.asas?v=2

http://www2.arpalombardia.it/qariafiles/RelazioniAnnuali/RQA_MI_2014.pdf

http://www.cartadelrischio.it/

http://www.isprambiente.gov.it/it/pubblicazioni/quaderni/ambiente-e-societa/limpatto-dellinquinamento-atmosferico-sui-beni-di

http://www.google.it/maps

http://www.visitfai.it/villanecchi/

http://www.comune.milano.it/wps/portal/ist/it/servizi/mobilita/Area_C